UNI TY
Of M GAN
JAI 1958
ENGINEERING
LIBRARY

JOURNAL OF FLUID MECHANICS

VOLUME 3 PART 3

DECEMBER 1957

Published by

CAMBRIDGE UNIVERSITY PRESS

BENTLEY HOUSE, 200 EUSTON ROAD, LONDON, N.W.1
AMERICAN BRANCH: 32 EAST 57th STREET, NEW YORK 22, N.Y.

Price 20*s*. (*U.S.A.* $3.25)

The JOURNAL OF FLUID MECHANICS exists for the publication of theoretical and experimental investigations of all aspects of the mechanics of fluids, and is issued in six parts per volume.

Editor:

Dr. G. K. BATCHELOR, Cavendish Laboratory, University of Cambridge, Cambridge, England.

Assistant Editors:

Dr. T. B. BENJAMIN, Dr. I. PROUDMAN, Dr. P. G. SAFFMAN.

Associate Editors:

Prof. G. F. CARRIER, Pierce Hall, Harvard University, Cambridge 38, Massachusetts, U.S.A.

Dr. W. C. GRIFFITH, Research and Development Laboratory, Missile Systems Division, Lockheed Aircraft Corporation, Palo Alto, California, U.S.A.

Prof. M. J. LIGHTHILL, Department of Mathematics, The University, Manchester, England.

Authors wishing to have papers published in the JOURNAL should communicate them to any one of the persons named above, choosing one in their own country where possible.

Authors are urged to ensure that their papers are written clearly and attractively, in order that their work will be readily accessible to readers.

Manuscripts should be typed in double spacing on one side of the paper only, with references listed at the end in alphabetical order of authors. Drawings should be done on a large scale in Indian ink on tracing cloth or drawing paper, captions being typed on a separate sheet. Proofs of papers from overseas will usually be despatched to authors by airmail. Authors are entitled to receive 50 offprints of a paper in the JOURNAL free of charge, and additional offprints can be purchased from the publisher.

SUBSCRIPTIONS

The subscription price for a volume of six parts is £5 10*s*. net, post free, payable in advance. Separate parts 20*s*. net, plus postage. Subscriptions may be sent to any bookseller, or to the Cambridge University Press, Bentley House, 200 Euston Road, London, N.W.1.

Subscribers in the United States should send their orders to the Cambridge University Press, American Branch, 32 East 57th Street, New York 22. Subscription price per volume $18.50 post free, payable in advance; separate parts $3.25, plus postage.

Some shock tube experiments on the chemical kinetics of air at high temperatures

By SAUL FELDMAN
AVCO Research Laboratory, Everett, Massachusetts

(*Received* 1 *March* 1957 *and in revised form* 15 *August* 1957)

SUMMARY

This paper is concerned with the rates at which atoms and molecules react in the air that flows over a body flying through the atmosphere at hypersonic speeds. Using air as a working fluid, a series of shock tube experiments were carried out to provide information about these rates. Mach angle measurements were made to determine the state of the gas in three situations of interest.

(*a*) Flow over flat plates was used to determine the state of the gas behind the incident normal shock; temperatures in the gas that passed through the shock varied between 2000 and 6000° K and densities between standard and 1/80 of standard density.

(*b*) Flow over wedges was employed to decelerate the flow behind the incident shock to a small supersonic Mach number; here temperatures downstream of the oblique shock increased, at most, 2000° K above the free stream value.

(*c*) A Prandtl–Meyer expansion was used to cool rapidly the dissociated gas, so that the recombination process could be investigated; temperatures dropped at most 2500° K and the densities varied between standard and 1/200 of the standard value. In some cases, the initial degree of dissociation of air was over 45%.

The results (figure 11) indicate that the dissociation and recombination relaxation times of the chemical species found in air are very fast, when compared to the time it takes a particle of gas to flow either around a blunt body in hypersonic flight or past small models in shock tubes. Thus the shock tube is shown to be an instrument capable of supplying air at high temperatures in thermodynamic equilibrium (figure 5).

In the case of a non-melting blunt body of about 1 ft. diameter flying through the atmosphere at hypersonic speeds, the present results imply that, when the gas behind the detached shock is in thermodynamic equilibrium, the flow will also be in equilibrium as it expands around the body, provided its speed is greater than 10 000 ft./sec at altitudes below 180 000 ft. (figure 12).

1. Introduction

The kinetic energy of a blunt object flying through the atmosphere at hypersonic speeds is sufficient to dissociate the oxygen and some of the nitrogen in air. At high enough velocities, some of the molecules will also be ionized. These phenomena occur when the gas particles cross the standing bow shock that moves with the body.

Consider a body entering the atmosphere from space. At the point where the velocity is 25 000 ft./sec and the altitude is 140 000 ft., the stagnation point temperature could be anywhere between 30 000° K and 7500° K, depending on whether the molecular excitation and reaction rates are infinitely slow or infinitely fast respectively. Figure 1 shows how the concentration of the most important species in the gas at the stagnation point varies along a typical entry trajectory, assuming infinitely

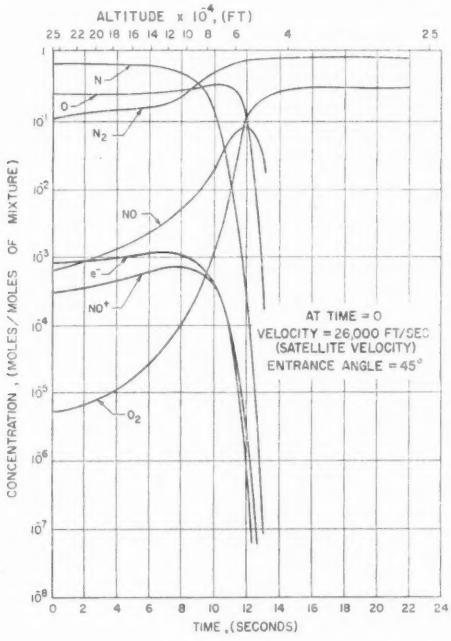

Figure 1. Concentration of the most important chemical species in equilibrium air at the stagnation point for a typical entry trajectory.

fast reaction rates (i.e. equilibrium composition; Gilmore 1955). When we consider the cooling of the gas from the stagnation region as it expands around the body, the question of the rate with which atoms recombine in the inviscid flow and in the boundary layer becomes important. If electromagnetic waves are to be used to send or receive information from a flight object, it is necessary to have an accurate knowledge of the electron

concentration in the inviscid flow. This requires an accurate knowledge of the temperature. A knowledge of the recombination rate is essential if the theory of the inviscid gas flow around the body is to be complete. An important problem, then, is to determine the *dissociation and recombination rates in air*.

The chemical reactions that go on in high temperature air are so complicated that the only reasonable method of approach to the problem, at the present time, is to carry out experiments that simulate the flow situations of interest.

Before discussing the experiments, some of the terminology used in chemical kinetics will be introduced. The recombination of two atoms A, which collide with a third body B to form a molecule A_2, is represented by the relation

$$A + A + B \underset{k_r}{\rightarrow} A_2 + B, \tag{1}$$

where B in the right-hand side is an excited particle which carries away the energy of recombination and k_r is the so-called recombination rate coefficient defined by the differential equation

$$\{d[A]/dt\}_r = -2k_r[A]^2[B], \tag{2}$$

where the square brackets denote concentrations in gm-moles/cm^3, the units of k_r are cm^6 moles^{-2} sec^{-1}, t denotes time, and the subscript r means recombination. Equation (2) says that the time rate of disappearance of atoms is proportional to the concentration of each of the species that take part in three-body collisions. The reaction rate coefficient k_r depends on temperature.

Similarly, the dissociation process is governed by the reverse of (1), and is determined by the dissociation rate constant k_d. (The subscript d will be used again later to denote dissociation.) It should be noted that, in a gas mixture like air, dissociation may occur by other more complicated paths than the one given by the inverse of (2).

In equilibrium chemical thermodynamics (Penner 1955), it is shown that at a given temperature the thermodynamic equilibrium constant K_c is given by

$$k_d/k_r = K_c. \tag{3}$$

(The subscript c denotes that K_c is defined in terms of concentrations.) If one assumes that even in a non-equilibrium state the molecules in their different energy levels have an equilibrium statistical distribution, then (3) still holds.

Knowing the atomic and molecular properties of the species involved in a reaction, K_c can be obtained from statistical mechanical calculations. The values of K_c are well known for the species in air. Therefore, in order to determine the reaction rates, it is necessary to determine experimentally only one of the reaction rates in (3).

2. Chemical kinetic experiments

The shock tube is a useful tool for obtaining air at temperatures and pressures that simulate, in the laboratory, the flight conditions of a body

in hypersonic flight through the atmosphere (Rose & Stark 1957). This air can then be used for the purpose of measuring chemical reaction rates. The basic idea is to cool rapidly, by aerodynamic means, the hot and partially dissociated gas produced in a shock tube. The problem then is to find an observable flow parameter that changes as a function of the chemical reaction rates.

For the purpose of obtaining chemical kinetic data for air, there are two different approaches which can be used. One is to use each of the individual species found in air as a working fluid, in order to investigate the detailed kinetics of each species, and then attempt to reconstruct from that information the more complex behaviour of air. Another approach is to observe the behaviour of the composite gas during rapid changes of state; this last approach is used in the present experiments.

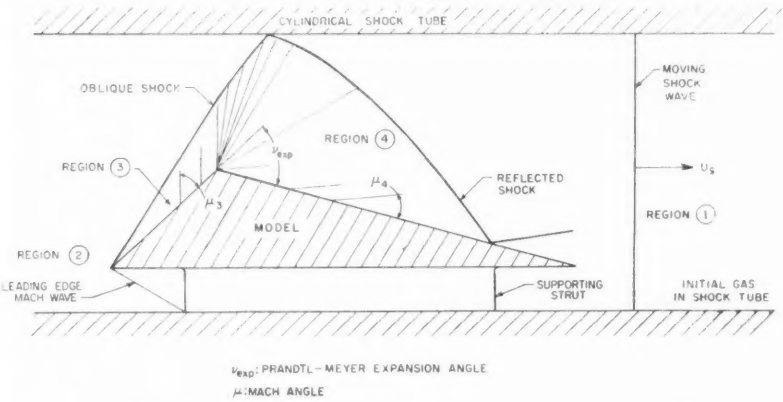

Figure 2. Flow configuration around compression–expansion models.

In one of our experiments, the air behind the moving normal shock is first compressed by means of a wedge (figure 2) spanning the shock tube test section, and is then expanded around a corner (Prandtl–Meyer expansion)*. The two-dimensional model is scribed transversely on the forward and rear surface so that the flow Mach number along the model wall can be determined by taking schlieren photographs of the small disturbances caused by the scratches†. The suddenly cooled gas is then observed as it relaxes towards equilibrium. If the relaxation times are of the appropriate order of magnitude, it would be possible to observe changes of Mach angle with distance along the wall, downstream of the expansion.

* Dr Harry E. Petschek, of the AVCO Research Laboratory, originally suggested the possibility of investigating recombination rates by studying the Prandtl–Meyer expansion of a dissociated gas flowing around a flat plate placed in the shock tube at angle of attack.

† Mach angle measurements have been used in experimental aerodynamics by Hertzberg & Kantrowitz (1950) and by Hertzberg (1956).

This rate of change of Mach angle with distance could be used to calculate the reaction rates. The possible observable difference in Mach angles in region 4 (see figure 2) is largest when the flow upstream of the expansion (region 3) is sonic. The oblique shock compression, then, has the purpose of lowering the Mach number of the initial flow behind the incident shock wave (region 2).

In order to analyse the Prandtl–Meyer expansion in a reacting gas and obtain some understanding of the experimental evidence, it is necessary to know the state of the gas upstream of the expansion. It is therefore important to investigate, first, the flow of air through moving normal shocks in the shock tube, and second, the flow of this shocked air through a standing oblique shock.

3. Experimental determination of the state of the gas behind the incident shock. Flat plate shock tube experiments

The experimental arrangement consists of a flat plate with a sharp leading edge which spans the width of a round shock tube at the point where glass windows have been inserted tangentially to the tube (figure 3).

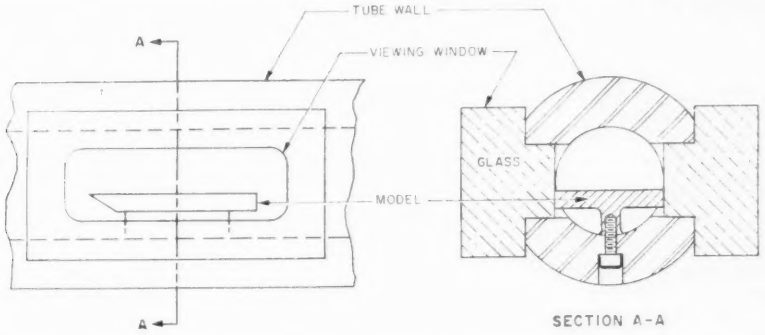

Figure 3. Experimental arrangement of model in schlieren test section in chemical kinetic experiments with the shock tube.

The model is supported by a diamond-shaped strut bolted to the bottom of the test section. Lines perpendicular to the flow are scribed on the model. These lines cause Mach waves in the flow downstream of the incident shock (i.e. in the gas usually used for test purposes; region 1 denotes the undisturbed gas in the shock tube before rupture of the diaphragm). A schlieren photograph of the Mach line pattern of the flow using a model with a highly polished surface and finely scribed lines is shown in figure 4 (*a*) (plate 1). Note the narrow Mach lines coming off the centre portion of the plate. Subsequently, heavier lines were scribed on the same model in addition to the fine lines already there. The result of this change is shown in figure 4 (*b*) (plate 1). Here the heavier lines are seen to fan out. A comparison of the fine and broad waves indicates that the trailing edge

of the strong waves proceeds with the same angle as the weak waves. The result of this comparison becomes useful when interpreting schlieren photographs where only broad waves appear. In figure 4(*c*) (plate 1) a plate scribed so that all lines are identical to each other demonstrates that there is *no measurable Mach number gradient in the flow direction.* The dark lines were drawn at the measured Mach angle to help the visualization of departures from parallelism.

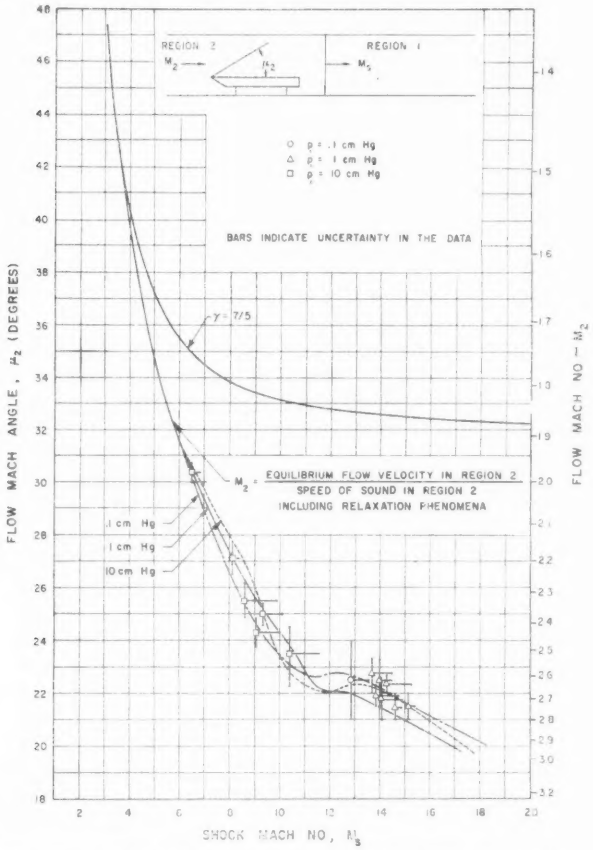

Figure 5. Estimate of flow Mach number downstream of moving shock. (Relaxation phenomena are included when computing sound velocities.) A comparison between frozen flow ($\gamma = 7/5$) and the flat plate Mach line experiments.

It should be remarked that the thickness of the Mach waves can be justified by the finite size of the disturbances and the finite breadth of the test section, and are definitely in no way associated with any relaxation phenomena. Additional experimental confirmation of this fact is given by schlieren photographs of the small disturbances taken in argon in a Mach number range for which no relaxation phenomena occur; the waves appear to have the same thickness as in air.

Since the dissociation rates are not known, the experimental Mach angle μ_2 of the flow downstream of the incident shock is compared (figure 5) with two different theoretical values obtained by making the following two extreme alternative assumptions about the relaxation times and the speeds of sound*:

(*a*) the gas is chemically frozen at room temperature composition, i.e. $\gamma = 7/5$, γ denoting the ratio of specific heats (vibration of the molecules remains unexcited);

(*b*) the flow velocity downstream of the shock is determined by assuming thermodynamic equilibrium across the shock wave, and the choice of the proper speed of sound is determined by the ratio of the vibrational (Blackman 1956) and chemical relaxation times (based on the lower limit of the recombination rates determined in § 6) to the flow times across the Mach waves (cf. Appendix).

The uncertainty in the data shown in figure 5 is due to the spread of the Mach waves, of the order of 1°, and to attenuation of the incident normal shock wave. Figure 5 shows definitely that the dissociation rate is so fast that *the flow in the slug of gas used in our shock tube tests is in thermodynamic equilibrium.* Since the photographs are taken after the incident shock is well out of the field of view, no information was obtained as to the length of the relaxation region in the neighbourhood of the incident shock.

4. Shock tube experiments with wedges

The next question that has to be answered is whether the gas that passed through the incident shock, and which is in thermodynamic equilibrium, will again be in equilibrium when it goes through an oblique shock attached to a wedge located in the shock tube.

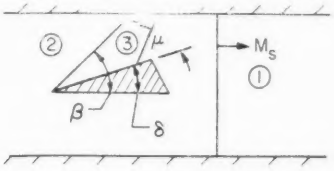

Figure 6. Notation for experiments with wedges.

Experiments have been carried out with wedges, in which the shock angle β was measured as a function of the deflection angle δ (see figure 6). The flow Mach angle μ_3 downstream of the oblique shock (denoted as region 3 in figure 2) was also determined with the scribing technique already mentioned.

A comparison can be made here of the experimental value (β_{exp}) with two different theoretical values of β, obtained by making the following two assumptions:

(*a*) the gas is in chemical equilibrium across the incident shock, and chemically frozen across the oblique shock, but vibration is fully excited (β_{cf});

(*b*) the gas is in equilibrium through both shocks (β_{ee}).

* A discussion of frozen and equilibrium flow, as well as some limiting cases of the speeds of sound in a reacting gas, is given in the Appendix.

The results are given in table 1, where the angles in the columns labelled β_{exp}, β_{ec} and β_{ef} should be compared. There is excellent agreement between the results of the experiments and the calculations assuming full equilibrium.

Run no.	p_1	M_s	δ	β_{exp}	β_{ec}	β_{ef}	μ_{3exp}	$\mu_{3fnc}-\mu_{3exp}$	$\mu_{3fcc}-\mu_{3exp}$	$\mu_{3e}-\mu_{3exp}$
F-145	0·1	15·60	26·0	39·5	39·5	48·1	—	—	—	—
F-146	0·1	16·00	26·0	39·0	39·2	47·9	—	—	—	—
F-70	0·1	14·75	27·0	41·0	41·0	50·2	—	—	—	—
F-141	0·1	14·15	33·0	49·0	49·6	*D*	—	—	—	—
F-74	0·1	12·57	41·0	63·0	63·0	*D*	61·1	3·7	−0·1	−12·3
F-50	0·1	14·15	43·0	63·7	64·3	*D*	69·1	5·0	0·0	−12·0
F-140	0·1	16·90	43·0	59·6	59·4	*D*	—	—	—	—
F-232	1	13·15	20·0	37·5	37·5	40·1	—	—	—	—
F-142	1	13·35	25·0	41·5	41·9	46·6	33·0	2·2	1·0	−2·2
F-143	1	14·60	25·0	40·7	40·7	45·8	33·0	0·4	−0·7	−3·8
F-47	1	13·85	25·7	41·8	42·1	47·3	—	—	—	—
F-129	1	13·65	26·0	43·0	42·4	47·8	—	—	—	—
F-130	1	14·40	26·0	41·5	41·9	47·4	—	—	—	—
F-131	1	14·65	26·0	42·0	41·7	47·2	—	—	—	—
F-133	1	15·15	26·0	40·7	41·2	47·0	—	—	—	—
F-76	1	13·65	26·7	43·3	43·2	48·9	—	—	—	—
F-8	1	14·10	28·8	45·6	45·0	52·1	36·3	1·3	0·0	−3·6
F-53	1	14·85	33·0	50·8	49·4	63·7	—	—	—	—
F-56	1	15·25	36·3	54·0	53·5	*D*	—	—	—	—
F-20	1	14·40	37·0	55·3	55·7	*D*	—	—	—	—
F-19	1	15·30	37·0	54·8	54·5	*D*	44·9	8·1	5·9	−0·2
F-25	1	14·91	38·0	57·0	56·7	*D*	50·7	2·3	0·1	−6·0
F-27	1	14·72	41·0	63·7	63·2	*D*	56·4	3·1	0·0	−7·2
F-54	1	15·65	43·0	67·0	67·1	*D*	—	—	—	—
F-147	10	9·80	20·8	40·0	40·0	41·7	—	—	—	—
F-138	10	8·10	26·0	49·8	50·2	58·2	—	—	—	—
F-144	10	8·10	30·0	56·0	56·3	*D*	—	—	—	—
F-139	10	8·40	30·0	54·9	55·4	*D*	—	—	—	—
F-137	10	8·80	30·0	53·8	53·8	*D*	—	—	—	—
F-136	10	9·80	30·0	52·7	52·3	*D*	—	—	—	—

Table 1. Resumé of oblique shock experiments. p_1 is given in cm Hg, and the angles in degrees. *D* denotes shock detachment.

The last four columns of table 1 give a comparison of the Mach angles μ_{3exp} of the gas flowing over the forward part of the wedge with the theoretical values obtained by using three different speeds of sound. The indication is that of these three speeds of sound, the one that gives best

agreement with experiments is the speed of sound a_{fcv} calculated by freezing the chemical composition at the equilibrium value behind the oblique shock and by letting the vibration participate in the changes across a sound wave. The reason why the Mach angle μ_3 is so sensitive to the different speeds of sound (see the last four columns of table 1) is that the flow over the wedges is only slightly supersonic. On the other hand, this transonic flow is also sensitive to boundary layer constrictions in the shock tube; these may cause the flow not to be truly steady and two-dimensional, and consequently, introduce the longitudinal gradients that were observed in some cases. Also, it should be pointed out that a 1% uncertainty in the shock Mach number M_s produces a 2% error in the Mach number M_3 of the flow over the wedge. Since the experiments are performed in a heated gas produced by an attenuating shock, the conclusions drawn from the Mach number measurements in region 3 may still be opened to question. The effect that these gradients have on the flow after the Prandtl–Meyer expansion (region 4 in figure 2) can be shown to be negligible.

Evidence of the steadiness of the flow around the models in the shock tube has been obtained by taking drum camera photographs of the self-luminosity of the flowing gas. On the outside surface of the window (figure 3) a slit is positioned with respect to the compression–expansion model, as indicated on the lower portion of figure 7 (plate 2). Note in the upper portion of the figure (which is the drum camera photograph) that after the first 10 μsec the oblique shock remains in a steady position for approximately 20 μsec; a sufficient time to gather experimental data. This time, called the testing time, is a function of p_1, M_s and shock tube length.

From the evidence given in the last two sections, it may be concluded that *the gas upstream of the Prandtl–Meyer expansions is in thermodynamic equilibrium*. This is the information needed as a starting point for the interpretation of the recombination experiments.

5. Prandtl–Meyer expansion experiments

A typical schlieren photograph of the air flow about the compression–expansion models is given in figure 8 (plate 3). The calculated shock angle can be seen to agree with the experimental one*. The oblique shock

* The shock curvature upstream of the start of the Prandtl–Meyer expansion is due to an expansion wave which comes from the upper-left corner of the flow field, where the viewing window joins the shock tube (cf. figures 3 & 4 (*a*) (plate 1)). The experiments reported here have been repeated in a square cross-sectional test-section, the windows and walls being on the same plane, and no premature curvature of the oblique shock was detected.

The flow along the model wall, downstream of the expansion, is not affected by the tube-window-joint expansion. The reason for not publishing the schlieren photographs taken in the square section is that the lines downstream of the Prandtl–Meyer expansion were not defined well enough to be reproduced clearly by the photo-offset method.

appears to have a large thickness because the boundary layer on the windows thickens along the intersection with the shock plane. The oblique shock is reflected by the cylindrical wall of the tube. The Mach lines, produced by scribing the model, are clearly seen on the back surface and faintly on the front wedge.

In all the experiments that have been carried out, no measurable variation has been found in the Mach angle of the flow downstream of the Prandtl–Meyer expansion. This means that we are dealing with either the extreme cases in which the gas is chemically frozen across the expansion, or that in which all the recombination has taken place by the time the gas emerges from the last wave of the expansion fan. It will now be necessary to calculate the Prandtl–Meyer expansion for the extreme cases of either frozen flow or equilibrium flow.

For *chemically frozen flow*, the two values of γ from (A.5) and (A.7) of the Appendix can be used first to determine the speed of sound behind the oblique shock, and then to calculate the Mach number M_3 in this region. (Although the differences between the two Mach numbers and the experimental value are small, one value consistently agrees better with experiment than the other.) Starting with the Mach numbers just determined (γ and the expansion angle ν are known) it is possible to calculate, using the usual Prandtl–Meyer formulae, two possible Mach numbers for the chemically frozen flow after the expansion, $M_{4f_{nv}}$ (frozen, no vibration) and M_{4fcv} (frozen, classical vibration). A typical result for frozen flow, classical vibration, is shown in figure 8 (plate 3) where it can be seen that the calculated Mach angle (black lines) is very different from the experimental one (white waves). If the vibration were also assumed to be frozen, the lack of agreement would be greater.

The alternative extreme case is obtained if we assume that the recombination rate is infinitely fast, and that *the flow is in equilibrium* beyond the expansion. It can be shown, by writing the usual relation

$$d\nu = \sqrt{(M^2-1)}\, du/u$$

in terms of enthalpy, that the condition after an expansion of ν radians is given by the integral equation

$$\nu = \frac{1}{2}\int_{H_3}^{H_4}\left[\left(\frac{u}{a}\right)^2 - 1\right]^{1/2}\frac{dH}{H} = \frac{1}{2}\int_{H_3}^{H_4}\left(\frac{2H}{a^2}-1\right)^{1/2}\frac{dH}{H}, \tag{4}$$

evaluated along an isentrope, where $H = h_t - h = \frac{1}{2}u^2$, h_t, h and u denote, respectively, total enthalpy of the flow, local enthalpy, and velocity in the expansion, a is the local speed of sound, and subscripts 3 and 4 denote conditions before and after the expansion respectively. For the purpose of integrating (4), it is convenient to have a Mollier chart that has lines of constant equilibrium speed of sound a_e, as given by (A.9). When the integral is evaluated (numerically or graphically) it is possible to plot the expansion angle ν *vs* the full equilibrium Mach number M_{4e}, where

$$M_{4e} = \sqrt{(2H)}/a_e. \tag{5}$$

Entering this plot with the experimental expansion angle ν_{exp}, the value of M_{4e} for the particular experiment can be determined.

If one assumes that the characteristics in a supersonic stream of reacting gas propagate with the equilibrium speed of sound, but that a finite disturbance could travel with the 'locally' frozen speed of sound, it is possible to obtain two other Mach numbers for the expanded flow. The value of ν obtained from (4) by using a_e may be plotted alternatively *vs* $\sqrt{(2H)}/a_{fnv}$ and *vs* $\sqrt{(2H)}/a_{fev}$*; this leads to M_{4efnv} and M_{4efev}. There are, therefore, depending on the relaxation times that are unknown, five possible ways of computing the flow Mach number. They give M_{4fnv}, M_{4fev}, M_{4efnv}, M_{4efev}, M_{4ee}. These are then compared with the experimental value M_{4exp}. In figure 9 (plate 3), the calculated Mach lines that agree best with the experimental values (they correspond to M_{4efev}) have been superposed on the photograph; the agreement is very good.

It should be emphasized that in all the Mach numbers that contain an e in their subscripts, the relation between ν and μ is obtained assuming thermodynamic equilibrium. The three different Mach numbers M_{4efnv}, M_{4efev} and M_{4ee} differ only in the manner in which the corresponding speed of sound is defined.

Run no.	p_1	Ms	δ	β_{exp}	β_{th}	ν	μ_{4exp}	$\mu_{4fnv}-\mu_{4exp}$	$\mu_{4fev}-\mu_{4exp}$	$\mu_{4ee}-\mu_{4exp}$	$\mu_{4efnv}-\mu_{4exp}$	$\mu_{4efev}-\mu_{4exp}$
F-135	0·1	15·25	40·0	55·0	56·0	50·0	25·7	−11·0	−9·7	−5·0	−1·8	−2·7
F-74	0·1	12·57	41·0	63·0	63·0	56·2	20·1	−5·2	−3·5	0·8	1·6	2·7
F-50	0·1	14·15	43·0	63·7	64·3	58·0	23·8	−9·8	−8·0	−3·0	0·0	−0·9
F-142	1	13·35	25·0	41·5	41·9	58·0	16·8	−7·8	−5·2	−1·7	−0·3	−1·0
F-143	1	14·60	25·0	40·7	40·7	58·0	16·5	−1·9	0·3	−1·7	−0·1	−0·7
F-8	1	14·10	28·8	45·9	45·0	43·4	19·0	−4·3	−3·0	−0·3	2·1	2·3
F-25	1	14·91	38·0	57·0	56·7	50·0	21·9	−6·5	−5·1	−1·1	2·2	1·0
F-122	1	15·00	40·1	59·9	60·1	50·0	24·3	−7·6	−6·0	−1·7	1·5	0·5
F-27	1	14·72	41·0	63·7	63·2	53·0	23·6	−8·5	−7·0	−2·7	0·3	−0·6

Table 2. Mach angles after Prandtl–Meyer expansion. A comparison between experiments and theory. The notation is given in figure 2.

The region in a Mollier diagram covered by the compression–expansion experiments is shown in figure 10, where the stagnation conditions have been plotted for the trajectories of several bodies of possible interest.

The significant data in these experiments, and the results of calculations for the flow Mach angle after the Prandtl–Meyer expansion, are presented in table 2. A comparison of the last five columns shows that, except for small wedge angles where the experiment is insensitive, *the flow Mach angle μ_4 is significantly closer to the calculated equilibrium values.* The speed of sound in the reacting gas used in the equilibrium calculations which agree best with the experimental results seems to be

$$a_{fnv} = \gamma_{nv} ZRT, \quad \text{where } \gamma_{nv} = \frac{4+3Z}{4+Z}.$$

* The notation used for the speeds of sound is given in the Appendix.

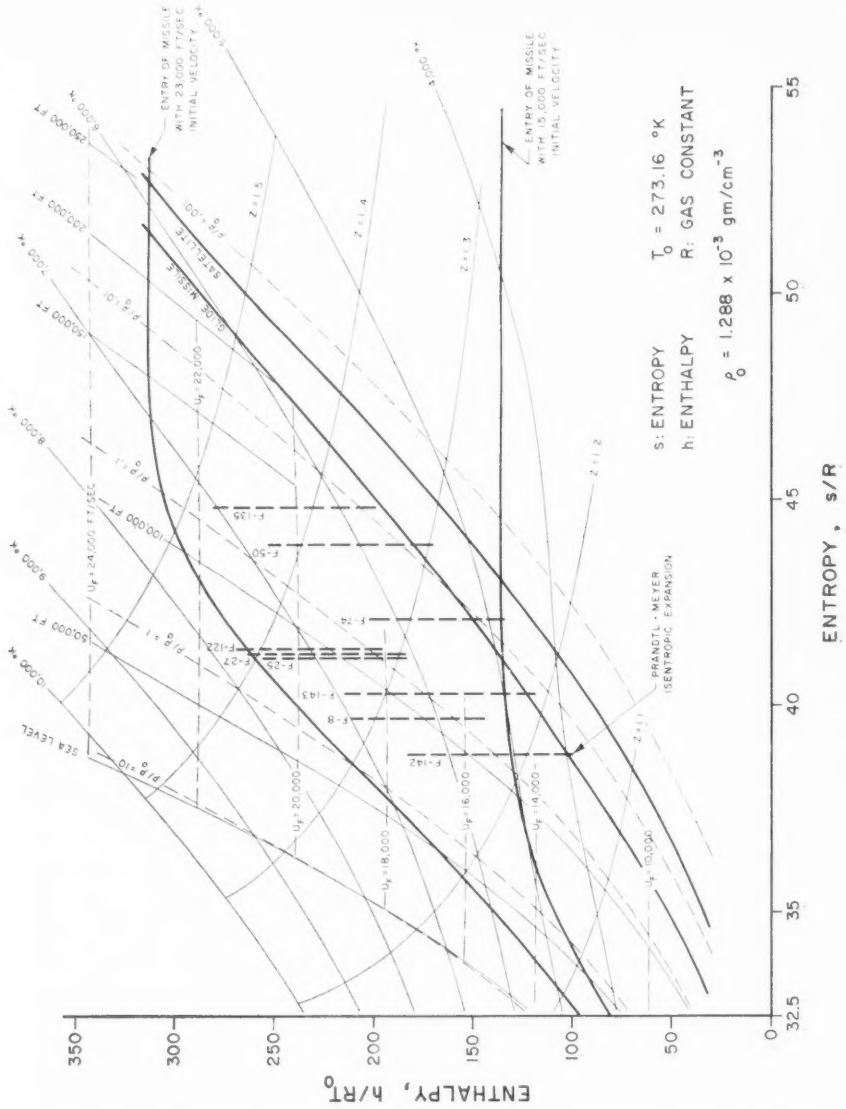

Figure 10. Comparison between the state of gas at the stagnation point of several bodies, and the Prandtl–Meyer expansion in the chemical kinetic experiments with air.

The fact that the experiments agree better with the speed of sound without excitation of the vibration of the molecules is in agreement with Blackman's vibrational relaxation times (although in the present case we also have the possibility of chemical reaction). These times, when compared with the times for a gas particle to traverse the thickness of one of the disturbances used to determine the flow Mach number in region 4 of figure 2, show that the vibration should be frozen in the present measurements.

On the other hand, if the flow around the expansion, as close to the corner as can be measured, is in chemical equilibrium, it does not seem plausible that the flow across a sound wave should be chemically frozen. Since the experimental angles that appear in the schlieren photographs are not sufficiently sharp, the use of the speed of sound defined by the last equation cannot be defended too strongly.

The question concerning the proper speed of sound to use in the equilibrium calculations is a difficult one to answer with the present evidence. Regardless of the outcome, *the data indicate that the flow is definitely not frozen but maintains a state very close to equilibrium.*

6. Estimate of a lower limit for the recombination rate

From the Prandtl–Meyer expansion experiments, it is possible to estimate a lower limit for the recombination rate. An analytic expression which will permit us to do this calculation will now be derived.

The rate equation (2) will be rewritten in terms of weight fractions defined by

$$y_i = \frac{\text{gm of species } i \text{ per unit volume}}{\text{gm of mixture per unit volume}}.$$

Subscripts a and m will denote atoms and molecules respectively. Since $y_a + y_m = 1$, we have

$$[A] = \rho y_a/W_a, \quad [A_2] = \rho y_m/W_m, \quad [B] = [A] + [A_2] = \rho(1+y_a)/W_m, \tag{6}$$

where ρ is the gas density and W_m the molecular weight of undissociated gas. The insertion of (6) into (2) yields

$$\{dy_a/dt\}_r = -(2\rho/W_m)^2 k_r y_a^2(1+y_a). \tag{7}$$

If account is also taken of the dissociation reaction

$$A_2 + B \underset{k_d}{\rightarrow} A + A + B,$$

the net rate can be expressed as

$$dy_a/dt = \{dy_a/dt\}_d + \{dy_a/dt\}_r. \tag{8}$$

The reaction rate for dissociation can be expressed as

$$\{d[A]/dt\}_d = 2k_d[A_2][B] = 2k_d(\rho/W_m)^2(1-y_a^2), \tag{9}$$

which together with (7) can be inserted in (8) to yield

$$dy_a/dt = (\rho/W_m)^2(1+y_a)[2k_d(1-y_a) - 4k_r y_a^2]. \tag{10}$$

At equilibrium $dy_a/dt = 0$, and the above expression gives

$$k_d = 2k_r y_{ae}^2/(1-y_{ae}) \tag{11}$$

which, together with (10), gives for the recombination rate k_r

$$k_r = \left(\frac{W_m/2\rho_0}{\rho/\rho_0}\right)^2 \frac{u\, dy_a/dx}{(1+y_a)[y_{ae}^2(1-y_a)/(1-y_{ae})-y_a^2]}, \tag{12}$$

where x denotes length measured along a streamline and u is the flow velocity.

Since the atomic weight fraction y_a is given in terms of the compressibility Z by

$$y_a = Z - 1,$$

equation (12) may be written as

$$k_r = \left(\frac{W_m/2\rho_0}{\rho/\rho_0}\right)^2 \frac{u(dZ/dv)(dv/dx)}{Z[(Z_e-1)^2(2-Z)/(2-Z_e)-(Z-1)^2]}, \tag{13}$$

where ν is the Prandtl–Meyer expansion angle.

Equation (13) can be used for an order of magnitude calculation in the following way. We will choose a streamline 1 mm away from the forward wedge wall (this being the closest to the wall of those streamlines that

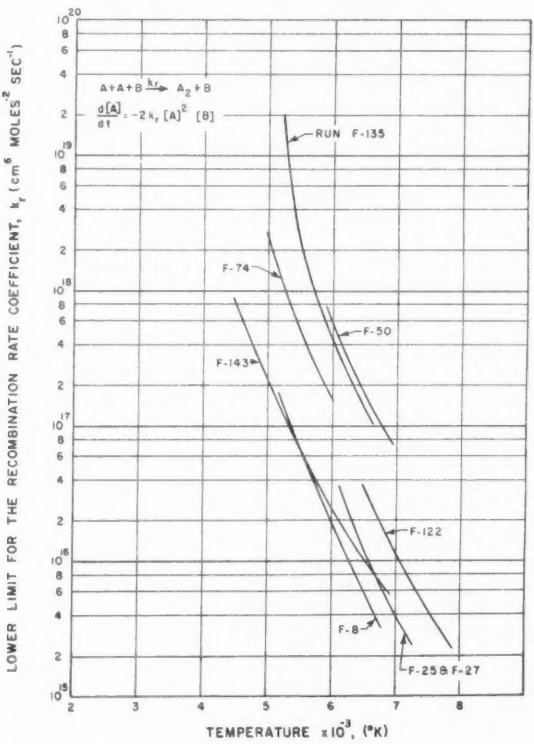

Figure 11. Lower limit for the recombination rate coefficient obtained from the Prandtl–Meyer expansion experiments.

can be seen flowing around the corner in the schlieren photographs), and follow it around the Prandtl–Meyer expansion. Consider the flow through a small expansion angle $\Delta\nu$. The problem is to decide what to use for Z and Z_e in (13). Since the experimental evidence is that after any expansion we get equilibrium, the value of Z_e to be used in (13) should be the equilibrium value *after* the expansion. On the other hand, since there is no experimental evidence for the value of Z *within* the expansion, we could assume, as an extreme condition, that Z stays at the equilibrium value at the *beginning* of the expansion. Any other choice of Z would give a larger value of k_r. Thus, the values of k_r calculated by using the local properties of the gas through the expansion are a *lower limit for the recombination rates*. The results are given in figure 11 as a function of temperature. These experiments have covered roughly a density range of standard to 1/200 of standard density.

The chemical kinetic theory that interprets the experimental results still remains to be developed.

7. Conditions for thermodynamic equilibrium in flight

Let the criterion for equilibrium flow require that the time for a gas particle to traverse the body length is ten times the chemical relaxation time. Making use of the relation

$$k_r \geqslant 10^{18} \text{ cm}^6 \text{ mole}^{-2} \text{ sec}^{-1}, \tag{14}$$

it is possible, when adopting the equality sign in the recombination rate of (14), to find an altitude (for a given body) below which the flow will stay in thermodynamic equilibrium as it flows around the body, provided the gas behind the detached shock is in equilibrium. (The effect of other limiting values of k_r will be discussed later.) This has been done for blunt bodies of 1 and 10 ft. surface length (figure 12). If the stagnation point gas is in thermodynamic equilibrium, the shaded area covers the region where the flow around a 1 ft. body may be expected to be in equilibrium. The corresponding result for a 10 ft. body is also given in figure 12. The shape and location of the two curves are insensitive to body shape, provided the body is blunt and smooth. The curves of y_{ae} = const. indicate the flight conditions at which the air at the stagnation point of a blunt body has a noticeable degree of dissociation. If a recombination rate k_r larger by a factor of 10 be adopted, the effect on the curve for the 1 ft. body is to displace it to where the 10 ft. curve is now. On the other hand, if the criterion for equilibrium flow requires the flow transit time to be 100 times the relaxation time (instead of 10), the 1 ft. curve is displaced downward in figure 12 by approximately 40 000 ft. Several typical trajectories (Masson & Gazley 1956) have also been included in figure 12. It can be seen that the flow around a satellite entering the atmosphere may not be in thermodynamic equilibrium. This points towards the importance of designing chemical kinetic experiments on a faster time scale than for those described here.

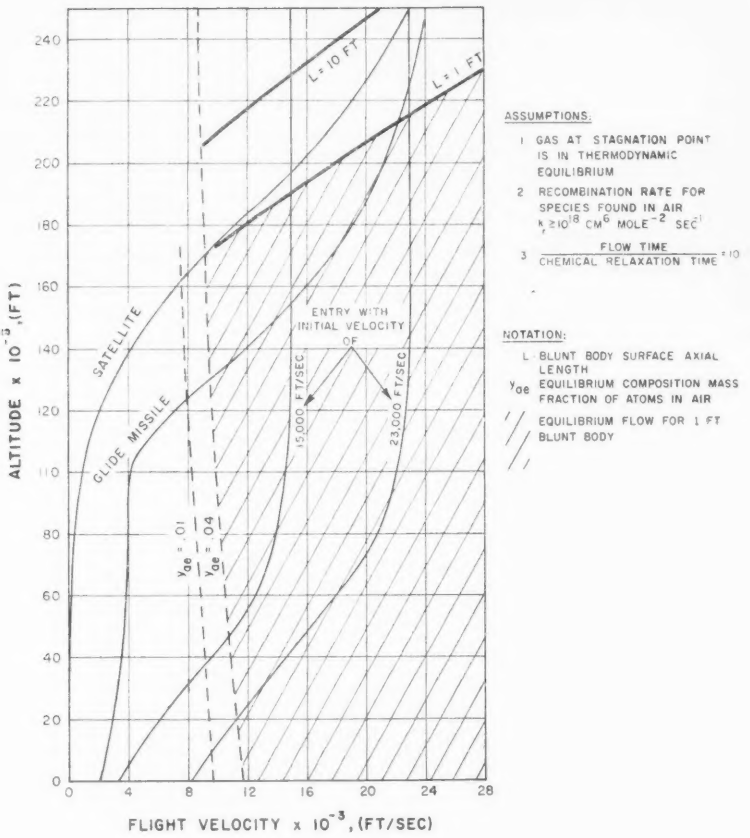
ALTITUDE x 10^{-3},(FT)
FLIGHT VELOCITY x 10^{-3},(FT/SEC)
L = 10 FT
L = 1 FT
SATELLITE
GLIDE MISSILE
ENTRY WITH INITIAL VELOCITY OF
15,000 FT/SEC
23,000 FT/SEC
Y_{oe} = .01
Y_{oe} = .04
Y_{oe} = .1
ASSUMPTIONS:
1 GAS AT STAGNATION POINT IS IN THERMODYNAMIC EQUILIBRIUM
2 RECOMBINATION RATE FOR SPECIES FOUND IN AIR $K_r \geq 10^{18}$ CM^6 MOLE^{-2} SEC^{-1}
3 $\frac{\text{FLOW TIME}}{\text{CHEMICAL RELAXATION TIME}} \geq 10$
NOTATION:
L BLUNT BODY SURFACE AXIAL LENGTH
Y_{oe} EQUILIBRIUM COMPOSITION MASS FRACTION OF ATOMS IN AIR
EQUILIBRIUM FLOW FOR 1 FT BLUNT BODY

Figure 12. Flight conditions for which equilibrium flow may be expected around a blunt body. Some typical trajectories for bodies entering the atmosphere are also shown.

This work has been sponsored by the Ballistic Missile Division, Air Research and Development Command, U.S. Air Force, under contract AF04(645)–18. The author wishes to express his appreciation to the staff members of the AVCO Research Laboratory who contributed to this work, especially to Dr Arthur Kantrowitz, director of the laboratory, and to Professor James A. Fay, of the Massachusetts Institute of Technology and consultant to AVCO, for helpful discussions during the course of this work. Thanks are due to Mr James E. Trider for having carried out the shock tube experiments, and without whose cooperation and enthusiasm the experimental work would have not progressed to the stage reported here.

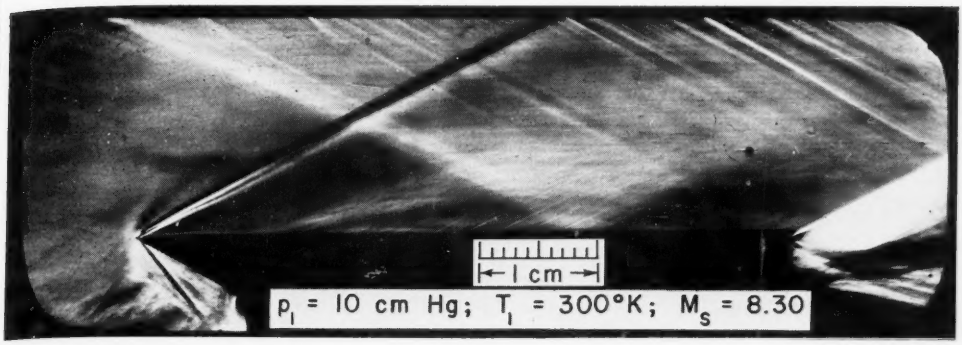

(*a*) Model scribed with very fine lines.

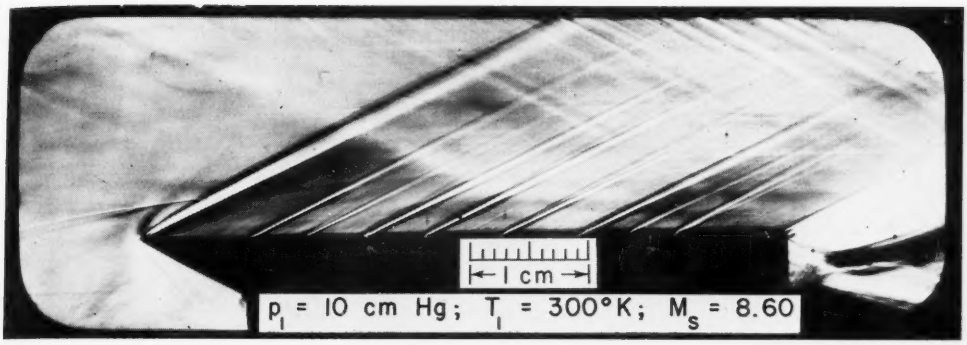

(*b*) Heavy lines scribed in addition to fine lines of figure 4 (*a*).

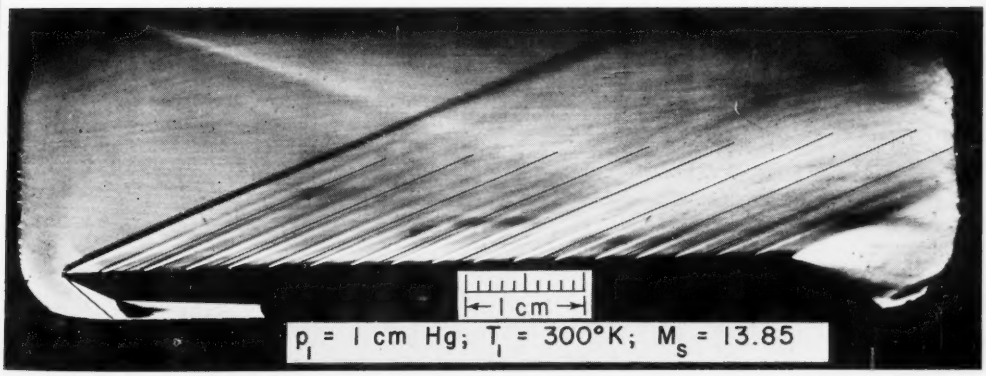

(*c*) Model scribed with heavy lines identical with each other.

Figure 4. Flow over flat plates in the shock tube. Subscript 1 refers to region 1 in figure 2. M_s is the ratio of the shock velocity to the speed of sound in region 1.

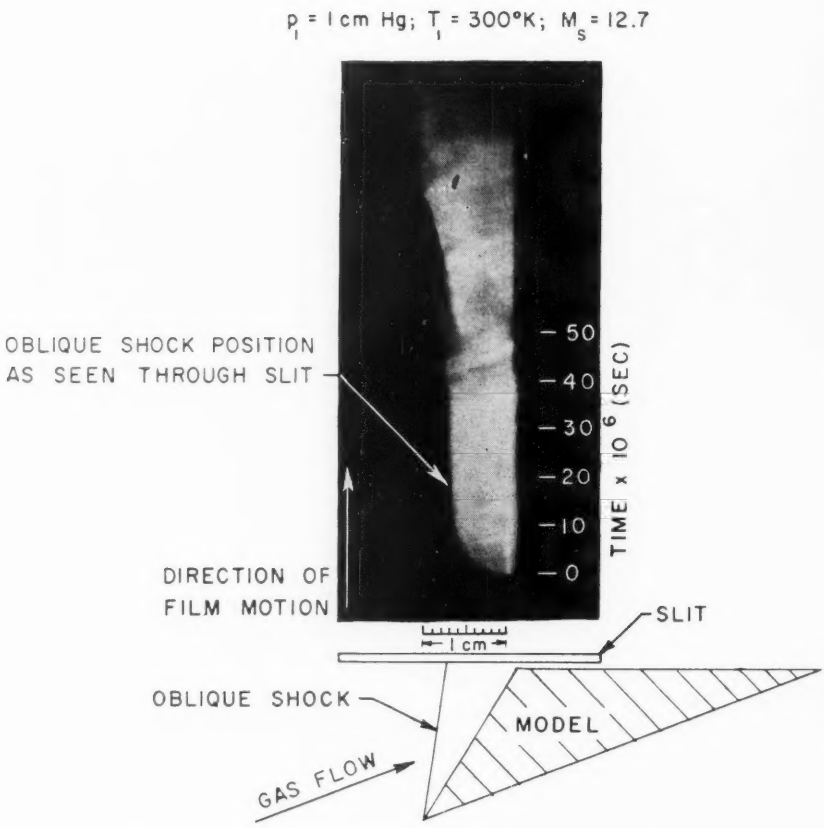

Figure 7. Drum camera photograph of flow around wedge.

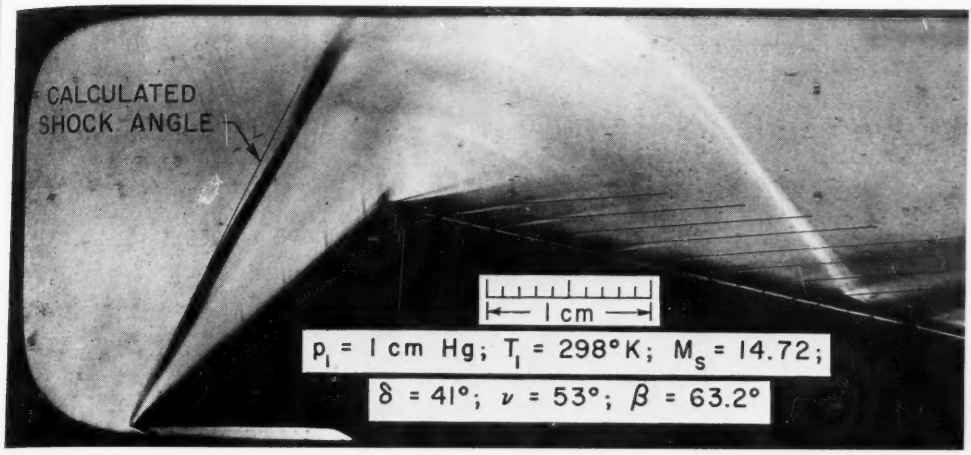

Figure 8. Comparison with experiment of Mach lines for frozen flow, classical vibration. ($\gamma = 1{\cdot}375$, $M_{4fnc} = 3{\cdot}50$, $\mu_{4fnc} = 16{\cdot}6°$.)

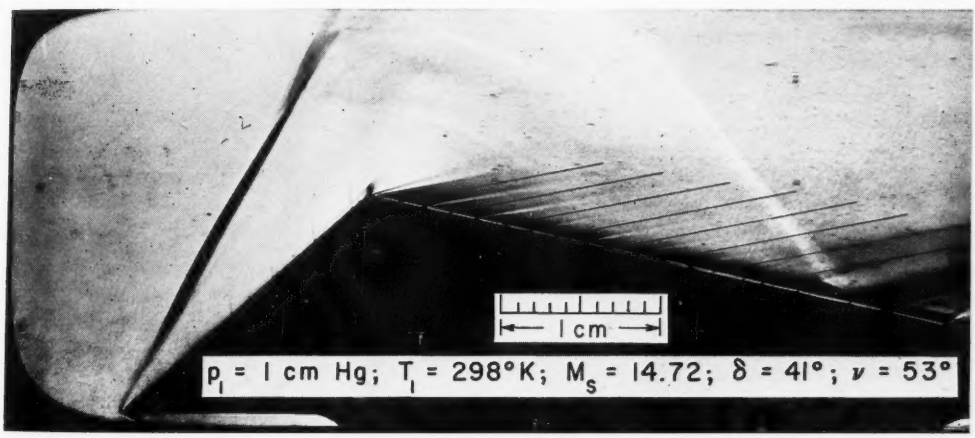

Figure 9. Comparison with experiment of Mach lines for equilibrium velocity and frozen speed of sound, classical vibration. ($M_{4efcc} = 2{\cdot}56$, $\mu_{4efcc} = 23{\cdot}0°$.)

Appendix. Frozen and equilibrium flow. Some limiting cases of the speed of sound in a reacting gas

The speed with which a small disturbance, called a sound wave, propagates in a reacting gas is known to depend on the rates at which the atomic and molecular internal degrees of freedom can adjust themselves to small changes in the thermodynamic coordinates. If the gas is chemically reactive, the sound speed depends also on the reaction rates, or the chemical relaxation times. The relaxation time τ for a process is defined by

$$\frac{1}{\tau} = \frac{1}{y-y_e}\frac{d(y-y_e)}{dt}, \tag{A.1}$$

where y may denote instantaneous concentration in the case of chemical reactions, or energy in the case of energy excitation of external or internal degrees of freedom. The subscript e denotes the equilibrium value of y. The value of τ is constant when the process involved is exponential, i.e. near equilibrium.

If the typical time necessary for a particle of gas to flow over a body of interest is denoted by τ_{flow} and if

$$\tau_{\text{flow}}/\tau \ll 1, \tag{A.2}$$

the flow is called *frozen flow*, i.e. no reaction occurs during the time a particle spends flowing over the body. Conversely, *equilibrium flow* is defined by

$$\tau/\tau_{\text{flow}} \ll 1. \tag{A.3}$$

Frozen and equilibrium flow having been defined, the discussion that follows will be concerned with the speeds of sound. It will be implied that the rotational relaxation times, for the diatomic molecules in air, are negligibly small when compared with the vibrational and chemical relaxation times (Hertzfeld 1955). The vibrational relaxation times in pure oxygen and nitrogen and their mixtures have been measured by Blackman (1956). There are four possibilities of interest for the speeds of sound, and two for the ratio of specific heats γ.

(*a*) The chemical reaction rate is very slow, no change in composition occurring across a sound wave, and the rotation of the molecules participates in the change, but the vibration of the molecules does not. The speed of sound so defined will be called *frozen speed of sound, frozen vibration*. Its value can be shown to be

$$a_{fnc}^2 = \gamma_{nc} ZRT, \tag{A.4}$$

where $Z = p(\rho RT)^{-1}$ gives a measure of the degree of dissociation of the gas (Z can be obtained from a Mollier chart for equilibrium air, Feldman 1957), R is the undissociated gas constant, and λ_{nc} the ratio of specific heats* is defined by

$$\gamma_{nc} = \frac{4+3Z}{4+Z}. \tag{A.5}$$

* The specific heat ratio can be obtained by writing the expressions for the enthalpy and internal energy of a mixture of atoms and diatomic molecules, and taking their derivatives with respect to temperature to obtain the specific heats.

(*b*) The same as case (*a*), except that here vibration participates in the changes in a sound wave (i.e. the vibrational relaxation times are very short). This sound speed will be called *frozen speed of sound, equilibrium vibration*. For the purpose of calculation, it will be assumed that the contribution of the vibrational degree of freedom to the heat capacities is the classical value RT, which is nearly true for the conditions of interest. This speed of sound will be called *frozen speed of sound, classical vibration*, and is given by

$$a_{fcv}^2 = \gamma_{cv} ZRT, \tag{A.6}$$

where the ratio of specific heats γ_{cv} is

$$\gamma_{cv} = \frac{8+Z}{8-Z}. \tag{A.7}$$

(*c*) The chemical reaction rates and the excitation of the rotation of the molecules are infinitely fast. Vibration of the molecules does not participate. This sound speed is called *equilibrium speed of sound, frozen vibration*, and is defined by

$$a_{env}^2 = (\partial p/\partial \rho)_{s = \text{const.}}, \tag{A.8}$$

where $\partial p/\partial \rho$ could be evaluated, along an isentrope, on a Mollier chart which includes a fixed value for the vibrational energy of the molecules.

(*d*) The chemical reaction rates, rotation and vibration are fast enough to follow completely the changes in a sound wave. This is the *full equilibrium speed of sound* and is found from the usual expression

$$a_e^2 = (\partial p/\partial \rho)_{s = \text{const.}}. \tag{A.9}$$

The relative magnitudes of these speeds of sound are

$$a_{fnv} < a_{fcv} < a_{env} < a_e, \tag{A.10}$$

the difference between the extreme values being of the order of 10 to 20% in the range of temperatures encountered in hypersonic flight.

References

Blackman, V. 1956 *J. Fluid Mech.* **1,** 61.

Feldman, S. 1957 Hypersonic gas dynamic charts for equilibrium air, *Avco Research Laboratory Handbook*.

Gilmore, F. R. 1955 Equilibrium composition and thermodynamic properties of air to 24,000° K, *Rand Corp., Report* no. RM-1543.

Hertzberg, A. & Kantrowitz, A. R. 1950 *J. Appl. Phys.* **21,** 874.

Hertzberg, A. 1956 *Jet Propulsion* **26,** 549.

Hertzfeld, K. F. 1955 Relaxation phenomena in gases, section H of *Thermodynamics and Physics of Matter*. Princeton University Press.

Masson, D. J. & Gazley, C. 1956 *Aero. Eng. Rev.* **15,** 46.

Penner, S. S. 1955 Introduction to the study of chemical reactions in flow systems, *AGARDograph* no. 7. London : Butterworths Scientific Publications.

Rose, P. H. & Stark, W. I. 1957 *J. Aero. Sci.* (to be published).

The diffraction of a rarefaction wave by a corner

By J. B. L. POWELL
Department of Mathematics, University of Bristol

(*Received* 1 *August* 1957)

SUMMARY

An investigation is made of the effect of a small disturbance on the flow in a complete rarefaction wave, for example, the flow produced by the rupture of a membrane originally separating a compressible gas from a vacuum. The perturbation arises from a rigid boundary slightly inclined to the direction of flow. The growth of the perturbed region is studied and the pressure field is calculated for diatomic gases.

The nature of the expanding boundary of the perturbed region is investigated. Arguments are put forward which suggest that this boundary can be a weak shock in certain circumstances. A second shock may also appear in some cases, following the first and of greater strength.

In an appendix the solutions are extended to monatomic gases and to fluids with an adiabatic index of 2. The latter results are suitable for a comparison with hydraulic experiments.

1. INTRODUCTION

The term 'complete rarefaction wave' is the name given to the flow produced when a membrane separating a compressible gas from a vacuum is ruptured, or a piston is retracted at the so-called escape speed of the gas (see Courant & Friedrichs 1948, p. 105). If u_1 is the particle velocity and c_1 the speed of sound in the flow, then

$$u_1 = (1-\mu^2)\{(X/t) - c_0\}, \tag{1}$$

$$c_1 = \mu^2(X/t) + (1-\mu^2)c_0, \tag{2}$$

$$\mu^2 = (\gamma-1)/(\gamma+1), \tag{3}$$

where γ is the adiabatic index and c_0 is the speed of sound in the undisturbed gas which previous to the time $t = 0$, when the membrane is removed, occupied the region $X \geqslant 0$.

At the head of the wave adjoining the undisturbed fluid, $X = c_0 t$, and so by equations (1) and (2) $u_1 = 0$, $c_1 = c_0$. The tail of the wave represents the limit of penetration into the vacuum where $c_1 = 0$, and its position is given by

$$u_1 = -\left(\frac{1-\mu^2}{\mu^2}\right)c_0, \qquad \frac{X}{t} = -\left(\frac{1-\mu^2}{\mu^2}\right)c_0.$$

A small perturbation on the flow in the rarefaction wave is produced by a rigid boundary slightly inclined to the direction of flow. The boundary

takes the form of two plane surfaces intersecting in the plane $X = 0$. Their equations are respectively $Y = -(\delta_1 + \delta_2)X$, for $X < 0$ and $Y = -\delta_2 X$ for $X \geqslant 0$ where δ_1 and δ_2 are small angles (see figure 1). Thus there is a corner in the wall surface at the initial position of the membrane which is concave to the flow for $\delta_1 > 0$. The ensuing flow is assumed to be isentropic. Viscosity and heat conduction are neglected. Thus the only physical constants defining the problem are p_0 and c_0, the pressure and speed of sound in the undisturbed gas and δ_1 and δ_2, the inclination of the walls.

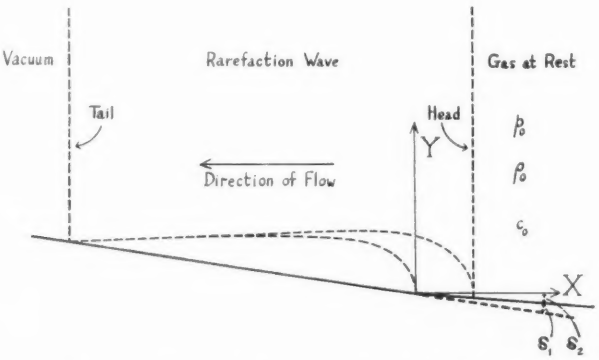

Figure 1. The configuration in the physical plane.

The above conditions have been assumed in order to provide a tractable problem. In fact, rarefaction waves occurring in practice are always incomplete, even under ideal conditions and solutions for such cases are discussed in § 7.

2. General solution of the basic equations

It may easily be shown that the velocity potential of the flow in the undisturbed rarefaction wave is

$$\tfrac{1}{2}(1-\mu^2)(c_0^2 t + X^2 t^{-1} - 2c_0 X).$$

If the velocity potential of the flow in the perturbed region is

$$\tfrac{1}{2}(1-\mu^2)(c_0^2 t + X^2 t^{-1} - 2c_0 X) + \phi$$

and squares and products of ϕ and its derivatives are neglected, ϕ satisfies the equation (Chester 1954)

$$\phi_{\eta\eta} - \alpha \frac{x}{\eta} \phi_{x\eta} = \phi_{\zeta\zeta}, \tag{4}$$

where x, η and ζ are new variables given by

$$\left.\begin{aligned} x &= \mu^2(X/c_0 t) + (1-\mu^2) \\ \eta &= \mu^2 X + (1-\mu^2)c_0 t \\ \zeta &= (1-2\mu^2)^{1/2} Y \end{aligned}\right\}, \tag{5}$$

and

$$\alpha = 2\mu^2/(1-2\mu^2). \tag{6}$$

In the problem considered here, ϕ may be further simplified by writing it in the form

$$\phi = c_0 \zeta f(x, y), \tag{7}$$

where

$$y = \eta/(\eta^2 - \zeta^2)^{1/2}. \tag{8}$$

Here the function f is non-dimensional and depends only on non-dimensional combinations of the variables x, η and ζ. This is required because of the lack of a fundamental length or time scale in the data defining the problem. The variable y remains finite and real in the interior of the perturbed region for, as will appear later, $\eta > \zeta$ except at the tail of the rarefaction wave where $\eta = \zeta = 0$. Since $\eta \geqslant 0$ it also follows that $y \geqslant 1$.

Substitution of (7) in equation (4) gives the equation

$$y(y^2-1)f_{yy} - \alpha x(y^2-1)f_{xy} + 3y^2 f_y = 0, \tag{9}$$

with the solution

$$f_y = (y^2-1)^{-3/2}\psi(x^{1/\alpha}y), \tag{10}$$

where $\psi(x^{1/\alpha}y)$ is an arbitrary function of $x^{1/\alpha}y$. From equations (2) and (5), $x = (c_1/c_0) \geqslant 0$ and hence $x^{1/\alpha}$ is real and positive.

Beyond the head of the rarefaction wave, that is for $X \geqslant c_0 t$, $Y \geqslant 0$ or $x \geqslant 1$, $y \geqslant 1$, the gas is at rest. Thus ϕ is identically zero for $x \geqslant 1$, $y \geqslant 1$. The same is true of f_y and hence by (10) $\psi(x^{1/\alpha}y) = 0$ for $x^{1/\alpha}y > 1$. Thus to the present order of approximation no perturbation exists outside the boundary $x^{1/\alpha}y = 1$. Moreover inside this boundary $x \to 0$ as $y \to \infty$ and so, by continuity, it follows from equation (8) that $\eta^2 - \zeta^2$ is of constant sign in the perturbed region. At the wall surface, $\zeta = 0$, so that in the perturbed region $\eta > \zeta$. This is in agreement with the assumption made earlier in this section.

For $x^{1/\alpha}y < 1$, ψ is determined by the boundary condition at the wall surface. In a linearized form, the condition of zero normal velocity becomes

$$\left.\begin{aligned} \frac{\partial \phi}{\partial Y} &= -(\delta_1 + \delta_2)(1-\mu^2)\{(X/t) - c_0\} \qquad \text{for } X < 0 \\ \frac{\partial \phi}{\partial Y} &= -\delta_2(1-\mu^2)\{(X/t) - c_0\} \qquad \text{for } X > 0 \end{aligned}\right\}, \tag{11}$$

the velocity along the wall surface being given to the first order by equation (1). Equations (11) are equivalent to

$$\frac{\partial \phi}{\partial \zeta} = -c_0 \lambda(x-1)\{\delta_2 + \delta_1 H(1-\mu^2-x)\}, \tag{12}$$

where λ is a constant defined by

$$\lambda = \frac{1-\mu^2}{\mu^2(1-2\mu^2)^{1/2}}, \tag{13}$$

and $H(x)$ is the Heaviside unit function defined by

$$\left.\begin{aligned} H(x) &= 0 \qquad x < 0 \\ H(x) &= 1 \qquad x > 0 \end{aligned}\right\}. \tag{14}$$

From equations (7) and (10) it follows that

$$\frac{\partial \phi}{\partial \zeta} = c_0 \int_{x^{-1/\alpha}}^{y} x^{1/\alpha} y \psi'(x^{1/\alpha} y) \frac{dy}{(y^2-1)^{1/2}}, \tag{15}$$

where the prime denotes the derivative of ψ and the lower limit in the integration is chosen so that $\partial\phi/\partial\zeta = 0$ on the boundary $x^{1/\alpha}y = 1$. In their present form equations (12) and (15) combine to give ψ as the solution of a Volterra integral equation of the first kind. It is, however, of a particularly simple form since by the transformations

$$y_1 = \frac{1}{y^2 x^{2/\alpha}}, \tag{16}$$

$$\chi(y_1) = \tfrac{1}{2} y^3 x^{3/\alpha} \psi'(x^{1/\alpha} y), \tag{17}$$

it may be reduced to Abel's integral equation

$$-\lambda(x-1)x^{1/\alpha}\{\delta_2 + \delta_1 H(1-\mu^2-x)\} = \int_1^{x^{-2/\alpha}} \frac{\chi(y_1)}{(x^{-2/\alpha}-y_1)^{1/2}}\, dy_1. \tag{18}$$

This has the explicit solution (Bocher 1914, p. 10)

$$\chi(y_1) = \frac{2\lambda}{\alpha\pi} \frac{d}{dy_1} \int_1^{y_1^{-\alpha/2}} \{\delta_2 + \delta_1 H(1-\mu^2-x)\} \frac{(x-1)\, dx}{x^{(1+\alpha)/\alpha}(y_1 - x^{-2/\alpha})^{1/2}}, \tag{19}$$

whence we may obtain

$$\psi(x^{1/\alpha} y) = \frac{2\lambda}{\alpha\pi} x^{1/\alpha} y \int_{x^{1/\alpha}}^{1} \{\delta_2 + \delta_1 H(1-\mu^2-\nu)\} \frac{(1-\nu)\, d\nu}{\nu(\nu^{2/\alpha} - x^{2/\alpha} y^2)^{1/2}}, \tag{20}$$

which together with equation (10) gives the complete solution for the region $x^{1/\alpha}y < 1$.

3. The nature of the boundaries when $\gamma = 1{\cdot}4$

It will be convenient henceforth to use the value $\gamma = 1{\cdot}4$ appropriate to a diatomic gas. Equation (20) may then be integrated in terms of elliptic functions, and clearly the results may be similarly developed for more general γ. Those for $\gamma = \frac{5}{3}$ and 2 are given in the Appendix.

When $\gamma = 1{\cdot}4$ we have

$$\mu^2 = \tfrac{1}{6}, \qquad \alpha = \tfrac{1}{2}, \qquad \lambda = 5(\tfrac{3}{2})^{1/2}, \tag{21}$$

and the surface $x^{1/\alpha}y = 1$ which marks the boundary of the perturbed region becomes $xy^{1/2} = 1$. When $\delta_2 = 0$ it is clear from equation (20) that ψ and hence f, is zero for $xy^{1/2} \geqslant \frac{5}{6}$. Thus there is a second surface, $xy^{1/2} = \frac{5}{6}$, inside the first, which marks the limit of the perturbation due to the displacement δ_1.

The equations of the two boundaries in the physical plane are

$$\left(\frac{X}{c_0 t} + 5\right)\left\{1 - K\left(\frac{X}{c_0 t} + 5\right)^4\right\}^{1/2} = \sqrt{24}\, \frac{Y}{c_0 t}, \tag{22}$$

where $K = 6^{-4}$ for the outer boundary, $K = 5^{-4}$ for the inner boundary. They are both characteristics of the original hyperbolic equation (9) and in § 6 arguments are put forward which suggest that in some circumstances these boundaries take the form of weak shocks.

Both boundaries are similar in shape and expand uniformly about the corner. The tail of the rarefaction wave ($X = -5c_0 t$), the wall, and the two boundaries meet in a point which is the furthest penetration downstream of the disturbances. At this point the gradients of the two boundaries are identical and

$$\left(\frac{dY}{dX}\right)_{X=-5c_0 t} = \left(\frac{1}{24}\right)^{1/2}. \tag{23}$$

The upstream extremities of the inner and outer boundaries are respectively the corner $X = Y = 0$, and the intersection of the wall and the head of the rarefaction wave $X = c_0 t$, $Y = 0$. In each case the boundary is perpendicular to the wall. The shape of the curves is given in figure 2.

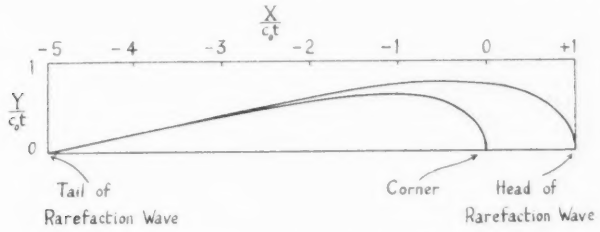

Figure 2. The shape of the two independent regions of perturbed flow.

4. The velocity and pressure fields at the wall surface

For $\gamma = 1{\cdot}4$, equation (20) may be integrated to give

$$f_y = \frac{20}{\pi}\left(\frac{3}{2}\right)^{1/2}\frac{1}{(y^2-1)^{3/2}}\left\{\delta_2\left[\tfrac{1}{2}\cos^{-1}x^2y - 2^{-1/2}xy^{1/2}\,\mathrm{cn}^{-1}(xy^{1/2})\right] + \right.$$
$$\left. + \delta_1 H\left(\tfrac{5}{6}-xy^{1/2}\right)\left[\tfrac{1}{2}\cos^{-1}\left(\frac{36}{25}x^2y\right) - 2^{-1/2}xy^{1/2}\,\mathrm{cn}^{-1}\frac{6xy^{1/2}}{5}\right]\right\}, \tag{24}$$

where cn^{-1} is the inverse function corresponding to the jacobian elliptic function cn of modulus $\frac{1}{2}\sqrt{2}$. It may be expressed alternatively in the form

$$\mathrm{cn}^{-1}x = \sqrt{2}\int_x^1 \frac{dx}{(1-x^4)^{1/2}} = F(\cos^{-1}x), \tag{25}$$

where $F(\cos^{-1}x)$ is the elliptic integral of the first kind of amplitude $\cos^{-1}x$ and modulus $\frac{1}{2}\sqrt{2}$.

The potential throughout the perturbed region is given by an integration of equation (24); however, the pressure and velocity fields at the wall surface may be obtained otherwise. The normal component of the perturbation velocity $\partial\phi/\partial Y$ is given explicitly by equation (11). The tangential component $\partial\phi/\partial X$ is obtained from equations (7) and (8). Thus

$$\frac{\partial\phi}{\partial X} = \frac{(y^2-1)^{1/2}c_0}{6y}\{xf_x - y(y^2-1)f_y\}, \tag{26}$$

or alternatively (since f satisfies equation (9)) in terms of f_y,

$$\frac{\partial \phi}{\partial X} = -\frac{(y^2-1)^{1/2}c_0}{6y}\int_y^{x^{-2}} \{f_y + x[1+\tfrac{1}{2}(1-y^2)]f_{xy}\}\,dy. \tag{27}$$

The integrand is given immediately by equation (24). Furthermore the only contribution to $\partial\phi/\partial X$ at $y = 1$ is due to the value of the integrand in the neighbourhood of $y = 1$. Thus, at $y = 1$,

$$\frac{\partial \phi}{\partial X} = -\frac{10}{3\pi}\left(\frac{3}{2}\right)^{1/2} c_0\left\{\delta_2\left[\tfrac{1}{2}\cos^{-1}x^2 - \sqrt{2x}\,\mathrm{cn}^{-1}x\right] + \right.$$

$$\left. + \delta_1 H(\tfrac{5}{6}-x)\left[\tfrac{1}{2}\cos^{-1}\left(\frac{36x^2}{25}\right) - \sqrt{2x}\,\mathrm{cn}^{-1}\frac{6x}{5} - \frac{6x^2}{(5^4-6^4x^4)^{1/2}}\right]\right\}. \tag{28}$$

There is a singularity in the tangential velocity component at the corner where

$$\frac{\partial \phi}{\partial X} \sim \frac{5}{6}c_0\frac{\delta_1}{\pi}\left(-\frac{6}{5}\frac{X}{c_0 t}\right)^{-1/2} \qquad \text{as } X \to -0. \tag{29}$$

As $x \to 0$ or $X \to -5c_0 t$, the perturbation velocity components tend to the finite non-zero limits,

$$\frac{\partial \phi}{\partial X} = -\frac{5\sqrt{6}c_0}{12}(\delta_1+\delta_2), \qquad \frac{\partial \phi}{\partial Y} = \frac{5c_0}{6}(\delta_1+\delta_2),$$

giving a first-order velocity discontinuity across the boundary of the perturbed region at the tail of the wave.

To the present order of approximation the flow is isentropic and the pressure field is determined explicitly by the change in sound speed. Denote the pressures in the perturbed and unperturbed rarefaction wave by p_2 and p_1 respectively. Then $p_2 = p_1$ when $\delta_1 = \delta_2 = 0$. Let the speed of sound in the disturbed region of the rarefaction wave be $c_1 + \Delta c$. Then

$$\frac{p_2 - p_1}{p_1} = \frac{7\Delta c}{c_1}. \tag{30}$$

The increase in sound speed Δc is obtained from Bernoulli's equation. Chester (1954) has shown that, in terms of the perturbation potential ϕ,

$$\Delta c = -\frac{1}{c_1}\left\{\frac{1}{5}\frac{\partial \phi}{\partial t} + \frac{1}{6}\left(\frac{X}{t} - c_0\right)\frac{\partial \phi}{\partial X}\right\}. \tag{31}$$

By a transformation into the (x, y)-plane this gives

$$\Delta c = \frac{(y^2-1)^{1/2}c_0}{6y}\int_y^{x^{-2}} \{f_y - x[\tfrac{1}{5} - \tfrac{1}{2}(1-y^2)]f_{xy}\}\,dy, \tag{32}$$

with f_y given by equation (24). Consequently the increase in sound speed is determined on $y = 1$ by the behaviour of the integrand at $y = 1$. From equation (30) the pressure distribution at the wall surface is

$$\frac{p_2 - p_1}{p_1} = \frac{35\sqrt{6}}{3\pi}\left\{\delta_2\left[-\frac{4}{5\sqrt{2}}\,\mathrm{cn}^{-1}x + \frac{1}{2x}\cos^{-1}x^2\right] + \right.$$

$$+ \delta_1 H(\tfrac{5}{6}-x)\left[-\frac{4}{5\sqrt{2}}\mathrm{cn}^{-1}\frac{6x}{5} + \frac{1}{2x}\cos^{-1}\left(\frac{36x^2}{25}\right) + \right.$$

$$\left.\left. + \frac{6x}{5(5^4-6^4x^4)^{1/2}}\right]\right\}. \tag{33}$$

The pressure is singular on the downstream side of the corner where

$$\frac{p_2-p_1}{p_1} \sim \frac{7\delta_1}{5\pi}\left(-\frac{6X}{5c_0 t}\right)^{-1/2} \quad \text{as } X \to -0. \tag{34}$$

Both p_2 and p_1 remain finite and approach zero as $x \to 0$ but the non-dimensional pressure $(p_2-p_1)/p_1$ is singular.

Values of $(p_2-p_1)/(p_1\delta_1)$ and $(p_2-p_1)/(p_1\delta_2)$ are exhibited in figure 3 for the respective cases $\delta_2 = 0$, $\delta_1 = 0$. This serves to separate the respective contributions due to the two displacements δ_1 and δ_2.

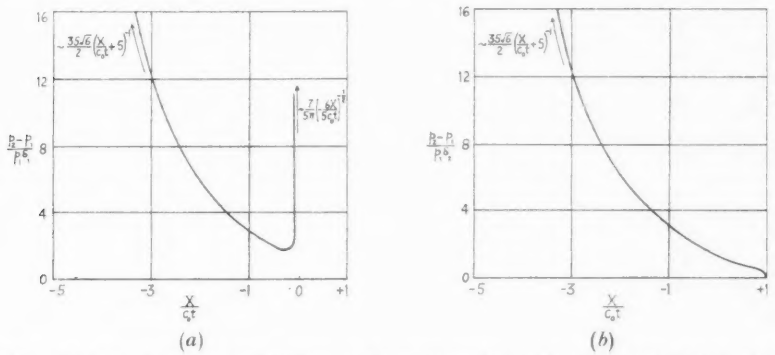

Figure 3. The pressure distribution at the wall surface. (*a*) $(p_2-p_1)/(p_1\delta_1)$ for the case $\delta_2 = 0$. (*b*) $(p_2-p_1)/(p_1\delta_2)$ for the case $\delta_1 = 0$.

5. The sonic line

In the absence of perturbation, the fluid reaches sonic speed on the plane $X = 0$ where $u_1 = -c_1 = -5c_0/6$. The perturbed region due to the displacement δ_1 lies entirely downstream of this plane. Consequently, such a displacement does not alter the position of the sonic line (this is not strictly correct near the corner; in § 6 it is shown that a concave corner causes small disturbances to propagate upstream). Thus we may take $\delta_1 = 0$ with no loss of generality.

In the perturbed region the sonic line is given by the equation

$$(c_1+\Delta c)^2 = \left(u_1+\frac{\partial\phi}{\partial X}\right)^2+\left(\frac{\partial\phi}{\partial Y}\right)^2.$$

By a substitution from equations (1) and (2) for u_1 and c_1, this becomes

$$\frac{X}{t}+\Delta c+\frac{\partial\phi}{\partial X} = 0, \tag{35}$$

correct to the first order, where Δc and $\partial\phi/\partial X$ are to be evaluated on $X = 0$. Equations (27) and (32) give the sonic line as

$$\frac{X}{c_0 t} = \frac{(y^2-1)^{1/2}}{6y}\int_y^{36/25} f_{xy}\,dy. \tag{36}$$

Hence by a substitution from equation (24) for f_{xy},

$$\frac{X}{c_0 t} = \frac{-5\sqrt{3}}{3\pi}\,\delta_2\,\frac{(y^2-1)^{1/2}}{y}\int_y^{36/25}\frac{\nu^{1/2}}{(\nu^2-1)}\,\mathrm{cn}^{-1}\left(\tfrac{5}{6}\nu^{1/2}\right)d\nu, \tag{37}$$

where y is such that

$$\frac{Y}{c_0 t} = \frac{5\sqrt{6}}{12} \frac{(y^2-1)^{1/2}}{y}. \tag{38}$$

The shape of the sonic line is given in figure 4, which shows that for $\delta_2 > 0$ the sonic line is moved downstream. The gradient of the sonic line is everywhere continuous and it reaches its maximum displacement from the plane $X = 0$ when it meets the wall at the point

$$\frac{X}{c_0 t} = -\frac{5\sqrt{3}}{3\pi} \delta_2 \operatorname{cn}^{-1} \tfrac{5}{6}.$$

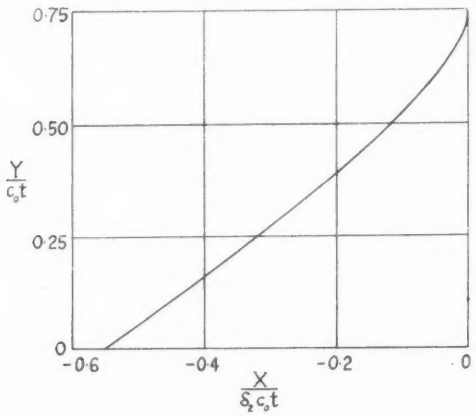

Figure 4. The shape of the sonic line in the perturbed region for the case $\delta_1 = 0$.

6. The nature of the boundaries of the perturbed regions

The above theory predicts singularities in the pressure and velocity fields at the corner and the head and tail of the rarefaction wave. These are just those points in which the boundaries $xy^{1/2} = \frac{5}{6}$, $xy^{1/2} = 1$, meet the wall surface. In the following paragraphs the behaviour at each of the three singular points is discussed briefly and suggestions are made with regard to the behaviour along the remainder of the boundaries.

At the tail of the wave $x = 0$ or $X = -5c_0 t$, the linear theory gives discontinuities in the perturbation velocity of amount

$$\frac{\partial \phi}{\partial X} = -\frac{5\sqrt{6}}{12} c_0(\delta_1 + \delta_2), \qquad \frac{\partial \phi}{\partial Y} = 5c_0(\delta_1 + \delta_2).$$

There is also a singularity in the perturbation pressure where by (33),

$$\frac{p_2 - p_1}{p_1} \sim \frac{35\sqrt{6}c_0}{12c_1}(\delta_1 + \delta_2) \quad \text{as } X \to -5c_0 t. \tag{39}$$

These values satisfy the conditions for a weak shock or rarefaction wave which to the first order lies along the line $2\sqrt{6}Y = X + 5c_0 t$ (both boundaries approximate to this line near the point $X = -5c_0 t$). The gas flows through the shock turning through an angle $\delta_1 + \delta_2$. Hence the

pressure change takes the form of a weak shock for $\delta_1+\delta_2 > 0$, and a Prandtl–Meyer expansion for $\delta_1+\delta_2 < 0$.

With the linear theory there is a singularity in the pressure at the corner for $\delta_1 \neq 0$ (see equation (34)). A more accurate picture is obtained from solving the full non-linear equations of motion by a series expansion in terms of the distance from the corner. Thus, it may be shown that for $\delta_1 < 0$ the flow in the neighbourhood of the corner is given by a Prandtl–Meyer fan of the sonic type. The flow upstream of the fan is undisturbed and the pressure change through the fan is $O(\delta_1^{2/3})$. However, for $\delta_1 > 0$ no solution can be obtained by a power series of the above form. The author has shown (Powell 1956, p. 90) that in this case the flow at the corner is just subsonic and disturbances are propagated upstream to a point whose distance from the corner is $O(\delta_1^{2/3})$. The pressure change at the wall surface is continuous and is $O(\delta_1^{2/3})$ but away from the wall it develops into a shock wave.

The circumstances at the head of the wave are different. On the linear theory the pressure behaves as

$$\frac{p_2-p_1}{p_1} \sim \frac{7\sqrt{6}\delta_2}{3\pi}(1-x)^{1/2}, \qquad \text{as } x \to 1, \tag{40}$$

with singularities in the pressure derivatives. In a small region near the head of the wave the full equations of motion may be solved by a series expansion. A solution exists for $\delta_2 < 0$ in which the flow accelerates continuously from rest to a value which is $O(\delta_2^2)$. When $\delta_2 > 0$ disturbances are propagated ahead of the head of the wave $X = c_0 t$. They travel into gas at rest in which the speed of sound is c_0. Hence they take the form of a shock wave which may be shown to have a strength $O(\delta_2^2)$.

We have shown that the extremities of the inner boundary $xy^{1/2} = 1$ are marked by shocks for $\delta_1 > 0$ and expansion regions for $\delta_1 < 0$. This would suggest that the shocks or expansions are continued around the entire boundary although perhaps in a diminished form. This is substantiated by an examination of the normal pressure derivative at the boundary. For a class of problems in cone-field theory, Lighthill (1949 b) has shown that the boundary of a perturbed region is a first approximation to a shock wave when the normal pressure derivative is singular and positive, and to a rarefaction wave otherwise. With certain assumptions, the author has indicated (Powell 1956) how Lighthill's proof may be extended to cover the present case. In this, there is a shock along the inner boundary for $\delta_1 > 0$ and an expansion region for $\delta_1 < 0$ with similar behaviour at the outer boundary for $\delta_2 > 0$ and $\delta_2 < 0$, respectively. However, the strengths of the two shocks differ. The shock at the inner boundary is of strength $O(\delta_1^{4/3})$ increasing to $O(\delta_1^{2/3})$ in the neighbourhood of the corner, whereas the shock at the outer boundary is $O(\delta_2^4)$ increasing to $O(\delta_2^2)$ at the head of the wave.

It is interesting to compare these results with the analogous problem of the diffraction of a shock wave by a corner (Lighthill 1949 a; Tan 1951).

In general, the boundary of the perturbed region behind the incident shock itself represents a shock wave or rarefaction wave whose strength is $O(\delta^2)$. But when the flow behind the incident shock is just sonic, the boundary remains attached to the corner and is locally of strength $O(\delta^{2/3})$ decreasing to $O(\delta^2)$ on the remainder of the boundary. Thus both the present problem and that of Lighthill are similar in the respect that they possess perturbed regions which are bounded by a shock wave or rarefaction wave whose strengths are respectively $O(\delta_1^{2/3})$ and $O(\delta^{2/3})$ at the corner. However, the analysis of the present section suggests that their strengths differ on the remainder of the boundary, being $O(\delta^2)$ in Lighthill's case and $O(\delta_1^{4/3})$ in the present case. This difference can to some extent be explained by the nature of the characteristic lines in the two problems. In Lighthill's problem the general equation of motion is elliptic inside the perturbed region and hyperbolic outside so that in the neighbourhood of the corner only one characteristic is generated which is continued around the entire boundary of the perturbed region. In the present problem, the equation of motion is hyperbolic everywhere (with the exception of a small region near the corner) and all characteristics generated near the corner are continued around the boundary of the perturbed region. It is reasonable to suppose that in the latter case a shock whose strength is of a higher order will be propagated around the boundary.

7. Conclusion

In practice, it is impossible to obtain a perfect vacuum behind the membrane and shock-tube experiments are usually performed with the pressure difference across the membrane obtained by a high compression of the gas on one side. The resulting flow differs from the complete rarefaction wave. When the membrane fractures, a shock wave travels down the tube into the region of rarefaction followed by a region of steady flow. An incomplete rarefaction wave spreads upstream also followed by a region of uniform flow and the two regions of uniform flow are separated by a contact discontinuity which moves downstream with the same velocity as the fluid (e.g. Holder 1953).

Clearly in the above case, the region of perturbation will extend not only through the rarefaction wave but also into the regions of steady flow between the rarefaction wave and the shock wave. However, the solution obtained in the previous sections will still hold in the rarefaction wave since equation (8) is hyperbolic and the flow is determined by conditions on the wall alone.

For the resulting rarefaction wave to be near enough to completeness to extend as far downstream as $(X/c_0 t) = -4{\cdot}5$ requires an initial pressure ratio of thirty million. This is impracticable, but pressure ratios of 10^4 have been obtained and in this case the wave extends downstream to about $(X/c_0 t) = -3$, i.e. two-thirds of the complete rarefaction wave are present.

The author wishes to thank Dr W. Chester for suggesting the subject to him and for much helpful discussion on the problem. During the major part of the research the author was in receipt of a maintenance grant from the Department of Scientific and Industrial Research.

Appendix

(*a*) $\gamma = \frac{5}{3}$

Gases other than air are commonly used in the shock-tube. For example, argon may be used on the low pressure side of the membrane with hydrogen on the high pressure side. The rarefaction wave will always occur in the gas which originally occupies the high pressure region; thus in the above example the previous results will still hold since hydrogen is a diatomic gas.

For monatomic gases such as helium and argon we may approximate to $\gamma = 5/3$. In this case equation (20) may be integrated in terms of elementary functions. Thus the perturbed region is bounded by the curve

$$\left(\frac{X}{c_0 t}+3\right)\left\{1-\frac{1}{k^2}\left(\frac{X}{c_0 t}+3\right)^2\right\}^{1/2} = 2\sqrt{2}\,\frac{Y}{c_0 t},$$

where $k = 4$ for $\delta_2 \neq 0$, $k = 3$ for $\delta_2 = 0$. The boundary extends from $X = c_0 t$ to $X = -3c_0 t$ and apart from a contraction in the X-direction it resembles in general shape the boundary of § 4.

The perturbation velocity along the wall surface is given by

$$\frac{\partial\phi}{\partial X} = \frac{3\sqrt{2}c_0}{2\pi}\left\{\delta_2[2x\cosh^{-1}(1/x)-\cos^{-1}x]+\right.$$
$$\left.+\delta_1 H(\tfrac{3}{4}-x)\left[2x\cosh^{-1}\frac{3}{4x}-\cos^{-1}\frac{4x}{3}+\frac{x}{(9-16x^2)^{1/2}}\right]\right\},$$

and the pressure distribution by

$$\frac{p_2-p_1}{p_1} = \frac{5\sqrt{2}}{2\pi}\left\{\delta_2\left[\frac{3}{x}\cos^{-1}x-2\cosh^{-1}\frac{1}{x}\right]+\right.$$
$$\left.+\delta_1 H(\tfrac{3}{4}-x)\left[\frac{3}{x}\cos^{-1}\frac{4x}{3}-2\cosh^{-1}\frac{3}{4x}+\frac{1}{(9-16x^2)^{1/2}}\right]\right\}.$$

(*b*) $\gamma = 2$

Results for $\gamma = 2$ are useful for a comparison with hydraulic theory by the so-called hydraulic analogy. In this, the two-dimensional flow of a compressible gas is compared with the flow of water through a channel (e.g. Black & Mediratta 1951).

In this case the boundary of perturbation is given by

$$\left(\frac{X}{c_0 t}+2\right)\left\{1-\frac{1}{k}\left(\frac{X}{c_0 t}+2\right)\right\}^{1/2} = \sqrt{3}\,\frac{Y}{c_0 t},$$

where $k = 3$ for $\delta_2 \neq 0$, $k = 2$ for $\delta_2 = 0$. The perturbation velocity distribution is

$$\frac{\partial\phi}{\partial X} = \frac{4\sqrt{3}c_0}{3\pi}\left\{\delta_2[2x^{1/2}(1-x)^{1/2}-\cos^{-1}x^{1/2}]+\right.$$
$$\left.+\delta_1 H(\tfrac{2}{3}-x)\left[2x^{1/2}(\tfrac{2}{3}-x)^{1/2}-\cos^{-1}\left(\frac{3x}{2}\right)^{1/2}+\frac{(3x)^{1/2}}{6(2-3x)^{1/2}}\right]\right\},$$

and the pressure distribution is given by

$$\frac{p_2-p_1}{p_1}=\frac{8\sqrt{3}}{3\pi x}\left\{\delta_2[2\cos^{-1}x^{1/2}-x^{1/2}(1-x)^{1/2}]+\right.$$
$$\left.+\delta_1 H(\tfrac{2}{3}-x)\left[2\cos^{-1}\left(\frac{3x}{2}\right)^{1/2}-x^{1/2}(\tfrac{2}{3}-x)^{1/2}+\frac{(3x)^{1/2}}{6(2-3x)^{1/2}}\right]\right\}.$$

References

Black, J. & Mediratta, O. P. 1951 *Aeronaut. Quart.* **2,** 227.

Bocher, M. 1914 *An Introduction to the Study of Integral Equations*, 2nd Ed. Cambridge University Press.

Chester, W. 1954 *Quart. J. Mech. Appl. Math.* **7,** 247.

Courant, R. & Friedrichs, K. O. 1948 *Supersonic Flow and Shock Waves.* New York : Interscience.

Holder, D. W. 1953 A note on shock tubes, *Aero. Res. Counc., Lond., Rep.* no. 14,879.

Lighthill, M. J. 1949 a *Proc. Roy. Soc.* A, **198,** 454.

Lighthill, M. J. 1949 b *Phil. Mag.* (7) **40,** 1202.

Powell, J. B. L. 1956 Ph.D. Thesis, Bristol University.

Tan, H. S. 1951 *J. Aero. Sci.* **18,** 768.

A note on Mott-Smith's solution of the Boltzmann equation for a shock wave

By AKIRA SAKURAI

*Department of Applied Mathematics, Weizmann Institute of Science, Israel**

(*Received* 10 *July* 1957)

SUMMARY

After a modification, the interpolation formula of Mott-Smith (1951) for the shock wave problem is found to be a solution of the Boltzmann equation at large Mach number in a finite region of molecular velocity space. This modification gives a unique determination of the shock wave thickness, removing the ambiguity for this in Mott-Smith's formula.

Since the classical paper by Becker, it has been believed that the problem of shock wave structure must be considered in the light of the kinetic theory of gases. Many attempts have been made to find the solution of the basic Boltzmann equation, especially in the case of weak shock waves where the solution might be considered to be not so different from the Maxwell distribution. However, according to recent experiments on weak shock waves by Talbot & Sherman (1956), measured shock profiles are in rather better agreement with the predictions of the Navier–Stokes equations than with the results of the approximate solutions of the Boltzmann equation for weak shock waves. An approximate solution for a strong shock was given by Mott-Smith (1951). He considered that the molecular velocity distribution in a strong shock wave must be bimodal because of the effects of bounding supersonic and subsonic regions where the velocity distributions are of Maxwell type with different physical constants. Since the series of monocentric functions used in the approximate solutions for weak shock waves are inappropriate to represent such a bimodal distribution, Mott-Smith's approximate solution consisting of a sum of the two Maxwell distributions seems to be a more reasonable solution of the shock wave problem.

If we write $f(\mathbf{c}, x)$ for the distribution function of molecular velocity $\mathbf{c}$ in a plane shock wave whose normal is in the x direction, Mott-Smith's approximation $f^{(0)}$ has the form

$$f^{(0)} = \nu_\alpha(x) f_\alpha + \nu_\beta(x) f_\beta, \tag{1}$$†

where f_α, f_β signify the Maxwell distributions in the uniform super and

* Now at Tokyo Electrical Engineering College, Kanda, Tokyo.

† The definitions of f_α, f_β differ from Mott-Smith's by the factors $\nu_\alpha(x)$, $\nu_\beta(x)$ respectively.

subsonic regions respectively and are given by

$$f_\alpha = n_\alpha \left(\frac{m}{2\pi k T_\alpha}\right)^{3/2} \exp\left\{-\frac{m}{2kT_\alpha}(\mathbf{c}-\mathbf{i}u_\alpha)^2\right\}, \tag{2}*$$

$$f_\beta = n_\beta \left(\frac{m}{2\pi k T_\beta}\right)^{3/2} \exp\left\{-\frac{m}{2kT_\beta}(\mathbf{c}-\mathbf{i}u_\beta)^2\right\}, \tag{3}*$$

where n_α, n_β are the number densities, T_α, T_β are the temperatures, $\mathbf{i}u_\alpha$, $\mathbf{i}u_\beta$ are the stream velocities and m is the mass of the molecule.

To determine the functions $\nu_\alpha(x)$, $\nu_\beta(x)$, Mott-Smith utilized the transport equation for an arbitrary function $\Phi(\mathbf{c})$

$$\frac{\partial}{\partial x}\left(\int u\Phi(\mathbf{c}) f\, d\mathbf{c}\right) = \iiint \{\Phi(\mathbf{c}') - \Phi(\mathbf{c})\} f f_1 g\, d\Omega d\mathbf{c}_1\, d\mathbf{c},$$

which is equivalent to an averaging of the one-dimensional Boltzmann equation

$$L(f) \equiv u\frac{\partial f}{\partial x} - \iint (f'f_1' - ff_1) g\, d\Omega d\mathbf{c}_1 = 0, \tag{4}$$

in the velocity-space $\mathbf{c}$ with the weight $\Phi(\mathbf{c})$, where g is the magnitude of the relative velocity $\mathbf{g} = \mathbf{c}_1 - \mathbf{c}$ of a colliding pair; f_1, f', f_1' represent $f(\mathbf{c}_1, x), f(\mathbf{c}', x), f(\mathbf{c}_1', x)$; and $\mathbf{c}'$, $\mathbf{c}_1'$ denote the velocities of a colliding pair after collision; and $d\Omega$ is a differential cross-section. Taking $\Phi(\mathbf{c}) = u^2, u^3$, it was found that

$$\nu_\alpha(x) = \nu(-x), \qquad \nu_\beta(x) = \nu(x), \qquad \nu(x) = \tfrac{1}{2}(1 + \tanh 2x/X), \tag{5}$$

where X is a function of Mach number $M = u_\alpha/c_\alpha$ (c_α is the velocity of sound in the supersonic flow) and gives the thickness of the shock wave.

Now the form of the function $X(M)$ depends on the choice of the function $\Phi(\mathbf{c})$ but the forms of the functions $\nu_\alpha(x)$, $\nu_\beta(x)$ are always the same for any $\Phi(\mathbf{c})$ and are given by (5). The purpose of the present note is to show that if we take a special form for the function $X(M)$, the equation

$$f^{(0)} = \nu(-x) f_\alpha + \nu(x) f_\beta \tag{6}$$

satisfies directly the Boltzmann equation (4) at large M for a finite, fixed value of c. This choice of $X(M)$ may be useful in removing the ambiguity about the function $X(M)$ caused by its dependence on $\Phi(\mathbf{c})$.

Substituting from (6) into (4) and utilizing the relations

$$\frac{d}{dx}\nu(x) = -\frac{d}{dx}\nu(-x) = \frac{4}{X}\nu(x)\nu(-x), \tag{7}$$

$$f_\alpha' f_{\alpha 1}' = f_\alpha f_{\alpha 1}, \qquad f_\beta' f_{\beta 1}' = f_\beta f_{\beta 1}, \tag{8}$$

we get

$$L(f^{(0)}) = \nu(x)\nu(-x) L_c(f^{(0)}), \tag{9}$$

where

$$L_c(f^{(0)}) = \frac{4}{X} u(f_\beta - f_\alpha) - \iint (f_\alpha' f_{\beta 1}' + f_{\alpha 1}' f_\beta' - f_\alpha f_{\beta 1} - f_{\alpha 1} f_\beta) g\, d\Omega d\mathbf{c}_1.$$

It is to be noted that the dependence on x and $\mathbf{c}$ is separated in (9), and $L(f^{(0)}) \to 0$ as $x \to \pm\infty$ since $\nu(x)\nu(-x) = \frac{1}{4}\,\mathrm{sech}^2(2x/X)$. The term $L_c(f^{(0)})$

* The definitions of f_α, f_β differ from Mott-Smith's by the factors $\nu_\alpha(x)$, $\nu_\beta(x)$ respectively.

in (9) will be shown to become small for a special $X(M)$ when M becomes large for finite, fixed c.

To do this, we shall first transform $L_c(f^{(0)})$. It follows from (8) that

$$f'_\alpha f'_{\beta 1} = f_\beta f_{\beta 1} \frac{f'_\alpha}{f'_\beta}, \qquad f'_{\alpha 1} f'_\beta = f_\beta f_{\beta 1} \frac{f'_{\alpha 1}}{f'_{\beta 1}},$$

and hence

$$\int\int (f'_\alpha f'_{\beta 1} + f'_{\alpha 1} f'_\beta - f_\alpha f_{\beta 1} - f_{\alpha 1} f_\beta) g \, d\Omega d\mathbf{c}_1$$

$$= \int\int f_\beta f_{\beta 1} \left(\frac{f'_{\alpha 1}}{f'_{\beta 1}} + \frac{f'_\alpha}{f'_\beta} - \frac{f_{\alpha 1}}{f_{\beta 1}} - \frac{f_\alpha}{f_\beta} \right) g \, d\Omega d\mathbf{c}_1. \quad (10)$$

Putting $$\mathbf{p}_\beta = (m/2kT_\beta)^{1/2}(\mathbf{c} - \mathbf{i}u_\beta), \qquad \mathbf{g}_\beta = \mathbf{p}_{\beta 1} - \mathbf{p}_\beta, \quad (11)$$

the right-hand side of equation (10) becomes

$$\left(\frac{2kT_\beta}{m} \right)^{1/2} n_\beta f_\beta J_\beta \left(\frac{f_\alpha}{f_\beta} \right),$$

where $$J_\beta(h) = \pi^{-3/2} \int\int \exp(-p_{\beta 1}^2)(h'_1 + h' - h_1 - h) g_\beta \, d\Omega d\mathbf{p}_{\beta 1}. \quad (12)$$

Then $L_c(f^{(0)})$ becomes

$$L_c(f^{(0)}) = -f_\alpha u_\alpha \left[\frac{4}{X} \left(1 + \frac{1}{u_\alpha} \left(\frac{2kT_\alpha}{m} \right)^{1/2} \right) \left(1 - \frac{f_\beta}{f_\alpha} \right) + \right.$$

$$\left. + \frac{1}{u_\alpha} \left(\frac{2kT_\beta}{m} \right)^{1/2} n_\beta \frac{f_\beta}{f_\alpha} J_\beta \left(\frac{f_\alpha}{f_\beta} \right) \right], \quad (13)$$

where $p_{\alpha x}$ is the x component of $\mathbf{p}_\alpha = (m/2kT_\alpha)^{1/2}(\mathbf{c} - \mathbf{i}u_\alpha)$.

From (2) and (3), we have

$$\frac{f_\beta}{f_\alpha} J_\beta \left(\frac{f_\alpha}{f_\beta} \right) = \exp(p_\alpha^2 - p_\beta^2) J_\beta \{ \exp(p_\beta^2 - p_\alpha^2) \}, \quad (14)$$

and utilizing the standard simplified form of the expression (12) (see, for example, Chapman & Cowling 1953),

$$J_\beta(h) = -K_0(\mathbf{p}_\beta) h(\mathbf{p}_\beta) - \int h(\mathbf{p}_{\beta 1}) K(\mathbf{p}_\beta, \mathbf{p}_{\beta 1}) \, d\mathbf{p}_{\beta 1},$$

where $$K_0(\mathbf{p}_\beta) = \pi^{-3/2} \int\int \exp(-p_\beta^2) g_\beta \, d\Omega d\mathbf{p}_{\beta 1}$$

and $K(\mathbf{p}_\beta, \mathbf{p}_{\beta 1})$ is a symmetric function of $\mathbf{p}_\beta$, $\mathbf{p}_{\beta 1}$, equation (14) reduces to

$$\frac{f_\beta}{f_\alpha} J_\beta \left(\frac{f_\alpha}{f_\beta} \right) = -K_0(\mathbf{p}_\beta) - \exp(p_\alpha^2 - p_\beta^2) \int \exp(p_{\beta 1}^2 - p_{\alpha 1}^2) K(\mathbf{p}_\beta, \mathbf{p}_{\beta 1}) \, d\mathbf{p}_{\beta 1}. \quad (15)$$

For the case of the elastic sphere model of diameter σ, we have

$$K_0(\mathbf{p}_\beta) = \pi^{1/2} \sigma^2 F(p_\beta^2), \qquad F(x^2) = e^{-x^2} + \frac{2x^2 + 1}{x} \int_0^x e^{-t^2} \, dt, \quad (16)$$

and

$$\exp(p_\alpha^2-p_\beta^2)\int \exp(p_{\beta 1}^2-p_{\alpha 1}^2)K(\mathbf{p}_\beta,\mathbf{p}_{\beta 1})\,d\mathbf{p}_{\beta 1}$$

$$=\pi^{1/2}\sigma^2\exp(p_\alpha^2-p_\beta^2)\left\{k^4F(p_\alpha^2)-\frac{2}{\pi}\int \exp(-p_{\alpha 1}^2+\omega_\beta^2)\frac{1}{g_\beta}\,d\mathbf{p}_{\beta 1}\right\}, \quad (17)$$

where $$\omega_\beta^2=\{[\mathbf{p}_\beta,\mathbf{p}_{\beta 1}]/g_\beta\}^2, \qquad k=(T_\alpha/T_\beta)^{1/2}. \quad (18)$$

Writing $$u_{\alpha\beta}=(m/2kT_\beta)^{1/2}(u_\alpha-u_\beta),$$

we have $$\mathbf{p}_\beta=k\mathbf{p}_\alpha+\mathbf{i}u_{\alpha\beta}. \quad (19)$$

Utilizing the Rankine–Hugoniot relation, k and $u_{\alpha\beta}$ become

$$\left.\begin{aligned} k &= (a-1)a^{-1/2}\frac{1}{M}\left(1+\frac{a-2}{M^2}\right)^{-1/2}\left(1-\frac{1}{aM^2}\right)^{-1/2},\\ u_{\alpha\beta} &= \left(\frac{a-2}{2}\right)^{1/2}\left(1-\frac{1}{M^2}\right)\left(1+\frac{a-2}{M^2}\right)^{-1/2}\left(1-\frac{1}{aM^2}\right)^{-1/2},\end{aligned}\right\} \quad (20)$$

where $a=2\gamma/(\gamma-1)$, and γ is the ratio of specific heats.

When M becomes large, k becomes small while $u_{\alpha\beta}$ remains finite and approaches the value $\{(a-2)/2\}^{1/2}$. Accordingly $\mathbf{p}_\beta$ in (19) lies near $\mathbf{i}u_{\alpha\beta}$ provided p_α is finite and fixed, and then $F(p_\beta^2)$ in (16) can be expressed as

$$F(p_\beta^2)\sim F(u_{\alpha\beta}^2)+2ku_{\alpha\beta}p_{\alpha x}F'(u_{\alpha\beta}^2)+k^2\{p_\alpha^2F'(u_{\alpha\beta}^2)+2u_{\alpha\beta}^2p_{\alpha x}^2F''(u_{\alpha\beta}^2)\}+\cdots, \quad (21)$$

where we have used the equation

$$p_\beta^2=u_{\alpha\beta}^2+2ku_{\alpha\beta}p_{\alpha x}+k^2p_\alpha^2$$

and primes in F means differentiation with respect to p_β^2.

The integral in (17)

$$\frac{2}{\pi}\int \exp(-p_{\alpha 1}^2+\omega_\beta^2)\frac{1}{g_\beta}\,d\mathbf{p}_{\beta 1}$$

will now be shown to be of the order of k^2. Utilizing the relations

$$g_\beta=kg_\alpha, \qquad d\mathbf{p}_\beta=k^3\,d\mathbf{p}_\alpha,$$

$$[\mathbf{p}_\beta,\mathbf{p}_{\beta 1}]/g_\beta=u_{\alpha\beta}[\mathbf{i},\mathbf{g}_\alpha/g_\alpha]+k[\mathbf{p}_\alpha,\mathbf{g}_\alpha/g_\alpha],$$

and under the assumption of finite and fixed p_α, we get

$$\frac{2}{\pi}\exp(p_\alpha^2-p_\beta^2)\int \exp(-p_{\alpha 1}^2+\omega_\beta^2)\frac{1}{g_\beta}\,d\mathbf{p}_{\beta 1}\sim k^2I(\mathbf{p}_\alpha)+\cdots, \quad (22)$$

where $$I(\mathbf{p}_\alpha)=\frac{2}{\pi}\exp(p_\alpha^2-p_\beta^2)\int \frac{1}{g_\alpha}\exp(-p_\alpha^2+u_{\alpha\beta}^2\sin^2\psi)\,d\mathbf{p}_{\alpha 1},$$

and ψ denotes the angle between $\mathbf{g}_\alpha$ and $\mathbf{i}$.

Now from (20) and the Rankine–Hugoniot relations,

$$\left.\begin{aligned}\frac{1}{u_\alpha}\left(\frac{2kT_\alpha}{m}\right)^{1/2} &= \left(\frac{2(a-2)}{a}\right)^{1/2}\frac{1}{M},\\ \frac{1}{u_\alpha}\left(\frac{2kT_\beta}{m}\right)^{1/2} n_\beta &= n_\alpha\{2(a-2)\}^{1/2}A(M),\\ A(M) &\equiv \left(1-\frac{1}{aM^2}\right)^{1/2}\left(1+\frac{a-2}{M^2}\right)^{-1/2},\end{aligned}\right\} \tag{23}$$

and equation (13) then finally becomes for finite and fixed p_α,

$$\begin{aligned}L_c(f^{(0)}) \sim -f_\alpha u_\alpha \Big[&\{(4/X)-\pi^{1/2}\sigma^2 n_\alpha\{2(a-2)\}^{1/2}A(M)F(u_{\alpha\beta}^2)\}\\ &+k\{2(a-2)\}^{1/2}\left\{\frac{4}{X(a-1)}\left(1+\frac{a-2}{M^2}\right)^{1/2}\left(1-\frac{1}{aM^2}\right)^{1/2}-\right.\\ &\left.-2\pi^{1/2}\sigma^2 n_\alpha A(M)u_{\alpha\beta}F'(u_{\alpha\beta}^2)\right\}p_{\alpha x}-k^2\pi^{1/2}\sigma^2 n_\alpha\{2(a-2)\}^{1/2}A(M)\times\\ &\times\{p_\alpha^2 F'(u_{\alpha\beta}^2)+2u_{\alpha\beta}^2 p_{\alpha x}^2 F''(u_{\alpha\beta}^2)-I(\mathbf{p}_\alpha)\}+\ldots\Big].\end{aligned} \tag{24}$$

By equating the first term in (24) to zero, we can determine $X(M)$ from

$$\frac{4l}{X}=\left(\frac{a-2}{\pi}\right)^{1/2}A(M)F(u_{\alpha\beta}^2), \tag{25}$$

where l is the mean free path defined by

$$1/l=\sqrt{2}\pi n_\alpha\sigma^2.$$

For the case of other molecular models, the second term in (15) is also likely to be small for large M and we may determine X from

$$\frac{4}{X}=n_\alpha\{2(a-2)\}^{1/2}A(M)K_0(\mathrm{i}u_{\alpha\beta}).$$

In the following table, values of l/X for $a=5$ in (25) and for various Mach numbers are compared with Mott-Smith's values and the results of

M	l/X	$(l/X)_R$	$(l/X)_{u^2}$	$(l/X)_{u^3}$
∞	0·703	—	0·628	0·468
10	0·685	—	0·600	0·455
5	0·630	—	0·527	0·419
4	0·596	0·495	0·478	0·397
3	0·520	0·414	0·397	0·346
2·5	0·474	0·355	0·332	0·304

Rosen (1954), determined by a restricted variational method using an expression of type (1) as a test function. In the table $(l/X)_R$ denotes the results of Rosen, while $(l/X)_{u^2}$, $(l/X)_{u^3}$ give Mott-Smith's values for the cases $\Phi=u^2$, u^3 respectively.

When X is given by (25), (24) reduces to

$$L_c(f^{(0)}) \sim kL_1+k^2L_2+\ldots,$$

where

$$L_1 = [2(a-2)]^{1/2}\frac{4}{X}\left\{\frac{1}{a-1}\left(1+\frac{a-2}{M^2}\right)^{1/2}\left(1-\frac{1}{aM^2}\right)^{1/2} - \right.$$
$$\left. - \sqrt{\frac{2}{\pi}}\frac{X}{4l}A(M)\,u_{\alpha\beta}\,F'(u_{\alpha\beta})\right\} p_{\alpha x},$$

$$L_2 = \frac{1}{l}\left(\frac{a-2}{\pi}\right)^{1/2} A(M)\{p_\alpha^2 F'(u_{\alpha\beta}^2) + 2u_{\alpha\beta}^2 p_{\alpha x}^2 F''(u_{\alpha\beta}^2) - I(\mathbf{p}_\alpha)\}.$$

This suggests that we may find a solution f in the form

$$f \sim f^{(0)} + k\phi^{(1)} + k^2\phi^{(2)} + \ldots .$$

$\phi^{(1)}$ can be found easily and is given by

$$\phi^{(1)} = -(4/X)L_1\,\nu(-x)\log\nu(-x),$$

where we have used the boundary conditions for f, equations (2) and (3). Since $L_1 \propto p_{\alpha x}$ and the mean density $\bar{n}$ is given by $\bar{n} = \int f\,d\mathbf{c}$, $\phi^{(1)}$ does not contribute to $\bar{n}$ and, accordingly, not to the thickness. It seems, however, difficult to find $\phi^{(2)}$, $\phi^{(3)}$, ... successively, mainly because $\phi^{(1)}$, $\phi^{(2)}$, ... are of ordinary order of magnitude only in a finite region of **c** space which depends on k, and we need to estimate the integrals in which they are included over the whole of **c** space.

References

Chapman, S. & Cowling, T. G. 1953 *Mathematical Theory of Non-uniform Gases.* Cambridge University Press.

Mott-Smith, H. M. 1951 *Phys. Rev.* **82,** 885.

Rosen, P. 1954 *J. Chem. Phys.* **22,** 1045.

Talbot, L. & Sherman, F. S. 1956 *Institute of Engineering Research, University of California, Rep.* no. HE-150-137.

The flow of swirling water through a convergent–divergent nozzle

By A. M. BINNIE, G. A. HOOKINGS* and M. Y. M. KAMEL
Engineering Laboratory, University of Cambridge

(*Received* 19 *July* 1957)

SUMMARY

Experiments with Perspex nozzles, which were arranged to discharge vertically downwards and in which the convergent part was followed by a short divergency, showed that at low swirls the flow was unstable. When the swirl was sufficiently large for an air core to be established, its effective magnitude was estimated from measurements, at the throat, of the core diameter and of the wall pressure. The former were in closer accord with inviscid theory than the latter. The results are presented in terms of dimensionless discharge and swirl coefficients. Measurements of core diameter and wall pressure were also made throughout one of the nozzles and compared with the theory. Reversed axial flow in the upper part of the nozzles was easily produced, and the limits of its appearance were determined. Low pressure tests with the reservoir top alternately submerged and uncovered revealed that the top had a marked influence on the nature of the flow in the nozzle; and measurements of the tangential and axial velocities in the upper part of the nozzle proved the inviscid theory to be seriously in error at high swirls. For purposes of comparison, similar experiments were performed on a convergent nozzle.

1. INTRODUCTION

In an earlier paper (Binnie & Teare 1956) an account was given of experiments on the passage of swirling water through a Perspex convergent nozzle of simple conical shape. As described below, the work has been continued with two convergent–divergent nozzles of much the same size as the nozzle previously used. The remainder of the equipment was again employed. Under these conditions a more satisfactory comparison could be made between the experiments and the inviscid theory of convergent–divergent motion, which is summarized in § 3. With the convergent nozzle it was necessary to assume that the throat lay in the plane of the nozzle outlet, but with the new nozzles the throat position was not, of course, in doubt. Moreover, better estimates of the effective swirl coefficient were possible. This coefficient cannot be reliably calculated from the wall

* On sabbatical leave from Auckland University College, New Zealand.

pressure in the convergent part of a nozzle remote from the throat because that pressure is so nearly equal to the supply head, and in a convergent nozzle the wall pressure falls rapidly to atmospheric as the outlet is approached—a state of affairs not contemplated in the theory. Thus, with more promising prospects, an attempt could now be made to determine the swirl coefficient from the throat value of the wall pressure or of the air-core diameter.

Before the new nozzles were used, for comparison some tests (described in § 4) were made on the convergent nozzle. The coreless flow that occurred at very low swirl was examined, and observations were made of the unstable conditions that set in while the air core was forming. In addition, the effect of the reservoir top on the velocity distribution in the nozzle was studied by means of low pressure tests first with the top slightly submerged and then with it slightly uncovered. In § 5 an account is given of numerous experiments on the convergent–divergent nozzles. At small swirls their action differed from that of the convergent nozzle. Under normal conditions with the core fully established, the observations at the throat of core diameter agreed much better with theory than those of wall pressure. Reverse flow was seen in the upper part of the nozzles even during high pressure tests, whereas in the convergent nozzle it occurred only at low heads. At high swirls the predictions of the inviscid theory were found very unreliable, and a detailed examination of these discrepancies was made by measuring not only the loss of total head in the nozzle but also the tangential and axial components of the velocity.

2. Description of apparatus

As shown in the upper part of figure 1, the convergent nozzle was modified by tail-pieces into alternative convergent–divergent shapes which will be designated A and B. Nozzle A was produced by attaching to the unaltered convergent nozzle a tail-piece in which the throat was a surface formed symmetrically by the revolution of a circular arc of radius 5 in. Nozzle B had a more gradual constriction, the radius of the circular arc forming the throat being 9·93 in.; before it was attached, the lower part of the convergent nozzle had to be removed. The throats of A and B were at the same level, and their diameters were respectively 0·940 and 1·088 in., the latter being identical with the throat diameter of the original convergent nozzle. The final divergent parts of both A and B were cones of semi-angle 10°, which was the same as the angle of convergence in the upper part of the nozzles.

As before, the nozzle in use was clamped to the circular base of the reservoir through an intermediate volute chamber. By this means the boundary layer formed inside the reservoir could be 'bled' off, and the maximum swirl that could be delivered to the nozzle was increased. The reservoir, which was 4 ft. 6 in. both in diameter and in height, was supplied by a vertical pipe, which entered at the centre of the top plate, and by a pair of horizontal tangential pipes. At the top of the reservoir

the modification indicated in figure 1(*d*) was made. A pipe of diameter $\frac{1}{4}$ in. was brought in to the centre of the underside of the baffle plate, and it was used to introduce air and permanganate solution and to draw off the neighbouring boundary layer. The pressures on the nozzle walls were

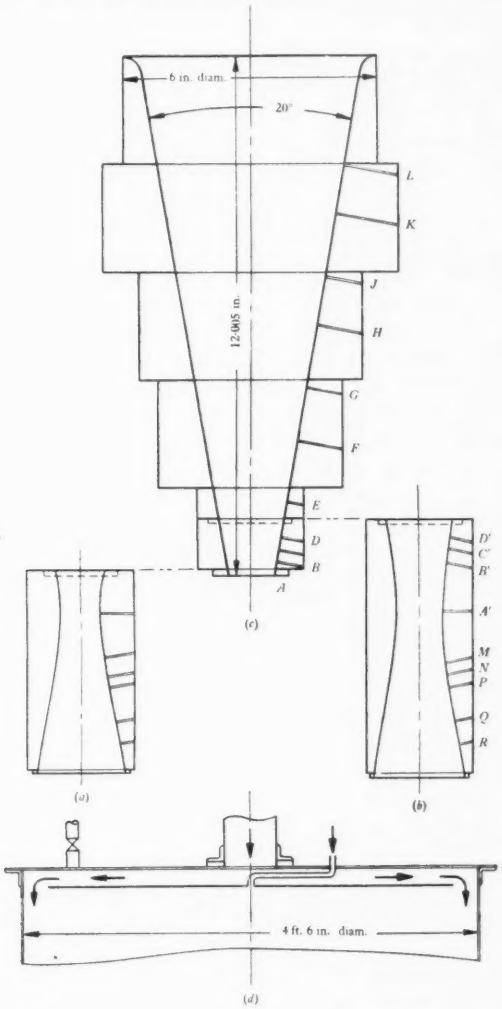

Figure 1. (*a*) tailpiece of nozzle A; (*b*) tailpiece of nozzle B; (*c*) convergent nozzle; (*d*) injection pipe at centre of baffle plate. The dimensions of nozzle B are as follows :

position	D'	C'	B'	A'	M	N	P	Q	R
axial distance from L (in.)	8·61	8·87	9·21	10·30	11·50	11·75	12·05	12·85	13·35
measured diameter (in.)	1·37	1·29	1·20	1·088	1·22	1·29	1·39	1·67	1·84

measured by tappings connected to conventional air–water and water–mercury manometers. The distribution of total head inside the nozzles was again explored through the tappings with a hypodermic tube having an outside diameter 0·027 in. and a side stagnation hole of diameter 0·014 in. Open tanks served to determine the discharge from the nozzles and the bleed. The diameter of the air core was obtained with a telescope fitted with a scale in the eyepiece but, owing to the irregular passage of waves on the core, the accuracy of these readings was not high. Refraction difficulties made this method unsatisfactory in the divergent part of the nozzle where the stream was thin, and there its radial thickness was measured with a fine wire pushed through the tappings by a micrometer screw.

3. Summary of the theory of inviscid flow

The discharge coefficient $\mathbf{K}$ and the swirl coefficient $\mathbf{X}$ are defined by

$$\mathbf{K} = \frac{\mathbf{Q}}{\pi a_t^2 (2g\mathbf{H})^{1/2}}, \qquad \mathbf{X} = \frac{\Omega}{a_t (2g\mathbf{H})^{1/2}}, \tag{3.1}$$

where $\mathbf{Q}$ is the discharge, $\mathbf{H}$ is the total head of the supply measured from the level of the throat, a_t is the nozzle radius at the throat, and Ω is the swirl constant equal to the product of radius and tangential velocity. For each test $\mathbf{K}$ could be calculated from the observations of $\mathbf{Q}$ and $\mathbf{H}$, but to obtain the effective value of $\mathbf{X}$ certain relations were required which can readily be deduced from the inviscid theory explained by Binnie & Harris (1950). They are

$$\mathbf{X}^2 = \frac{1}{2}\left(1 - \frac{3}{2}\frac{h_t}{\mathbf{H}}\right)\left[1 \pm \left\{1 - 2\frac{h_t^2}{\mathbf{H}^2}\left(1 - \frac{3}{2}\frac{h_t}{\mathbf{H}}\right)^{-2}\right\}^{1/2}\right], \tag{3.2}$$

and

$$\mathbf{X}^2 = 2\frac{b_t^4}{a_t^4}\left(1 + \frac{b_t^2}{a_t^2}\right)^{-1}, \tag{3.3}$$

which were used according as $\mathbf{X}$ was found from the throat wall pressure head h_t or from the core radius b_t at the throat. If the swirl is increased from a low value, $h_t/\mathbf{H}$ rises in accordance with the smaller root of (3.2) because the effect of the greater angular velocity exceeds the effect of the diminishing radial thickness of the stream. But a stage is attained when the two effects balance, and here $h_t/\mathbf{H}$ has its maximum possible value 0·343, to which the corresponding values of $\mathbf{X}$ and b_t/a_t are 0·493 and 0·644. Thereafter, since b_t increases continuously, h_t falls in accordance with the larger root of (3.2) until it reaches zero, when $\mathbf{X} = 1$, $b_t/a_t = 1$, and the discharge ceases. Thus, as Binnie & Hookings (1948) pointed out, an ambiguity arises when $\mathbf{X}$ is deduced from reading of the wall pressure, for it is impossible to distinguish between the stream with the small swirl and large radial thickness and the one with the large swirl and small thickness.

The theoretical relation between $\mathbf{K}$ and $\mathbf{X}$ may be found from (3.3) and the equation

$$\mathbf{K} = \left(1 - \frac{b_t^2}{a_t^2}\right)^{3/2}\left(1 + \frac{b_t^2}{a_t^2}\right)^{-1/2}, \tag{3.4}$$

the procedure being to insert in both a succession of values of b_t/a_t. The result is plotted in figures 5 and 6; it is very nearly a straight line over the range $0 < \mathbf{X} < 0{\cdot}6$. We shall also need to calculate, for specified values of $\mathbf{K}$ and for various cross-sections, the theoretical ratios of the core radius b to the nozzle radius a and of the wall pressure head h to the supply head $\mathbf{H}$. The ratio $h/\mathbf{H}$ is given by

$$\frac{h^3}{\mathbf{H}^3} - \left(1 - \mathbf{X}^2\frac{a_t^2}{a^2} - \mathbf{K}^2\frac{a_t^4}{a^4}\right)\frac{h^2}{\mathbf{H}^2} + 2\mathbf{K}^2\mathbf{X}^2\frac{a_t^6}{a^6}\frac{h}{\mathbf{H}} + \mathbf{K}^2\mathbf{X}^4\frac{a_t^8}{a^8} = 0, \qquad (3.5)$$

and then b/a is found from

$$\frac{b}{a} = \left(1 + \frac{1}{\mathbf{X}^2}\frac{a^2}{a_t^2}\frac{h}{\mathbf{H}}\right)^{-1/2}. \qquad (3.6)$$

The small difference in level between the throat and the section under consideration is here neglected; but when the calculations were carried out, the necessary correction to $\mathbf{H}$ was made. Equation (3.5) has two positive roots, the larger referring to the upstream side of the throat and the smaller to the downstream side; its last two terms were of little importance in the upper part of the nozzles where high powers of a_t/a were small.

4. Experiments on the convergent nozzle

(i) *At low swirl*

When a very small swirl was produced in the reservoir, its existence could be easily detected because, although no air core formed, the emergent jet slightly diverged. To throw light on the conditions prevailing inside the nozzle, horizontal traverses were made with the hypodermic tube inserted through a tapping. To ensure that the traverse was made across the axis of the flow, a stream of fine air bubbles was temporarily injected further upstream not far from the geometrical axis of the nozzle. The bubbles were rapidly forced to the effective axis and then discharged. In this way it was seen that usually the effective axis was distorted fairly steadily into a slightly helical shape in the same manner as an air core. Typical results of traverses extending a little way beyond the axis are plotted in figure 2, which relates to observations of total head $\mathbf{H}'$ through tappings E, F and G under constant flow conditions. When the swirl was raised as much as possible without an air core appearing, the losses of total head increased still more; and the observations followed a similar pattern to those shown in Binnie & Teare's figure 4, which were made round an air core. Again, the downward velocity near the axis was much higher than the mean. As might be expected in view of the great height of the reservoir, the loss at E was little greater than that at the higher tappings.

As the swirl was further increased, the air space within the emergent jet moved up; and when it succeeded intermittently in reaching the nozzle outlet, the flow was throttled and the reservoir pressure increased. Under these conditions readings could not be obtained. Fairly steady flow was, however, restored when a weak stream of air was injected on the axis,

either at the top of the reservoir or through one of the upper tappings, causing a minute core to appear. But as soon as the injection was stopped, the air was swept out and unsteady conditions again prevailed. This device was necessary over the range $0{\cdot}92 > \mathbf{K} > 0{\cdot}78$.

The swirl being raised, a tiny air core formed of its own accord with its top darting irregularly up and down. But as it was never driven out of the nozzle and its travel was in a region where the nozzle cross-section was relatively large, the head and the discharge were not subject to appreciable fluctuations. The top of the core reached higher as the swirl was increased, until at $\mathbf{K} = 0{\cdot}64$ it was always out of sight and steady conditions were apparently established.

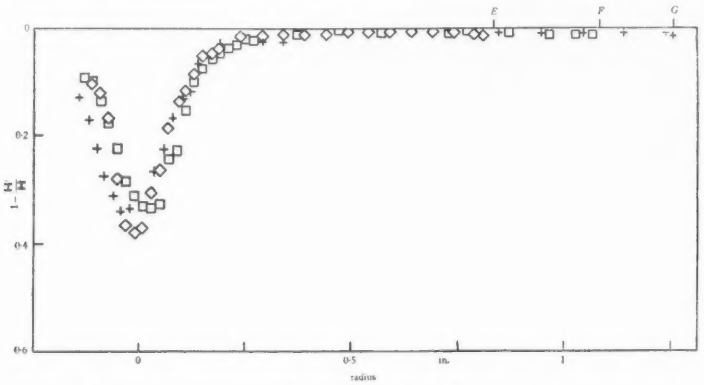

Figure 2. Fractional loss of total head in coreless flow in the convergent nozzle; + *G*; □ *F*; ◇ *E*.

The observations were continued up to the greatest available swirl, where $\mathbf{K} = 0{\cdot}48$, the final readings requiring the use of the bleed. All the above values of **K** were obtained at the constant head $\mathbf{H} = 25{\cdot}0$ ft. At $\mathbf{H} = 6{\cdot}6$ ft. the observations were unchanged except that the stage with a fluctuating self-induced core barely appeared, and the last stage occupied the range $0{\cdot}75 > \mathbf{K} > 0{\cdot}40$. No alterations in the limits were found when the tests were repeated with decreasing swirl.

(ii) *With the top of the reservoir uncovered*

To investigate the effect of the reservoir top on the flow through the nozzle, four pairs of tests were made. In the first part of each test the baffle plate (figure 1 (*d*)) was just submerged, and in the second the supply was reduced so that the baffle was just uncovered and a free surface was formed within the reservoir. In this second part, an air vent on the top plate was opened to ensure that the air pressure inside was truly atmospheric. The results of these experiments are set out in table 1 in order of diminishing swirl. Only at $\mathbf{K} = 0{\cdot}92$ was the flow coreless.

It will be seen that the submergence of the baffle plate considerably increased the discharge. In the first part, the insertion of colour through a tapping indicated a strong downward velocity close to the air core, and colour injected at the centre of the baffle was soon seen to pass through the same region. These observations confirmed Taylor's remark (1948) that the liquid, which is slowed up in the boundary layer on the back of reservoir, is unable to maintain its position, and it is quickly forced first to the core and then out through the nozzle. In the second part, there was a marked change in the appearance of the core, which was now larger in diameter and more disturbed by waves. The downward velocity near the core was greatly diminished; indeed, colour injected on the core surface was seen to move upwards an inch before being carried down by a transient train of waves.

Test	Supply	Bleed	**H** ft.	**K**
1	tangential	on	5·54	0·38
			5·29	0·30
2	tangential	off	5·50	0·57
			5·31	0·48
3	combined	off	5·41	0·73
			5·29	0·68
4	combined	off	5·56	0·92
			5·18	0·78

Table 1. The effect of a free surface inside the reservoir.

5. Experiments on the convergent-divergent nozzles

(i) *At low swirl*

The slightest introduction of swirl caused an increase in the area of contact between the stream and the divergency, and a spluttering noise was emitted, probably due to intermittent breaks in the vacuum near the throat as air from below forced its way into the zone of negative pressure. The swirl being slightly raised, the motion became quieter, and the contact between the jet and the nozzle wall was irregular (figure 3(*a*), plate 1). This state also was unstable and often reverted to the previous noisier condition. With a further increase in swirl, a loud noise was heard, and the emergent stream became wildly turbulent, drops of water being hurled out sideways with considerable velocity (figure 3(*b*), plate 1). As this highly unstable state developed, the discharge went up sharply, and the negative pressure at the throat reached its maximum value, which was about 26 ft. at $\mathbf{H} = 25$ ft. The micro-flash photographs showed that a bubble formed with its nose at the throat and with its tail in a violent state of commotion, and it may be regarded as a cavitation bubble since the

surrounding pressure was low. The admission of air through the throat tapping caused the flow to return to its previous quieter condition, but the violent state was quickly restored when the tapping was shut and the local velocity increased by the temporary insertion of a rod along the nozzle axis. At the next stage with rising swirl, the stream remained in complete contact with the whole of the divergency, but the air inside the emergent cone did not reach up above the throat. The states described in this paragraph will be referred to as phase (i). In all of them the motion was too unstable for accurate measurements to be possible. But when a small stream of air was admitted to the upper part of the nozzle, a tiny core formed exactly as described in § 4(i), and steady conditions were established. Observations made in this way have been inserted in table 2.

H ft.	Test	Phase (i)	Phase (ii)	Phase (iii)
25·0	*a*	0·97–0·71	0·68–0·58	0·54–0·45
	b	0·97–0·71	0·70–0·62	0·60–0·45
6·6	*a*	0·97–0·75	—	0·71–0·41
	b	0·97–0·70	—	0·66–0·40
5·0	*a*	—	—	0·71–0·31
	b	—	—	0·68–0·31

Table 2. Values of the discharge coefficient **K** for different phases in nozzle A.

The work was continued up to the highest available swirl. In what will be termed phase (ii), a core formed intermittently above the throat but always existed near the throat itself (figure 3(*c*), plate 1), the nature of the fluctuations being the same as those observed in the convergent nozzle. Ultimately in phase (iii) a core of steady diameter was seen throughout the nozzle (figure 3(*d*), plate 1).

Table 2 gives the values of **K** obtained with the three phases in nozzle A, no great effort being made to determine with extreme precision the limits between the phases. Three supply heads were used, and with the last the reservoir top was uncovered. In the tests labelled *a* the bleed was not used at low swirls, but it required opening more and more towards the end of each test; in those labelled *b* the bleed was always fully open. This difference in the supply conditions had little effect on the results. As in the convergent nozzle, phase (ii) at $\mathbf{H} = 6{\cdot}6$ ft. made only a fleeting appearance, and no readings of it were obtained. At $\mathbf{H} = 5{\cdot}0$ ft. air injection was not tried, and attention was confined to phase (iii), which extended to much lower values of **K** than those obtained with the top of the reservoir submerged. Almost identical results were obtained with nozzle B, and the figures in table 2 agree fairly closely with those set out in § 4 for the convergent nozzle.

(ii) *Comparative tests on nozzle B and the convergent nozzle*

Measurements of the core radius b and the wall pressure head h, made throughout the nozzle B at $\mathbf{H} = 24{\cdot}1$ ft., $\mathbf{Q} = 0{\cdot}111$ cu. ft./s, with the bleed discharging 0·127 cu. ft./s, are indicated by the solid points in figure 4. These conditions are almost identical with those under which the convergent nozzle had already been tested by Binnie & Teare (1956), and for purposes of comparison the observations displayed in their figure 5 have been transferred to figure 4 and plotted there as hollow points. For the above value of $\mathbf{Q}$, $\mathbf{K} = 0{\cdot}435$, the corresponding theoretical value of $\mathbf{X}$ being

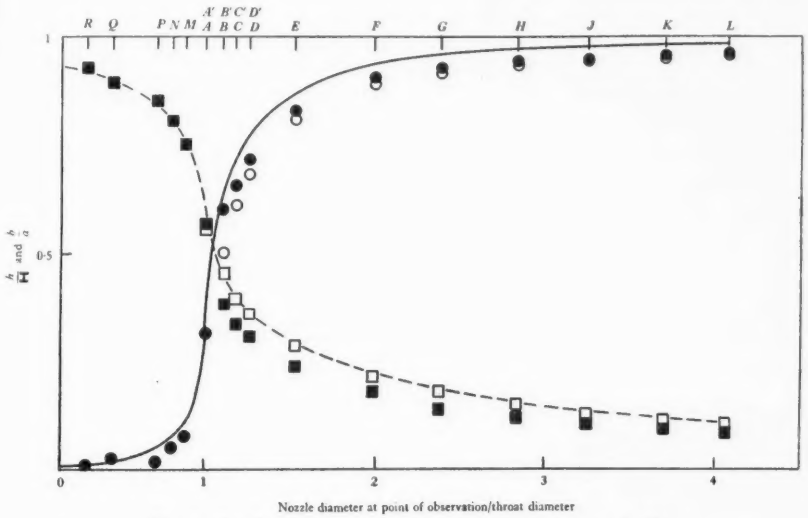

Figure 4. Core diameter and wall pressure in nozzle B.
b/a : ■ nozzle B; □ convergent nozzle; – – – theoretical relation.
$h/\mathbf{H}$: ● nozzle B; ○ convergent nozzle; ——— theoretical relation.

0·44, and the theoretical values of $h/\mathbf{H}$ and b/a are shown as curves on the diagram. As can be seen in figure 1, the throat of nozzle B was somewhat below the outlet of the convergent nozzle, which was assumed to be the effective throat. Therefore, in order that the same pair of theoretical curves might serve for both tests, the horizontal plotting in figure 4 has been done in terms of the ratio of the nozzle diameter at the point of observation to the throat diameter. Thus axial distances in the two nozzles are shown somewhat unequally in the neighbourhood of their throats. The positions of the tappings are indicated along the top of the diagram, which terminates on the left at the outlet of nozzle B.

In both tests there was fair conformity between the measured and theoretical core radii at the throat, but it must not be deduced that the flow in the nozzles closely followed the theoretical pattern. In the upper part of both, the values of h and b were less than the theoretical, and this

effect may be attributed to a reduction in swirl due to viscosity. Close to the throat, the discrepancies between the pressures continued and were more noticeable in the convergent nozzle than in nozzle B. In the former the pressure fell inevitably to atmospheric, and in the latter the pressure was bound to be diminished by the curvature of the wall. The theoretical pressure curve at the throat itself is very steep, and it is difficult to judge whether or not the observation in nozzle B is in good agreement.

Observations on reversed axial flow revealed another dissimilarity between the two tests. In the convergent nozzle reverse flow was seen only at much lower supply heads. In the test on nozzle B, however, it occurred at the level of tapping K, and colour injected at J revolved horizontally with only a slight tendency to ascend. A marked difference between the flows in the two nozzles was the adverse pressure at the throat of nozzle B, and this, it seems, promoted the formation of reverse flow. This conclusion is supported by Binnie's experiments (1957) in a cylindrical tube, which showed the importance of an obstruction downstream in causing reverse flow.

(iii) *Discharge and swirl coefficients*

The values of **K** and **X** obtained in five series of tests of nozzles A and B with full bleed are plotted in figures 5 and 6. In the former, **X** was calculated by means of (3.3) from the observed core radius b_t at the throat,

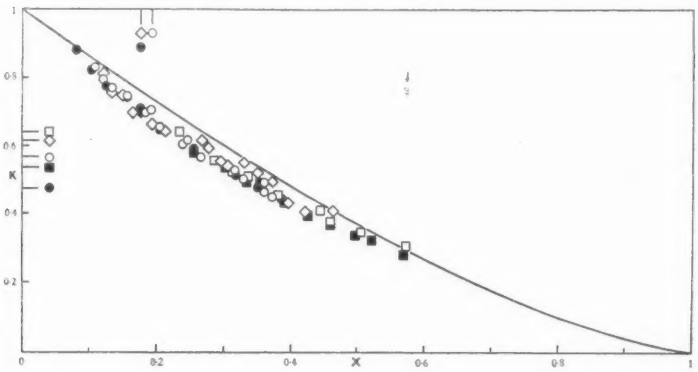

Figure 5. Observations of **K** and **X** with **X** calculated from b_t.

Head (ft.)	25·1	6·6	5·3
Nozzle A	○	◇	□
Nozzle B	●		■

——— theoretical relation.

and in the latter by means of (3.2) from the observed throat wall pressure h_t. For nozzle A, three tests were made at constant supply heads which were approximately the same as those set out in table 2, and again at the lowest

head the reservoir top was uncovered. For nozzle B, tests at the intermediate head were omitted. In three of the series, observations were made at very low swirls with the aid of the air injection method described in § 4(i), and the limits of injection are shown by the markings along the top of both figures. Reverse flow was seen in all five series, and the markings on the vertical axis of both figures indicate the limits below which reverse flow was visible. Now nozzle A had a smaller throat than B; thus reverse flow was assisted by an addition to the opposing wall pressure in the neighbourhood of the throat.

Figure 5 shows that the readings lie not far from the theoretical curve. Previous experience indicated that, in general, friction diminishes the swirl and the core radius, at the same time increasing the discharge. Thus a theoretical point is moved both to the left and upwards; and in spite of the difficulty of measuring b_t, an apparent agreement between theory and experiment was nearly obtained.

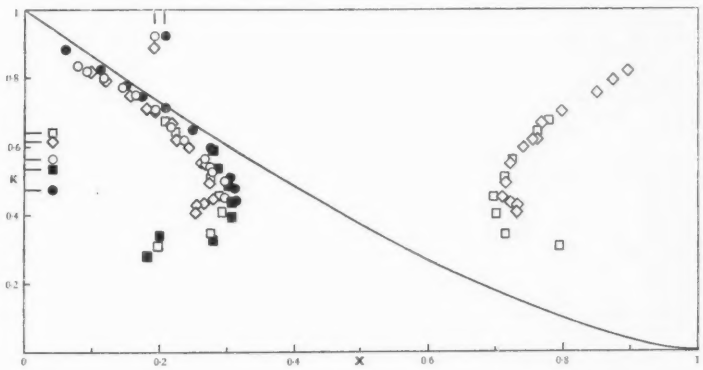

Figure 6. Observations of **K** and **X** with **X** calculated from h_t.
Plotting as in figure 5.

In contrast, figure 6 reveals serious discrepancies. As already explained, (3.2) yields two possible values of **X** for each observation of h_t. The main group of points lying to the left was derived from the smaller value of **X**; for some of the same readings the larger value was calculated, and this procedure resulted in the points on the right of the diagram. It is clear that the former supposition leads to better agreement with the theoretical curve, although at the lowest values of **K**, which were attained with the reservoir top uncovered, the higher value of **X** was less distant from the theoretical curve than the lower. It will be seen that the marked departures from the theoretical curve are associated with the formation of reverse flow, and an attempt to obtain details of these discrepancies is related in the next section.

(iv) *The velocity distribution in nozzle B*

Two tests designated (*a*) and (*b*) were made with pure tangential supply and with the bleed fully open so that the swirl was the greatest obtainable. In (*a*) at $\mathbf{H} = 6{\cdot}0$ ft., $\mathbf{K} = 0{\cdot}38$, the baffle plate at the top of the reservoir was just covered, and in (*b*) at $\mathbf{H} = 5{\cdot}3$ ft., $\mathbf{K} = 0{\cdot}28$, it was just uncovered. In the former, reverse flow extended down to *G*, and in the latter to *F*. To measure the tangential velocity v in the convergent part of the nozzle a vertical rod was supported in the air core by traversing gear, which was placed below the nozzle and which enabled the rod to be centred and moved vertically. From the top of the rod a short pin protruded, round which a nylon thread about 0·006 in. thick was looped, and a small ball was attached at the other end of the thread. Contrary to expectation the ball was found to rotate without winding the thread round the rod. Its revolutions were timed with a stroboscope; and since the inclination of the thread to the horizontal was not large, the mean radius of the path of the ball was determined from the length of the thread and from a visual measurement of the vertical distance between the top of the rod and the position of the ball as it passed in front of the rod. A trial with a lead ball of diameter about 0·1 in. proved unsatisfactory, for at small immersion the tangential velocity so determined was appreciably less than that given by the light-vaned wheel shown in Binnie & Teare's figure 2(*b*) (1956). It was eventually discovered that the rod was vibrating under the centrifugal force imposed by the ball, which should have been revolving at about 5000 rev/min, and the discrepancy was almost entirely removed when the lead ball was replaced by a lighter one of bitumastic material or by a thin disc of lead. At larger radii, where the centrifugal force was less, all three particles gave the same results.

For test (*a*) at the level of tapping *H*, figure 7 shows the values of v obtained with various lengths of thread, and two observations made with the vaned wheel are also included. Near the core, v was not proportional to the radius r as it would have been had there existed a zone of appreciable thickness moving with uniform angular velocity. Actually, the tangential velocity was almost constant for about $\frac{1}{2}$ in. and then diminished towards the wall. A check on these observations was made in the following way. The radial velocity was small; and if it is neglected, integration of the radial equation of inviscid motion (Goldstein 1938, pp. 103–4) gives an expression for the wall pressure head h in the form

$$h = \frac{1}{g}\int_b^a \frac{v^2}{r}\,dr. \tag{5.1}$$

This method was applied to the curve of v and yielded $h/\mathbf{H} = 0{\cdot}89$, which is in fair agreement with the manometer reading $h/\mathbf{H} = 0{\cdot}91$ obtained at the tapping.

An endeavour was then made to estimate the distribution of the axial velocity w by measuring on photographs the inclination of a thread of colour emitted from a hypodermic tube placed at various radii. Again with neglect of the radial velocity, w was calculated from the known value

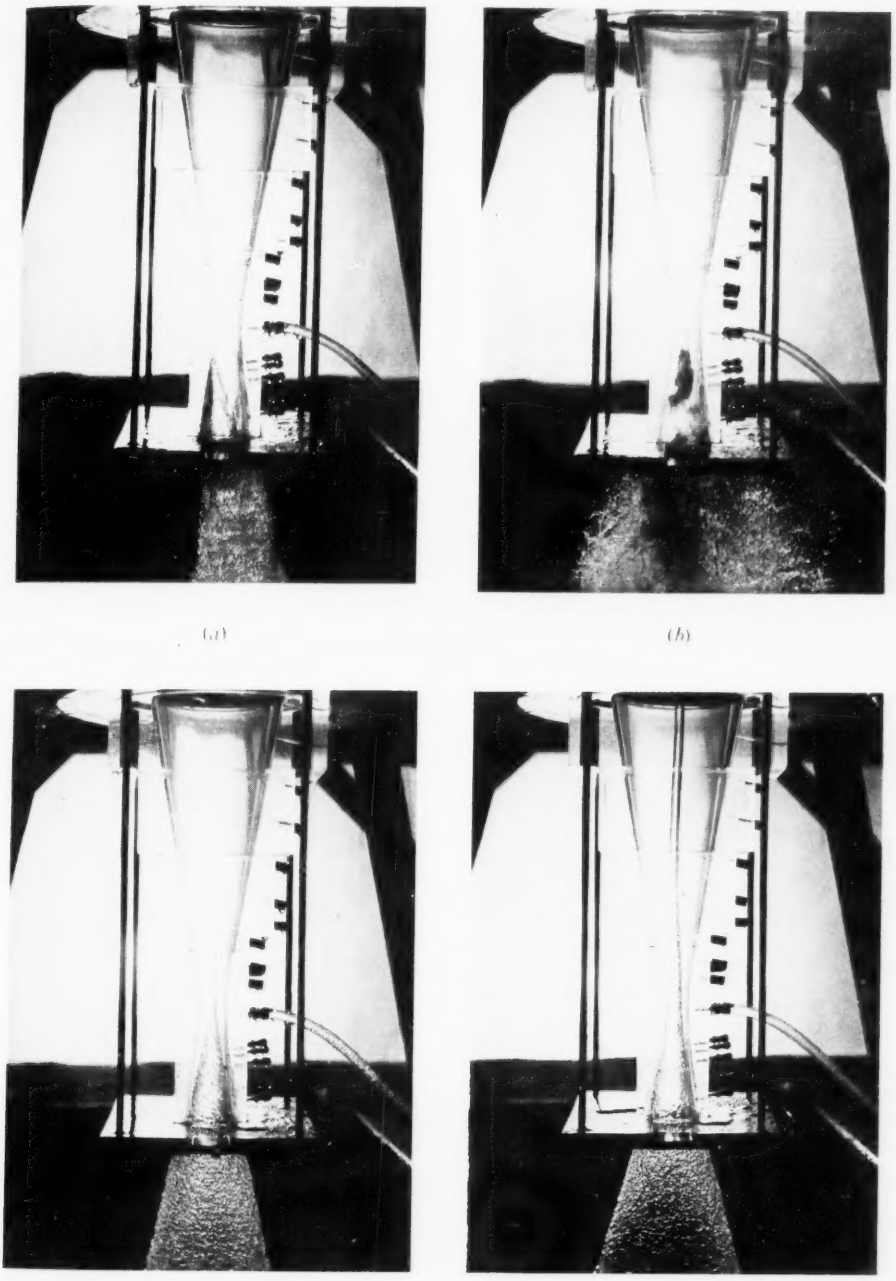

(*a*) (*b*)

(*c*) (*d*)

Figure 3. Development of air core in nozzle B as swirl was increased at constant head of 25 ft.

of v in each position. The results displayed in figure 7 confirm the qualitative observations described in §4(ii) and indicate a large axial velocity close to the core, falling away virtually to zero in the region of reverse flow where the upward velocity was slight, and at greater radii a measurable downward velocity existed. The velocity heads due to v and w were now known, and the pressure heads were calculated by applying (5.1) to intermediate radii. The variation of loss of total head was thus determined and is shown in figure 7 by solid circles. For comparison, the

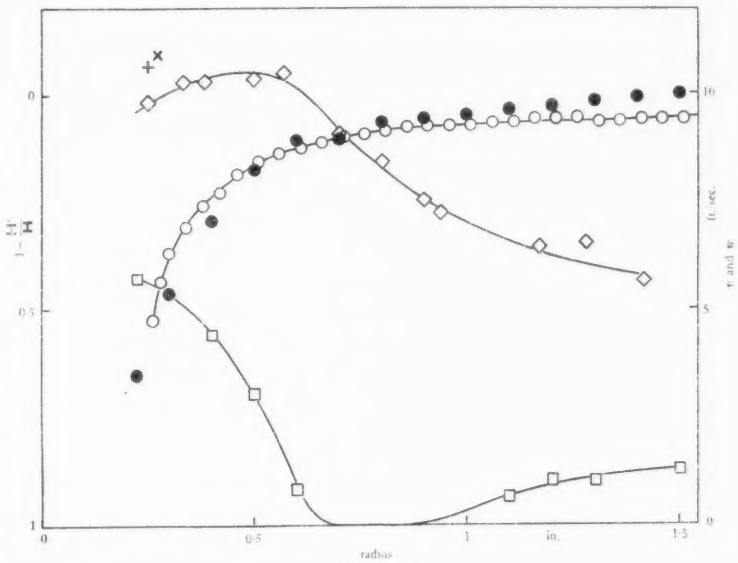

Figure 7. Velocity distribution in nozzle B with reservoir top covered. $\mathbf{H} = 6{\cdot}0$ ft.
◇ tangential velocity v measured with revolving particle.
\+ tangential velocity v measured with vaned wheel 0·55 in. O.D.
× tangential velocity v measured with vaned wheel 0·65 in. O.D.
□ axial velocity w.
● fractional loss of total head calculated from observed velocities.
○ fractional loss of total head measured with total-head tube.

measurements of total head loss made directly in the manner described in §4(i) are shown by hollow circles. The agreement is quite good, but the method did not provide a sensitive check on the observations of w because $w^2/(2g)$ was only a minor component of the total head. A more severe test was imposed by determining the discharge $\mathbf{Q}$ from the observations of w. This yielded $\mathbf{Q} = 0{\cdot}060$ cu. ft./s, which is not in accord with the measured value 0·048 cu. ft./s. Close to the core the pitch of the helix could be measured with fair precision, but at large radii, which made important contributions to the cross-section, the streak was ill-defined and

its inclination difficult to estimate; thus these latter observations were probably at fault. Nevertheless it is clear that the inviscid theory, which takes the axial velocity as uniform and the tangential velocity as varying inversely with the radius, cannot be a good approximation when the swirl is great. Similar results were found at the level of tapping F where the axial velocity was nearly but not quite reversed at a radius 0·8 in. The same checks were applied, and the agreement was somewhat better, the discharge as determined from the curve of w being 0·052 cu. ft./s. Test (*b*) failed because the core was so unstable that the $v-r$ relation could not be measured with sufficient accuracy.

It was observed that in reverse flow the injected colour moved at approximately constant radius. This is evidently due to the fact that the axial velocity w was small only in this part of the cross-section and its derivative with respect to axial distance z may be taken as zero there. A solution of the equation of continuity

$$\frac{1}{r}\frac{\partial}{\partial r}(ru) + \frac{\partial w}{\partial z} = 0 \tag{5.2}$$

is then $u = 0$.

References

Binnie, A. M. 1957 *Quart. J. Mech. Appl. Math.* **10,** 276.

Binnie, A. M. & Harris, D. P. 1950 *Quart. J. Mech. Appl. Math.* **3,** 89.

Binnie, A. M. & Hookings, G. A. 1948 *Proc. Roy. Soc.* A, **194,** 398.

Binnie, A. M. & Teare, J. D. 1956 *Proc. Roy. Soc.* A, **235,** 78.

Goldstein, S. (Ed.) 1938 *Modern Developments in Fluid Dynamics.* Oxford: Clarendon Press.

Taylor, G. I. 1948 *Proc. 7th Intern. Congr. Appl. Mech.* **2,** 280.

The structure of a shock wave in a fully ionized gas

By J. D. JUKES
Atomic Energy Research Establishment, Harwell, Berkshire

(*Received* 2 *August* 1957)

SUMMARY

The structure of a plane shock wave moving through a completely ionized plasma of protons and electrons is calculated. It is assumed that the two species of particles behave as two gases, each separately in a quasi-equilibrium state corresponding generally to two different temperatures. Navier–Stokes type equations with coefficients of viscosity and thermal conductivity appropriate to the two species are solved by numerical iteration.

For very strong shocks it is found that both the velocity of electrons and protons and the temperature of the protons change in a distance about twice the mean path for momentum transfer between protons in the hot (shocked) gas. The electron temperature changes in about eight of these mean free paths, causing a relatively wide zone of hot electrons at low density ahead of the usual velocity shock-front. The density and temperature gradients of protons and electrons create an electric field.

1. INTRODUCTION

A study of the structure of a shock wave requires consideration of the dissipative effects of viscosity and thermal conductivity. Suitable macroscopic equations can be derived from kinetic theory once the Boltzmann equation is solved for the velocity distribution function. Generally this function can only be found by a method of successive approximation with the Maxwell (equilibrium) distribution as the zero order term (see Chapman & Cowling 1939). To ensure convergence of this solution it is necessary for the ratio of the mean free path for momentum transfer in the fluid to be small compared with some characteristic length in which the distribution function changes appreciably. This is equivalent to an assumption of quasi-equilibrium conditions. Zero order terms give equations for a frictionless fluid and the result of a vanishingly thin shock front. First-order terms yield the familiar Navier–Stokes [N–S] equations, containing the effects of viscosity and thermal conductivity in two coefficients, μ and λ.

Becker (1923) solved the N–S equations assuming μ and λ to be constant. Later, Thomas (1944) included a temperature variation in μ and λ appropriate to a model gas of hard-sphere elastic molecules. This inclusion is important for strong shocks where there are large temperature and density changes because these variations lead to large changes in μ and λ. With this

inclusion, it is found that the shock front thickness tends to a finite limit as the Mach number M tends to infinity; a result not obtained with the simple Becker solution.

Mott-Smith (1951) has criticized the application of the N–S equations to strong shock waves ($M > 2$), where both experiments and more refined theory suggest that physical quantities and the distribution function change appreciably in distances only once or twice the mean free path for momentum transfer between molecules. It is unlikely that the expansion solution of Chapman & Cowling can be valid in these circumstances. Mott-Smith, although still only dealing with a gas of molecules of one type, assumes a distribution function composed of two Maxwellian distributions corresponding to upstream and downstream temperatures. Using these, he solves a transport equation. His theory predicts shocks whose limiting thickness as $M \to \infty$ is rather more than that of Thomas's theory.

The present paper develops the N–S equations for a fully ionized gas, such as may be encountered in some electrical gas-discharge. The treatment is similar to that of Thomas with the important difference that such a plasma is a mixture of two species of charged particles. Each species is assumed to behave as a gas in a quasi-equilibrium state. There is a separate, approximately Maxwellian, distribution for each gas, corresponding in general with two different temperatures for the proton and electron gases.

In the light of Mott-Smith's results this treatment should follow Thomas in arriving at a lower limit for the shock thickness, at the same time yielding the essential qualitative features of the shock front structure.

2. Plasma properties

The calculations are restricted to a plasma of protons and electrons in which simple equations of state are valid (Spitzer 1956). Any externally applied electric or magnetic fields are neglected. The equations of state are then,

$$p_e = n_e k T_e, \qquad p_i = n_i k T_i, \tag{2.1 a}$$

where k is Boltzmann's constant, p, n and T are the partial pressures, the number densities and the temperatures of electrons and protons as indicated by the suffices (i is for the heavy ion, a proton in this case). For a gas of single particles with no internal degrees of freedom the specific heat ratio, $c_p/c_v = \gamma$, is 5/3. In the hydrodynamic equations it will be supposed that the electrostatic force acting on the plasma is small compared to the fluid forces arising from the pressure and momentum. This assumption will be justified later when the electric field has been estimated. The assumption implies that the charge separation is negligible, so that to good approximation,

$$n_i \doteq n_e = n. \tag{2.1 b}$$

Because protons are nearly two thousand times heavier than electrons, the protons are chiefly responsible for the transport of momentum (viscosity) while the electrons are chiefly responsible for the transport of random, or

thermal, energy. It is therefore reasonable to take the viscosity to be a function of proton temperature alone and the thermal conductivity a function of electron temperature alone, provided

$$\lambda_e \frac{dT_e}{dx} \gg \lambda_i \frac{dT_i}{dx}$$

and

$$\mu_i \frac{du_i}{dx} \gg \mu_e \frac{du_e}{dx},$$

where λ_e denotes the thermal conductivity due to electrons alone, and so forth, and u_j is the streaming velocity of each species. The results are found to satisfy these conditions except possibly for very strong shocks ($M > 10$) where the second condition may not hold at the beginning of the shock. But the electron viscosity is there much smaller than the average viscosity throughout the shock so the qualitative results should not be invalid. The dependence of the coefficients μ and λ on the temperatures under the above conditions has been found by Chapman & Cowling and others.

As in other problems of dissipation in gases it is convenient to compute the Prandtl number $P = \mu C_p/\lambda$ of a plasma under equilibrium conditions. An exact treatment by Chapman & Cowling for a proton–electron plasma yields $P = 0{\cdot}065$. This is much less than is found for a one-particle gas ($\sim 0{\cdot}6$) because the mobility of electrons far exceeds that of protons by a factor of order $(m_i/m_e)^{1/2} \doteq 43$ when electron and proton temperatures are equal.

There is a slow interchange of energy between protons and electrons at different temperatures. Post (1956) gives the rate of energy transfer in collisions from a single proton to an electron gas at temperature T_e. By integrating over a Maxwell distribution of protons of temperature T_i, the rate of heat transfer per unit volume between the two gases is found to be

$$\left(\frac{32\pi}{m_e k}\right)^{1/2} e^4 \log_e \Lambda \frac{m_e n^2}{m_i T_e^{3/2}} (T_e - T_i), \tag{2.2}$$

where $\log_e \Lambda$ is the Coulomb logarithm of Spitzer's plasma theory (1956).

3. Equations

Suppose the plasma flows in planes parallel to the x-axis from $-\infty$ to $+\infty$ and that conditions of thermal equilibrium exist at upstream and downstream infinity, denoted by the points (1) and (2), with the usual Rankine–Hugoniot relations between them. Assume a steady state shock wave exists somewhere in the flow and consider each species of particle separately. For the jth species, the rate at which heat is supplied to an elemental unit volume moving with the flow is given by the mobile derivative,

$$\frac{DQ_j}{Dt} = ku_j\left(\frac{3}{2} n_j \frac{dT_j}{dx} - T_j \frac{dn_j}{dx}\right), \tag{3.1}$$

where $u_j = u$ = fluid velocity, and $n_j = n$ = number density. Carrying out the transformation from the moving axes to a system of axes fixed relative to the shock wave, the equations of energy transfer become:

$$ku\left(\frac{3}{2}n\frac{dT_i}{dx} - T_i\frac{dn}{dx}\right) = \frac{4}{3}\mu\left(\frac{du}{dx}\right)^2 + \frac{Kn^2}{T_e^{3/2}}(T_e - T_i), \tag{3.2}$$

$$ku\left(\frac{3}{2}n\frac{dT_e}{dx} - T_e\frac{dn}{dx}\right) = \frac{d}{dx}\left(\lambda\frac{dT_e}{dx}\right) - \frac{Kn^2}{T_e^{3/2}}(T_e - T_i). \tag{3.3}$$

K is a function of the atomic constants, and is found from the heat transfer term (2.2) to be $(32\pi/m_e k)^{1/2}e^4(m_e/m_i)\log\Lambda$.

The momentum equation, neglecting electrostatic forces, is

$$m\frac{du}{dx} = -\frac{dp_t}{dx} + \frac{d}{dx}\left(\frac{4}{3}\mu\frac{du}{dx}\right), \tag{3.4}$$

where $p_t \equiv p_e + p_i$ is the total pressure and

$$m = p_t u \tag{3.5}$$

is the mass flow per unit area. The continuity relation is

$$dm/dx = 0. \tag{3.6}$$

The integration of (3.4) and elimination of the constant of integration by means of the conditions at $x = \pm\infty$ gives

$$p_t + \rho_t u^2 - \frac{4}{3}\mu\frac{du}{dx} = (p_t + \rho_t u^2)_1 = (p_t + \rho_t u^2)_2. \tag{3.7}$$

(3.2), (3.3), (3.6) and (3.7) are the fundamental equations. We have, also,

$$\rho_t = n(m_i + m_e), \qquad p_t = nk(T_i + T_e),$$

and from (3.5) and (3.6)

$$p_t u = \text{constant} \doteqdot num_i = n_1 u_1 m_i, \tag{3.8}$$

and therefore

$$\frac{du}{dx} = -\frac{n_1 u_1}{n^2}\frac{dn}{dx}. \tag{3.9}$$

Add (3.2) and (3.3) and substitute $\mu(du/dx)$ from (3.7) to get the total energy equation

$$ku\left[\frac{3}{2}n\frac{d}{dx}(T_e + T_i) - (T_e + T_i)\frac{dn}{dx}\right] = [p_t + \rho_t u^2 - (p_t + \rho_t u^2)_1]\frac{du}{dx} + \frac{d}{dx}\left(\lambda\frac{dT_e}{dx}\right). \tag{3.10}$$

Substitute from (3.8) and (3.9) and then integrate (3.10) with respect to x to give

$$\frac{3}{2}u_1 n_1 k(T_e + T_i) = -\frac{2n_1^2 kT_1 u_1}{n} - \frac{n_1^2 m_i u_1^2}{n} + \frac{m_i u_1^2 n_1^2}{2n^2} + \lambda\frac{dT_e}{dx} + \text{const.} \tag{3.11}$$

At $x = -\infty$, $T_i = T_e = T_1$, and the elimination of the constant gives

$$\frac{3}{2}u_1 n_1 k(T_e + T_i) + \frac{2n_1^2 kT_1 u_1}{n} + \frac{n_1^2 m_i u_1^2}{n} - \frac{m_i u_1^2 n_1^2}{2n^2} - \lambda\frac{dT_e}{dx} = 5u_1 n_1 kT_1 + \frac{n_1 m_i u_1^2}{2}. \tag{3.12}$$

On substituting from (3.7) to (3.9), equations (3.3) and (3.7) become

$$n_1 u_1 k\left(\frac{3}{2}\frac{dT_i}{dx} - \frac{T_e}{n}\frac{dn}{dx}\right) = \frac{d}{dx}\left(\lambda\frac{dT_e}{dx}\right) - \frac{Kn^2}{T_e^{3/2}}(T_e - T_i), \tag{3.13}$$

and

$$\frac{4}{3}\mu\frac{n_1 u_1}{n^2}\left(\frac{dn}{dx}\right) = 2n_1 kT_1 + n_1 m_i u_1^2 - nk(T_e + T_i) - \frac{n_1^2 m_i u_1^2}{n}. \tag{3.14}$$

From now on we work with (3.12), (3.13) and (3.14), making them dimensionless by the substitutions

$$\nu \equiv n/n_1, \quad \tau \equiv T_e/T_1, \quad \theta \equiv T_i/T_1, \quad P \equiv \mu_1 c_p/\lambda_1, \quad \pi \equiv p_i/p_{i1}, \quad \xi \equiv x/l,$$

where l = mean free path of simple kinetic theory for ions ahead of the shock so that $l \equiv 4\mu_1/(3n_1 m_i c_1)$, c_1 being the velocity of sound ahead of the shock.

The Mach number of the shock front is

$$M^2 = \left(\frac{u_1}{c_1}\right)^2 = \frac{m_i u_1^2}{2\gamma kT_1}.$$

From (3.12), (3.13) and (3.14)

$$\frac{3}{2}(\theta+\tau) + \frac{2}{\nu} + \frac{2\gamma}{\nu}M^2 - \frac{\gamma M^2}{\nu^2} - \frac{\lambda}{\lambda_1}\left(\frac{3}{2}\frac{\gamma}{\gamma-1}\frac{1}{PM}\right)\frac{d\tau}{d\xi} = 5 + \gamma M^2, \tag{3.15}$$

$$\frac{\theta^{5/2}}{\nu^2}\frac{d\nu}{d\xi} = \frac{1}{\gamma M} - \frac{\nu}{2\gamma}\left(\frac{\tau+\theta}{M}\right) + M\left(1 - \frac{1}{\nu}\right), \tag{3.16}$$

$$\frac{3}{2}\frac{d\tau}{d\xi} - \frac{\tau}{\nu}\frac{d\nu}{d\xi} = \frac{3}{2}\frac{\gamma/(\gamma-1)}{PM}\frac{d}{d\xi}\left(\frac{\lambda}{\lambda_1}\frac{d\tau}{d\xi}\right) - \frac{EP}{M}\frac{\nu^2(\tau-\theta)}{\tau^{3/2}}. \tag{3.17}$$

E is a pure number, which, in terms of K, is

$$\frac{(\gamma-1)m_i\lambda_1 K}{3\gamma^2 k^{1/2}(kT_1)^{5/2}}.$$

Taking γ as 5/3, and using the value of λ_1 for zero current given by Spitzer, E is found to be 0·77.

Chapman & Cowling give

$$\mu/\mu_1 = \theta^{5/2} \quad \text{and} \quad \lambda/\lambda_1 = \tau^{5/2},$$

so that (3.15), (3.16) and (3.17) become

$$\frac{3}{2}(\theta+\tau) + \frac{2}{\nu} - \frac{10}{3}\frac{M^2}{\nu} - \frac{5}{3}\frac{M^2}{\nu^2} - \frac{15}{4}\frac{\tau^{5/2}}{PM}\frac{d\tau}{d\xi} = 5 + \frac{5}{3}M^2, \tag{3.18}$$

$$\frac{\theta^{5/2}}{\nu^2}\frac{d\nu}{d\xi} = \frac{3}{5M} - \frac{3\nu(\tau+\theta)}{10M} + M\left(1 - \frac{1}{\nu}\right), \tag{3.19}$$

$$\frac{3}{2}\frac{d\tau}{d\xi} - \frac{\tau}{\nu}\frac{d\nu}{d\xi} = \frac{15}{4PM}\frac{d}{d\xi}\left(\tau^{5/2}\frac{d\tau}{d\xi}\right) - \frac{EP}{M}\frac{\nu^2}{\tau^{3/2}}(\tau-\theta). \tag{3.20}$$

These equations reduce to,

$$N \equiv M\frac{d\nu}{d\xi} = \frac{\nu^2}{\theta^{5/2}}\left[M^2\left(\frac{\nu-1}{\nu}\right) + \frac{3}{5}\left\{1 - \frac{\nu(\tau+\theta)}{2}\right\}\right], \tag{3.21}$$

$$T \equiv M\frac{d\tau}{d\xi} = \frac{2PM^2}{5\tau^{5/2}}\left[\tau + \theta + \frac{4}{3\nu} - \frac{10}{3} - \frac{10}{9}M^2\left(\frac{\nu-1}{\nu}\right)^2\right], \tag{3.22}$$

$$H \equiv M\frac{d\theta}{d\xi} = \frac{2}{3}EP\frac{\nu^2}{\tau^{3/2}}(\tau-\theta)+$$
$$+\frac{1}{\theta^{5/2}}\left[\frac{20}{9}M^2\left(\frac{\nu-1}{\nu}\right)+\frac{4}{3}-\frac{2}{3}\tau\nu\right]\left[M^2\left(\frac{\nu-1}{\nu}\right)+\frac{3}{5}\left\{1-\frac{\nu(\tau+\theta)}{2}\right\}\right]$$
$$=\frac{2}{3}EP\frac{\nu^2}{\tau^{3/2}}(\tau-\theta)+\frac{N}{\nu^2}\left[\frac{20}{9}M^2\left(\frac{\nu-1}{\nu}\right)+\frac{4}{3}-\frac{2}{3}\tau\nu\right]. \tag{3.23}$$

4. Solutions

The integral curves of equations (3.21)–(3.23) lie in a τ, ν, θ-space as ξ goes from $-\infty$ to $+\infty$. We draw the surfaces N, H and $T = 0$ and examine the solutions in planes corresponding to fixed values of one of the variables (e.g. figure 1 shows the $\nu-\theta$ plane with $\tau = 1$). In the 3-space

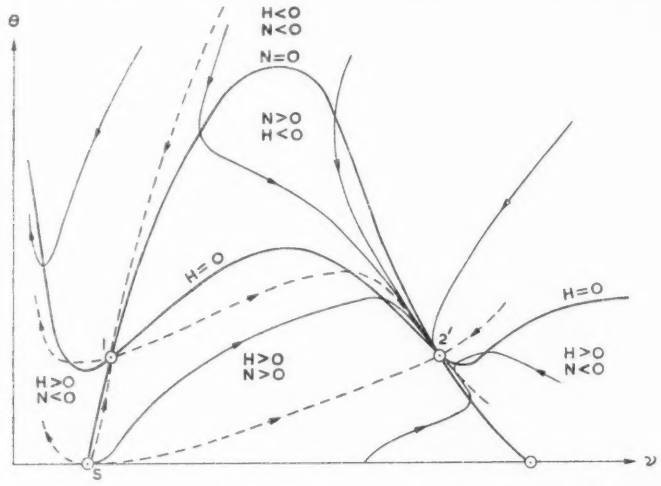

Figure 1. $\theta-\nu$ curves in $\tau = 1$ plane (not to scale). Arrows indicate ξ increasing. Strong shock, $M = 10$.

the curves pass through two saddle points (1) and (2) where $\xi = \mp\infty$, these being the intersections of the surfaces N, H, $T = 0$ by virtue of the boundary conditions. Singular points exist at $\tau = 0 = \theta$. Saddle point (1) contains the intersection of the planes ν, τ, $\theta = 1$ and saddle point (2) the planes ν, τ, $\theta = \nu_2$, τ_2, θ_2 respectively. In a 2-space, such as the plane shown in figure 1, the point of intersection of the plane $\tau = 1$ with the surfaces $N = 0 = H$ has been denoted by (2′) to distinguish it from the corresponding 3-space point (2). Similarly (2″) corresponds to (2) in figure 2.

It is necessary to investigate the behaviour of the solutions close to the saddle points and we do this by a linearization. There are two distinct sets of solutions for the extreme physical cases, (*a*) $M \gg 1$—a very strong shock, and (*b*) $M \gtrsim 1$—a weak shock, approximating to an acoustic wave.

Equations (3.15)–(3.17) may be written

$$a\frac{d^2\tau}{d\xi^2}+b\frac{d\tau}{d\xi}+c\frac{d\nu}{d\xi}=F(\tau,\nu),\qquad d\frac{d\tau}{d\xi}+f\frac{d\nu}{d\xi}=G(\nu), \tag{4.1}$$

where

$$\left.\begin{aligned} a&\equiv\frac{15\tau^{3/2}}{4P^2E\nu^2}, & b&\equiv\frac{5}{2}\frac{\tau^{5/2}}{PM}-\frac{3M}{2EP}\frac{\tau^{3/2}}{\nu^2}\\ c&\equiv\frac{M\tau^{5/2}}{EP\nu^3}, & d&\equiv\frac{3\tau^{5/2}\nu}{4PM^2}, \qquad f\equiv\frac{\theta^{5/2}}{\nu^2},\\ F(\tau,\nu)&\equiv 2\tau-\frac{10}{3}+\frac{4}{3\nu}-\frac{10M^2}{9}\left[1-\frac{2}{\nu}+\frac{1}{2\nu^2}\right],\\ G(\nu)&\equiv\frac{M}{3}\left(5-\nu-\frac{4}{\nu}\right)+\frac{(1-\nu)}{M}. \end{aligned}\right\} \tag{4.2}$$

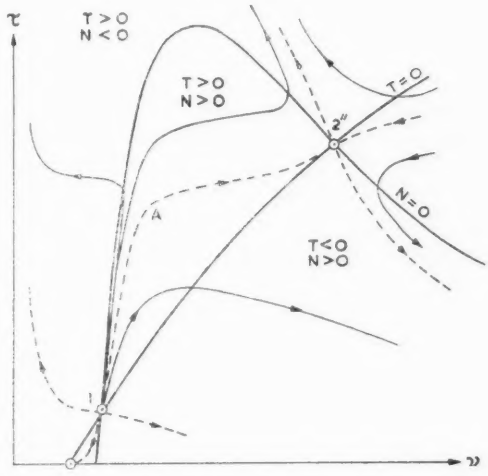

Figure 2. $\tau-\nu$ curves in $\theta=1$ plane (not to scale). Arrows indicate ξ increasing. Strong shock, $M=10$.

We linearize at points $i(=1, 2)$ by substituting

$$\left.\begin{aligned}\tau&=\tau_i+\Delta\tau\\ \nu&=\nu_i+\Delta\nu\\ \theta&=\theta_i+\Delta\theta\end{aligned}\right\},\qquad \left.\begin{aligned}\text{where }\Delta\tau&=H\exp\alpha\xi\\ \Delta\nu&=K\exp\alpha\xi\\ \Delta\theta&=L\exp\alpha\xi\end{aligned}\right\}, \tag{4.3}$$

in (4.1), obtaining a cubic equation in α

$$(af)\alpha^3+(bf-aG_\nu-cd)\alpha^2+(F_\nu d-fF_\tau-bG_\nu)\alpha+F_\tau G_\nu=0, \tag{4.4}$$

where $G_\nu\equiv\partial G/\partial\nu$, etc. Also, from (4.1), $\Delta\tau/\Delta\nu=(G_\nu-\alpha f)/(\alpha d)$ and

$$\frac{\Delta\theta}{\Delta\nu}=\left(\frac{5\alpha\tau^{5/2}}{2PM}-1\right)\frac{\Delta\tau}{\Delta\nu}+\frac{4}{3\nu^2}+\frac{20M^2}{9}\frac{(\nu-1)}{\nu^3}. \tag{4.5}$$

Strong shocks $M\gg 1$

We make use of the approximations $M^2\gg 1$, $\tau_2\doteq(5/16)M^2$, $\nu_2\doteq 4$, to find three (real) roots of α at points (1) and (2).

At (1),

$$\left.\begin{aligned}\alpha_{11} &= \frac{2}{5}PM + \frac{2}{3}\frac{EP}{M} + \text{... higher powers of } M^{-1}\\ \alpha_{12} &= M - \frac{4}{5M} + \ldots\end{aligned}\right\}, \quad \text{as } \xi = -\infty,$$

$$\alpha_{13} = -\frac{4EP}{3M} + \ldots, \qquad \text{as } \xi = +\infty. \quad (4.6)$$

At (2),

$$\left.\begin{aligned}\alpha_{21} &= -\frac{3{\cdot}1}{M^4} + \ldots\\ \alpha_{22} &= -\frac{47}{M^4} + \ldots\end{aligned}\right\}, \quad \text{as } \xi = +\infty,$$

$$\alpha_{23} = \frac{1{\cdot}5}{M^4} + \ldots, \qquad \text{as } \xi = -\infty.$$

A few typical integral curves are drawn on figures 1 and 2. The limiting integral curves which pass through both saddle points are shown by broken lines. To represent a physical solution satisfying the boundary conditions an integral curve must pass through both points (1) and (2). Also, ν, τ and θ must remain real, positive, non-zero and finite all along the curve $-\infty < \xi < +\infty$.

Reference to figures 1 and 2 shows that only one curve can be a physical solution. Also it must leave (1) with $\Delta\tau/\Delta\nu$ positive and arrive at (2) with $\Delta\theta/\Delta\nu$ negative, the sense of direction deriving from the increase of ξ. The values of $\Delta\tau/\Delta\nu$ and $\Delta\theta/\Delta\nu$ are given in (4.5) in terms of α. On substituting the values of α from (4.6) it is found that the physical solution leaves (1) with a slope corresponding to α_{11} and arrives at (2) with a slope corresponding to α_{21}.

We may note that even in the acceptable solution entropy does not increase monotonically between states (1) and (2). Of course the *net charge* of entropy is always positive between (1) and (2).

Weak shocks $M \gtrsim 1$

The analysis is similar to that for strong shocks, however, in this case we put $M = 1 + m$ and expand in power series in m, assuming m to be small.

We find two roots of (4.4) at (1) and (2)

$$\alpha_{11} \doteq \frac{4mP}{2P+1}, \qquad \text{as } \xi = -\infty,$$

$$\alpha_{21} \doteq -\frac{4mP}{2P+1}, \quad \text{as } \xi = +\infty.$$

In each case $\Delta\nu/\Delta\tau \doteq \frac{3}{2}$, $\Delta\theta/\Delta\tau \doteq 1$.

An analysis, as for strong shocks, shows that other roots of α give physically impossible solutions. An analytic solution, obtainable to this first order of approximation, shows that $\tau \doteq \theta$ throughout the wave.

Numerical integration for strong shocks

A qualitative appraisal of the physical solution for a strong shock is of great help in the numerical integration between points (1) and (2). We notice from (3.21) and (3.22) that $d\tau/dv = T/N \sim P \ll 1$, unless N is small too, and we trace the required integral curve in figure 2. Leaving (1) the integral curve runs very close to $H = 0 = N$ in the positive domain until it almost reaches the plane $\tau = \tau_2$. From some point A (say) the curve bends sharply away to approach (2). That the integral curve must proceed from A to (2) in a $\theta - v$ plane is clear from figure 1, for A lies in a domain where $N > 0$ and $v > 1$ close to the point (1).

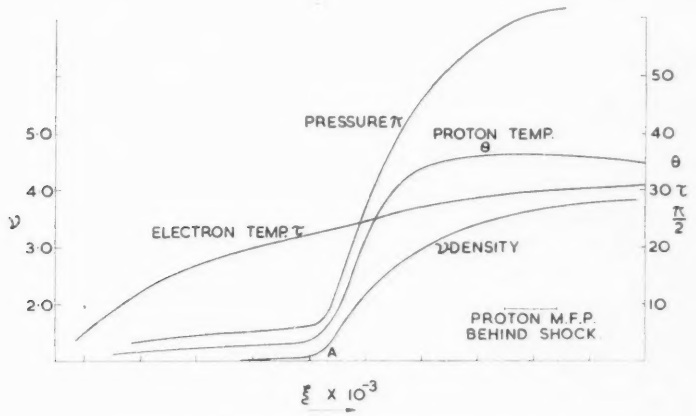

Figure 3. Shock profile. Strong shock, $M = 10$.

It is most important to note that the integral curves converge on point (2) in the $\theta - v$ plane, but on point (1) in the $\tau - v$ plane. To obtain a convergent solution by iteration one must take the following steps:

(i) Assume $\tau \doteq \tau_2$ with θ and $v \doteq 1$ between points (1) and A. Find v and θ at A.

(ii) Proceed from A to (2) solving for v and θ numerically.

(iii) Recalculate τ moving back from (2) to (1) using the first approximation to v and θ. Calculate a second approximation to τ.

(iv) Recalculate v and θ starting at (1), through A to (2). The iteration converges rapidly for $\tau_2 \gg 1$ (or $M \gg 1$).

(v) Integrate to obtain v, θ, τ as function of ξ.

A solution has been obtained for a typical, very strong shock of Mach number 10. The results are shown in figure 3.

5. Strong shocks

Certain features of the structure of strong shocks may easily be deduced.

The hot electron zone

In a zone between points (1) and A the electron temperature is much higher than the proton temperature. To estimate the profile of T_e we assume $\theta \doteqdot \nu \doteqdot 1$ and substitute in (3.23), which gives

$$\frac{d\tau}{d\xi} = \frac{2}{5} PM\left(\frac{\tau - 1}{\tau^{5/2}}\right). \tag{5.1}$$

This can be integrated directly and the solution made continuous at A. (5.1) has the correct asymptotic behaviour as $\xi \to -\infty$. The zone has a characteristic thickness L, given by

$$L \sim l_2/2P,$$

where l_2 is a mean free path for momentum transfer between protons *behind* the shock. Note that $l_2/l \sim \tau_2^2 \sim M^4$, so that L may be very large for strong shocks.

Peak proton temperature

A crude estimate of the peak proton temperature, $\theta_{\max}$, before protons and electrons attain equilibrium at T_2 can be made by neglecting all heat interchange between protons and electrons, i.e. putting $\tau = \tau_2$ and supposing too that θ reaches $\theta_{\max}$ as ν reaches $\nu_{\max} \doteqdot 4$. The computed solutions show that these assumptions are reasonable for the estimation of $\theta_{\max}$. From (3.21) and (3.23), it is found that

$$\theta_{\max} \doteqdot 1{\cdot}28\tau_2.$$

This is an overestimate as the heat interchange from protons to electrons is neglected and θ reaches $\theta_{\max}$ before ν reaches $\nu_{\max}$.

The electric field

An electric field is caused by polarization imposed by the boundary conditions. In a plasma an electric field, together with a density and thermal gradient of electrons, gives rise to a net electron drift or current relative to the ions. Spitzer (1956) has given the relation between them in terms of a coefficient of electrical conductivity σ and other coefficients which he has calculated. Evaluating these coefficients the expression for the electron current relative to the ions at rest is

$$j = \sigma\left[E + \frac{kT_e}{en_e}\frac{dn_e}{dx} + 1{\cdot}70\frac{k}{e}\frac{dT_e}{dx}\right]. \tag{5.2}$$

In a steady state the boundary conditions prohibit any total current and, therefore, $j = 0$ (neglecting any convected charge). From (5.2)

$$E = -\frac{dV}{dx} = -\frac{kT_e}{e}\frac{1}{l}\frac{d}{d\xi}[\log\nu + 1{\cdot}70\log\tau]. \tag{5.3}$$

Let $Q = eV/kT_1$, V being the potential, so that

$$\frac{dQ}{d\xi} = \tau\frac{d}{d\xi}[\log\nu + 1{\cdot}70\log\tau]. \tag{5.4}$$

If $\tau \doteqdot \tau_2$, equation (5.4) may be integrated by parts to give

$$Q - Q_1 = \tau_2 \log \nu + 1{\cdot}70(\tau - 1). \tag{5.5}$$

In particular,

$$Q_2 - Q_1 = \tau_2(\log 4 + 1{\cdot}70) = 3{\cdot}1\tau_2.$$

Equation (5.3) gives an estimate for E, so we are in a position to justify the neglect of the electrostatic force in (3.4) and the assumption that $n_i \doteqdot n_e$. Since $E \sim (kT)/(el)$, the ratio of the electrostatic 'pressure' $E^2/(8\pi)$ to the gas pressure p can be written

$$\frac{E^2}{8\pi p} \sim \left(\frac{d}{l}\right)^2,$$

where d is the Debye length defined as $d \equiv (kT/4\pi e^2 n)^{1/2}$.

Also, using $\operatorname{div} E = 4\pi e(n_i - n_e)$,

$$\frac{n_i - n_e}{n} \sim \left(\frac{d}{l}\right)^2.$$

Over an enormous range of conditions $l \gg d$, thus justifying the assumptions.

6. Conclusions

For a strong shock wave ($M > 2$), a quasi-equilibrium theory which assumes the protons and electrons to have separate equilibrium temperatures leads to the following results.

(*a*) Density and velocity and the proton temperature all change in one or two mean free paths (l_2) for momentum transfer in the hot (shocked) gas.

(*b*) The electron temperature changes more gradually over a larger distance ($\sim l_2/2P \doteqdot 8l_2$). This is equivalent to the mean free path for energy transfer between electrons and protons.

(*c*) The proton temperature rises to a maximum, which is only slightly higher than the final equilibrium temperature T_2.

(*d*) Density and total pressure increase monotonically through the shock.

(*e*) An electric field is set up across the shock caused by the density and temperature gradients of the electrons.

A weak shock ($M \doteqdot 1$) is broad ($L \sim l_2/\{4P(M-1)\}$) and in it electrons and protons are always in thermal equilibrium.

The author wishes to thank Mr R. Pease and Dr W. Marshall for their helpful reading of this paper.

References

Becker, R. 1923 *Z. Phys.* **8,** 321.

Chapman, S. & Cowling, T. G. 1939 *Mathematical Theory of Non-Uniform Gases.* Cambridge University Press.

Mott-Smith, H. M. 1951 *Phys. Rev.* **82,** 885.

Post, R. 1956 *Rev. Mod. Phys.* **28,** 338.

Spitzer, L. 1956 *Physics of Fully Ionized Gases.* New York : Interscience

Thomas, L. 1944 *J. Chem. Phys.* **12,** 449.

On fully-dispersed shock waves in carbon dioxide

By WAYLAND C. GRIFFITH and ANNE KENNY
Palmer Physical Laboratory, Princeton, New Jersey

(*Received* 26 *June* 1957)

A dispersed shock wave may be defined as one in which finite changes occur over distances large compared to the mean free path in the gas. In contrast a shock wave in air extends over only a few mean free paths. When internal motions in a molecule are excited rather slowly by collisions, as is the case for molecular vibration, the shock wave may be partly dispersed; then, the sharp shock front is followed by a diffuse tail leading to complete thermal equilibrium. Alternatively, it may be fully dispersed, so that adjustments in the energy in all the degrees of freedom proceed slowly and in parallel. The purpose of this note is to point out that within a narrow speed range, from a shock Mach number of 1 to 1·042, shocks in carbon dioxide are fully-dispersed in the above sense. Such waves have been observed experimentally using a shock tube and interferometer. The possible existence of such waves was first pointed out by Bethe & Teller (1941) purely as a matter of academic interest. This note treats the problem in the same spirit.

Lighthill (1956) views the problem of shock structure as one of finding a balance between convection of wave energy forward through the gas passed over by the shock and diffusion of energy by conduction, viscous friction, and vibrational relaxation. The latter process, described by the relaxation equation

$$\frac{dE_{\mathrm{vib}}}{dt} = \frac{E'_{\mathrm{vib}} - E_{\mathrm{vib}}}{\tau}, \tag{1}$$

dominates the other two in the phenomenon considered here. E_{vib} is the energy actually in the vibrational modes, the primed quantity is the energy appropriate to equilibrium, and τ is the vibrational relaxation time.

The speed of sound in an ideal gas is given by

$$a = (\gamma RT)^{1/2}. \tag{2}$$

Because the vibrational heat capacity cannot respond to sudden changes in the state of the gas, however, we see that a sharp shock front, suitable as the head of a partly-dispersed shock, can form only when the wave speed is greater than the speed of sound computed by not counting in the vibrational contribution to heat capacity. For any linear molecule this is

$$a' = (1{\cdot}4RT)^{1/2}. \tag{3}$$

In the speed range from $M = 1$ to $M = (1{\cdot}4/\gamma)^{1/2}$ a fully-dispersed wave must form. Its shape will be governed by equation (1).

Lighthill (1956) gives an approximate solution for the velocity profile of such a fully-dispersed shock wave, which is valid for very weak waves. More exact analysis gives

$$\frac{X}{v_1\tau} = \frac{(\gamma-1)}{(\gamma'-1)(M_1^2-1)}\left[\left(\frac{a_1'^2}{a_1^2}-M_1^2\right)\log\left(1-\frac{v}{v_1}\right)-\right.$$
$$\left.-\frac{a_2'^2}{a_1^2}\left(1-\frac{v_2^2}{a_2'^2}\right)\log\left(\frac{v-v_2}{v_1}\right)\right]. \quad (4)$$

Here, subscripts 1 and 2 refer to equilibrium conditions ahead of and behind the shock, respectively, and the primed quantities are to be computed without the inclusion of E_{vib}. For pure carbon dioxide at 300° K and 1 atmosphere, $\tau = 10\,\mu$sec, $\gamma = 1{\cdot}290$, and $a = 880$ ft./sec. A shock front would therefore be expected for $M \geqslant 1{\cdot}042$. Profiles for $M = 1{\cdot}01$, $1{\cdot}02$, $1{\cdot}03$ and $1{\cdot}04$ are shown in figure 1. Below $M = 1{\cdot}01$ the wave is symmetrical and of the same spatial extent as that shown for this Mach number.

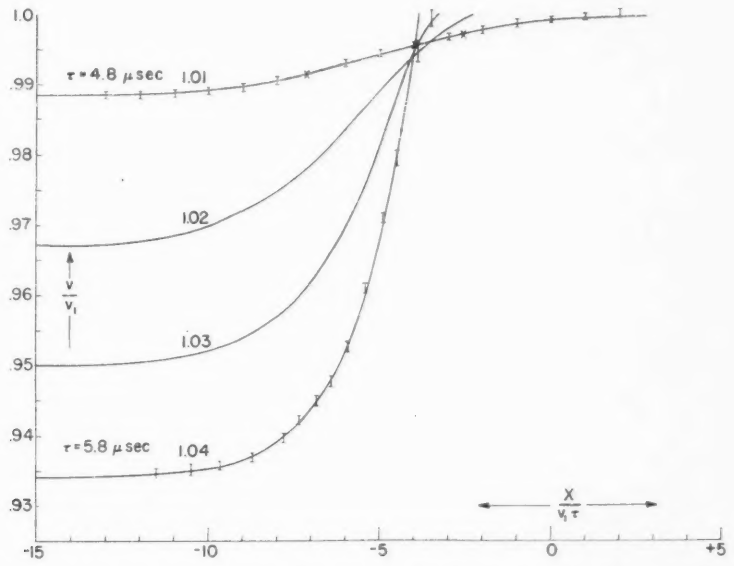

Figure 1. Calculated velocity profiles for shocks of Mach number 1·01, 1·02, 1·03 and 1·04 in carbon dioxide. The experimental data were obtained from the interferograms shown in figures 2 and 3 (plate 1). The one-quarter and three-quarters points are indicated by a cross.

The experimental values plotted on figure 1 were obtained from such interferograms as those shown in figures 2 and 3 (plate 1). Shock strengths were computed from the total observed fringe shifts since these waves are too weak to trip any of our timing circuits. The effective relaxation

time for each experiment was obtained by fitting the points corresponding to one-quarter and three-quarters of the total fringe shifts to the appropriate theoretical curve. This was necessary because the relaxation time, which determines the spatial scale factor, is very sensitive to minute gas impurities which we cannot control with precision. The values of τ thus computed are attached to the curves. It may be seen that these are somewhat below what we believe to be the value for a pure gas.

All gases with a mode that takes up energy over many collisions may be expected to exhibit a similar effect. The reason why it has not been seen before lies in the small vibrational heat capacity of most common gases, which makes the velocity shift small, or the very short relaxation time of most polyatomic gases, which makes the width of the diffuse wave small. Carbon dioxide offers the most favourable combination of these two properties. Above $M = 1{\cdot}042$ a shock front is observed and is followed by a relaxation region, as reported by Griffith, Brickl & Blackman (1956).

This work was supported by the Office of Naval Research. We are indebted to M. J. Lighthill for a stimulating discussion which led to this work.

References

Bethe, H. & Teller, E. 1941 Deviations from thermal equilibrium in shock waves, Cornell University unpublished report.

Griffiths, W., Brickl, D. & Blackman, V. 1956 *Phys. Rev.* **102**, 1209.

Lighthill, M. J. 1956 Viscosity in waves of finite amplitude; article in *Surveys in Mechanics*. Cambridge University Press.

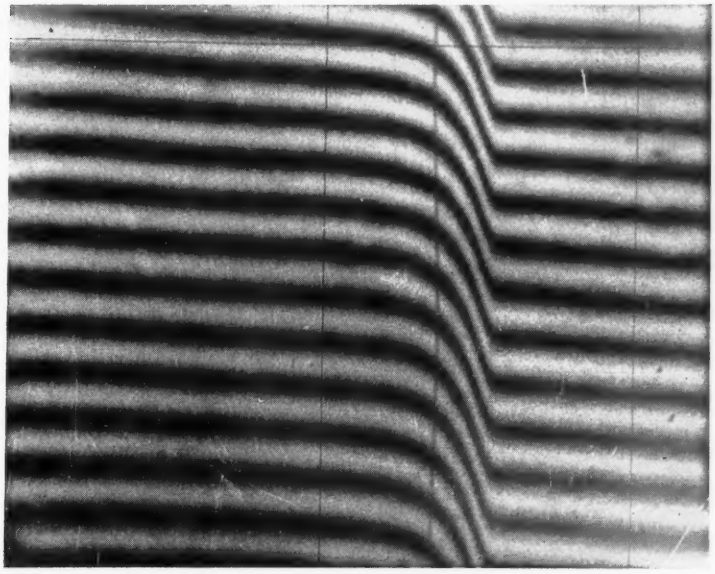

Figure 2. Interferogram of diffuse wave travelling to the right through carbon dioxide at a Mach number of 1·04. Vertical displacement of the fringes is proportional to the density. The outer two hairlines are one inch apart.

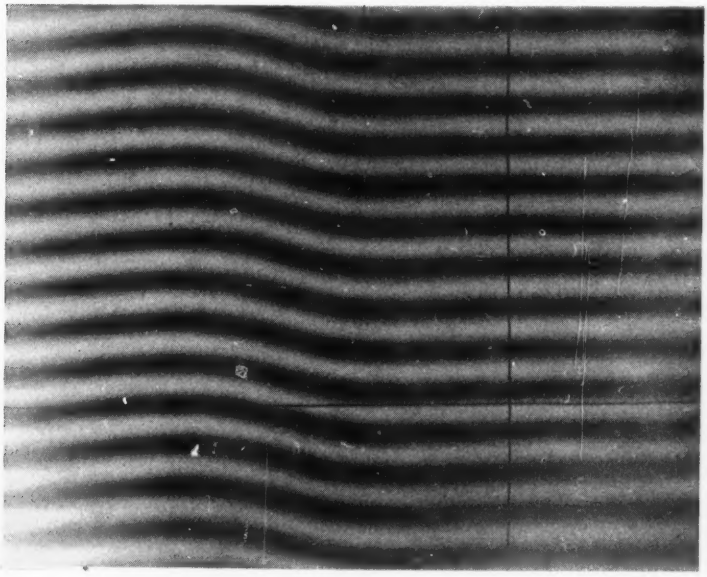

Figure 3. A wave of Mach number 1·01.

The instability of a shear layer between two parallel streams

By ROBIN E. ESCH
Pierce Hall, Harvard University

(*Received* 10 *July* 1957)

SUMMARY

An unbounded parallel flow, consisting of a linear shear layer between uniform streams, is investigated for stability. A conventional eigenvalue problem is formulated, and solved by both analytical and numerical methods. The region of instability in the plane of Reynolds number R and disturbance wave number α is determined, and typical growth rates in the unstable region are computed.

Unstable disturbances are found at all values of R. Results for $\alpha R > 100$ are found to agree closely with inviscid theory results. An analytic method useful for $\alpha R < 1$ is developed.

The extent to which the present results can be applied to the laminar boundary layer between free streams is discussed.

1. INTRODUCTION AND PREVIOUS RESULTS

The stability of parallel flows has been studied extensively; an account of such work, as well as a discussion of the general significance of the hydrodynamic stability problem, has been given by Lin (1955). Most of the work to date has dealt with flows confined by one or more solid boundaries. Since instability occurs only at high Reynolds numbers for such flows, most of this work has made use of mathematical methods appropriate to high values of the Reynolds number. The present investigation, however, deals with an unbounded flow, at both high and low Reynolds numbers, and novel methods are introduced to treat the problem.

The flow that will be treated consists of two uniform streams of fluid moving parallel to one another, separated by a laminar shear layer. Such a model is relevant to the investigation of the boundary layer separating a water current from adjacent still water. It is also useful in predicting what happens when a shock wave diffracts into the shadow zone behind an obstacle; for a brief time after the passage of the shock wave, the velocity field will be approximately parallel, and of the form considered here. Information of interest in such problems is the characteristic size of the disturbances which may be expected to appear, and the rate at which they grow. The transient character of such flows (the shear layer, of course, grows in width) is ignored in the models considered here. Only infinitesimal disturbances are considered.

Probably the first unbounded flow stability analyses were by Helmholtz (Lamb 1945)—hence the name 'Helmholtz instability'—and Rayleigh (1945). Helmholtz considered inviscid fluids with a discontinuous profile, shown as profile (*a*) of figure 1; the two streams are thus considered to be separated by a vortex sheet of zero thickness. An infinitesimal disturbance with wave number α was found to grow at the rate $e^{\alpha c_i t}$ where t is time, and c_i is a constant. This growth factor αc_i is graphed

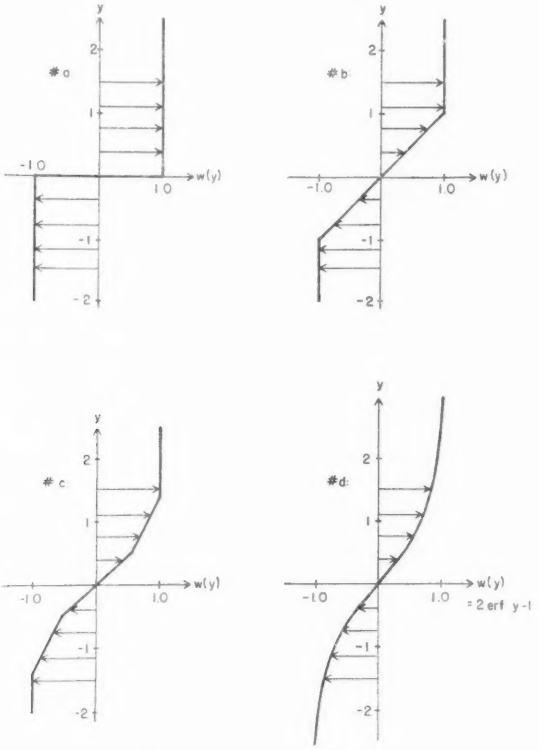

Figure 1. Velocity profiles.

in figure 2. Rayleigh, also assuming a perfect fluid, considered the piecewise linear profile (*b*) of figure 1. Such a profile is closer to the smooth profile to be expected in a real laminar boundary layer between two streams (similar to profile (*d*) in figure 1). The exponential growth factor found by Rayleigh is depicted in figure 2.

Carrier (1954), still considering zero viscosity, obtained an analytic solution for the piecewise linear profile (*c*) of figure 1, which is a closer approximation to profile (*d*). He also obtained a numerical solution for profile (*d*) itself. The results are shown in figure 2.

The first attempt to include viscosity in the analysis was made by Lessen (1950), who solved the boundary layer equations numerically to obtain a profile similar to (*d*) of figure 1. He obtained numerically the first two terms of an asymptotic approximation to the solution of the stability problem, thereby computing values of the disturbance growth factor for a certain region in the plane of Reynolds number R and disturbance wave number α. Lessen's results show that for such unbounded flows the physically interesting effects of viscosity occur at much lower Reynolds numbers than for flows confined by solid boundaries. Further, Lessen demonstrated that the slope of the neutral stability curve in the α, R plane is positive for very large R.

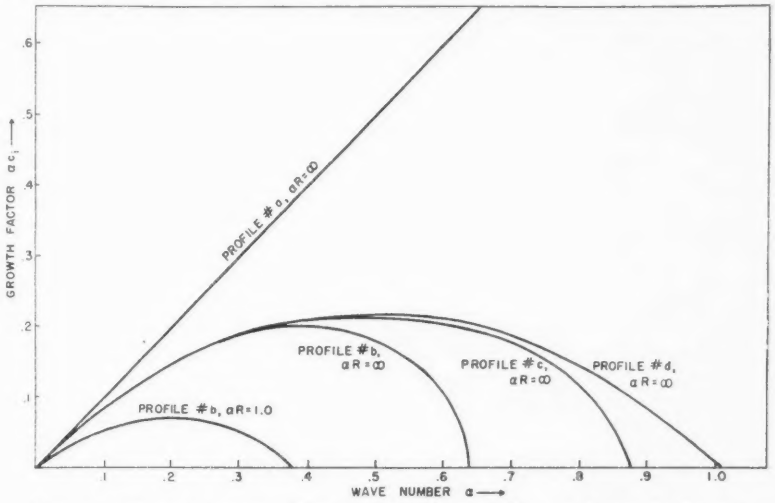

Figure 2. Growth factors. The corresponding profiles are shown in figure 1.

The present investigation treats the piecewise linear profile (*b*) of figure 1, extending the analysis to include the effects of viscosity. Although the resulting problem is only an approximate model for the physical problems stated earlier, the mathematical simplifications that result from this choice of profile allow exact solution of the eigenvalue problem at all values of Reynolds number. If the inviscid results may be taken as an indication, the present results will be quantitatively useful for profile (*d*) of figure 1 if the disturbance wave number α is small, but only qualitatively correct for larger values of α.

2. Mathematical formulation of the problem

The behaviour of small disturbances in the parallel flow of an incompressible fluid (cf. Lin 1955) are governed by the Orr–Sommerfeld equation

$$[w(y)-c](f''-\alpha^2 f)-w''(y)f = \frac{1}{i\alpha R}(f^{iv}-2\alpha^2 f''+\alpha^4 f) \qquad (1)$$

where $w(y)$ is the normalized steady velocity distribution whose stability is to be investigated; y is distance across the stream measured in units equal to the half-width H of the shear layer; and f, α, c, are defined by noting that the stream function associated with the disturbance velocity field is given by

$$\psi(x, y, t) = f(y)\exp[i\alpha(x-ct)]. \tag{2}$$

The Reynolds number R is $(U_m H/\nu)$, where U_m is the normalizing velocity, and ν is the kinematic viscosity of the fluid. The exponential growth factor is ac_i, where $c_i = \mathscr{I}(c)$; thus the steady velocity field is stable with respect to the disturbance if it is found that $c_i < 0$, and unstable if $c_i > 0$.

In the present problem the steady flow to be examined is

$$w(y) = \begin{cases} 1, & 1 \leqslant y, \\ y, & -1 \leqslant y \leqslant 1, \\ -1, & y \leqslant -1, \end{cases} \tag{3}$$

which is shown as profile (*b*) of figure 1. Equation (1) then becomes

$$(y-c)(f''-\alpha^2 f) = \frac{1}{i\alpha R}(f^{\mathrm{iv}} - 2\alpha^2 f'' + \alpha^4 f), \qquad -1 < y < 1, \tag{4}$$

$$(\pm 1 - c)(f''-\alpha^2 f) = \frac{1}{i\alpha R}(f^{\mathrm{iv}} - 2\alpha^2 f'' + \alpha^4 f), \qquad \begin{cases} y > 1, \\ y < -1. \end{cases} \tag{5}$$

It is to be noted that although the $w''f$ term of (1) does not appear in (4) and (5), its effect is not lost, but is merely concentrated on the sheets $y = 1$, $y = -1$. In fact, if the limits

$$\lim_{\epsilon \to 0} \int_{-1-\epsilon}^{-1+\epsilon} \{\text{Equation (1)}\}\, dy \text{ and } \lim_{\epsilon \to 0} \int_{1-\epsilon}^{1+\epsilon} \{\text{Equation (1)}\}\, dy$$

are considered, the $w''f$ term is found to lead to the requirement that

$$\left.\begin{aligned} \lim_{\epsilon \to 0}[f'''(-1+\epsilon) - f'''(-1-\epsilon)] &= -i\alpha R f(-1), \\ \lim_{\epsilon \to 0}[f'''(1+\epsilon) - f'''(1-\epsilon)] &= i\alpha R f(+1). \end{aligned}\right\} \tag{6}$$

The simple nature of equations (5) governing the *outer regions* $|y| > 1$ will allow the removal of these regions from the problem. The behaviour of the outer-region solutions, and the discontinuities in the derivative of $w(y)$, will then enter the problem in the form of boundary conditions on the centre-region equation (4). Equations (5) have the particular solutions

$$\left.\begin{aligned} f &= e^{\pm \alpha y}, \quad e^{\pm b_1 y}, \quad y > 1, \\ f &= e^{\pm \alpha y}, \quad e^{\pm b_2 y}, \quad y < -1, \end{aligned}\right\} \tag{7}$$

where $$b_1 = [\alpha^2 + i\alpha R(1-c)]^{1/2}, \qquad b_2 = [\alpha^2 - i\alpha R(1+c)]^{1/2}. \tag{8}$$

It will be assumed, and may be verified later, that $\mathscr{R}(b_1)$ and $\mathscr{R}(b_2)$ are never zero. Hence, with the appropriate choice of square root branches, b_1 and b_2 can be defined to have real parts greater than zero.

The general outer-region solutions will be linear combinations of the particular solutions (7). The boundary conditions at large $|y|$, which require that both components of disturbance velocity must decay, require the elimination of growing exponentials. Thus the outer-region solutions are

$$f = A_1 e^{-\alpha y} + A_2 e^{-b_1 y}, \qquad y > 1, \tag{9}$$

$$f = A_3 e^{\alpha y} + A_4 e^{b_2 y}, \qquad y < -1. \tag{10}$$

Returning to the equation governing $f(y)$ in the inner region $-1 < y < 1$, it is found that a general solution is

$$f = B_1 e^{\alpha y} + B_2 e^{-\alpha y} + B_3 f_3(y) + B_4 f_4(y), \tag{11}$$

where $e^{\alpha y}$, $e^{-\alpha y}$, $f_3(y)$ and $f_4(y)$ are four linearly independent solutions of (4). Applying the matching conditions, i.e. requiring f, f', and f'' continuous and f''' discontinuous as specified by (6), eight equations may be derived from (9) and (10). By eliminating the constants A_1, A_2, A_3, A_4 from these equations, the following four equations, which constitute boundary conditions on the inner-region solution (11), may be derived:

$$\left.\begin{aligned} f''(1) + (b_1 + \alpha) f'(1) + b_1 \alpha f(1) &= 0, \\ f'''(1) - (b_1^2 + b_1 \alpha + \alpha^2) f'(1) + (i\alpha R - b_1^2 \alpha - b_1 \alpha^2) f(1) &= 0, \\ f''(-1) - (b_2 + \alpha) f'(-1) + b_2 \alpha f(-1) &= 0, \\ f'''(-1) - (b_2^2 + b_2 \alpha + \alpha^2) f'(-1) + (i\alpha R + b_2^2 \alpha + b_2 \alpha^2) f(-1) &= 0. \end{aligned}\right\} \tag{12}$$

The centre-region equation, (4), plus these four boundary conditions, constitute a conventional eigenvalue problem, where $f(y)$ is the eigenfunction and c the eigenvalue. If equations (12), considered as equations in the unknown coefficients B_1, B_2, B_3, B_4, are to have non-trivial solutions, the determinant of the coefficients must vanish. Thus the secular equation (13) on p. 294 must be obeyed.

It remains to find acceptable representations for f_3 and f_4, the third and fourth solutions of (4), and to substitute them in (13), thereby obtaining a relationship among the parameters α, c and R. Solutions of (4) may be derived in the form of integrals of Bessel functions of order one-third, or integrals of Airy integrals (cf. Watson 1944, p. 188). However, representations of more immediate use may be obtained by taking the Fourier transform of equation (4). Defining

$$\phi(p) = \int_{-\infty}^{\infty} e^{-ipy} f(y)\, dy, \tag{14}$$

ϕ is found to obey the first-order equation

$$-i(p^2 + \alpha^2)\phi' + \left\{\frac{i}{\alpha R} p^4 + \left(c + \frac{2\alpha^2 i}{\alpha R}\right) p^2 - 2ip + \alpha^2 c + \frac{i\alpha^4}{\alpha R}\right\}\phi = 0, \tag{15}$$

which has the solution

$$\phi = 2\pi A \exp\left\{\frac{p^3}{3\alpha R} - i\left(c + \frac{i\alpha^4}{\alpha R}\right) p - \log[(p + i\alpha)(p - i\alpha)]\right\}. \tag{16}$$

$$\begin{vmatrix} 2\alpha(b_1+\alpha) & 0 & b_1\alpha f_3(1)+(b_1+\alpha)f_3'(1)+f_3''(1) & b_1\alpha f_4(1)+(b_1+\alpha)f_4'(1)+f_4''(1) \\ i\alpha R-2b_1^2\alpha-2b_1\alpha^2 & i\alpha Re^{-2\alpha} & (i\alpha R-b_1^2\alpha-b_1\alpha^2)f_3(1)- & (i\alpha R-b_1^2\alpha-b_1\alpha^2)f_4(1)- \\ & & -(b_1^2+b_1\alpha+\alpha^2)f_3'(1)+f_3'''(1) & -(b_1^2+b_1\alpha+\alpha^2)f_4'(1)+f_4'''(1) \\ 0 & 2\alpha(b_2+\alpha) & b_2\alpha f_3(-1)-(b_2+\alpha)f_3'(-1)+ & b_2\alpha f_4(-1)-(b_2+\alpha)f_4'(-1)+ \\ & & +f_3''(-1) & +f_4''(-1) \\ i\alpha Re^{-2\alpha} & i\alpha R+2b_2^2\alpha+2b_2\alpha^2 & (i\alpha R+b_2^2\alpha+b_2\alpha^2)f_3(-1)- & (i\alpha R+b_2^2\alpha+b_2\alpha^2)f_4(-1)- \\ & & -(b_2^2+b_2\alpha+\alpha^2)f_3'(-1)+f_3'''(-1) & -(b_2^2+b_2\alpha+\alpha^2)f_4'(-1)+f_4'''(-1) \end{vmatrix} = 0. \quad (13)$$

Consequently, defining for convenience

$$s = p(\alpha R)^{-1/3},$$

the desired function may be written

$$\left.\begin{aligned} f(y) &= \frac{1}{2\pi}\int e^{ipy}\phi(p)\,dp = AI, \\ \text{where} \qquad I &= \frac{1}{(\alpha R)^{1/3}}\int \frac{\exp(i\Gamma s+\frac{1}{3}s^3)}{(s+i\Delta)(s-i\Delta)}\,ds, \\ \Gamma &= (\alpha R)^{1/3}[y-c-(i\alpha^2/\alpha R)], \\ \Delta &= \frac{\alpha}{(\alpha R)^{1/3}}, \end{aligned}\right\} \tag{17}$$

and where the path of integration is either closed or approaches infinity in appropriate directions. That (17) is indeed a solution of (4) may easily be checked by direct substitution.

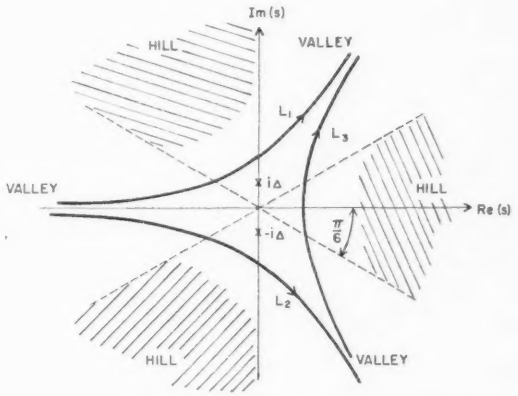

Figure 3. Paths in the s-plane.

Closed paths of integration about the simple poles at $s = i\Delta$ and $s = -i\Delta$ yield the two solutions $e^{-\alpha y}$. The remaining two independent solutions are obtained by considering paths with limits at infinity, such as L_1, L_2 or L_3 of figure 3. The corresponding integrals will be denoted I_1, I_2 and I_3. The paths must go to infinity in sectors in which the dominating factor of the integrand, $\exp(\frac{1}{3}s^3)$, is exponentially small. These sectors are the unshaded ones in figure 3.

3. Various methods of solution and results

Four methods, as enumerated below, were employed to obtain representations for f_3 and f_4 and thereby solve equation (13).

(*a*) *Large αR. Analytical method*

In most parallel flow stability investigations, the physically interesting phenomena have been found to occur at large Reynolds numbers (cf. Lin

1955). Consequently nearly all investigations to date have made use of asymptotic approximations valid for large Reynolds numbers. The first attack on the present problem made use of such a method.

Asymptotic approximations to the functions f_3 and f_4 were obtained from the integral representations (17) by the method of steepest descent integration (Watson 1944, p. 235ff). The following semi-convergent series in powers of $(\alpha R)^{-1/2}$ were thereby obtained:

$$I_1, I_2 = \begin{cases} I_b - I_a, & -I_a; \quad -\dfrac{3\pi}{2} < \arg\Gamma < -\dfrac{5\pi}{6}, \\ I_b, & -I_a; \quad -\dfrac{5\pi}{6} < \arg\Gamma < -\dfrac{\pi}{6}, \\ I_b, & I_b - I_a; \quad -\dfrac{\pi}{6} < \arg\Gamma < \dfrac{\pi}{2}, \end{cases} \tag{18}$$

where

$$\left.\begin{matrix} I_a \\ I_b \end{matrix}\right\} \sim \frac{\pi^{1/2}\exp\{\frac{7}{8}\pi i \pm (\frac{1}{4}\pi i + \frac{2}{3}e^{i(7/4)}\Gamma^{3/2})\}}{(\alpha R)^{3/4}[y-c-(i\alpha^2/\alpha R)]^{1/4}(y-c)} \times$$

$$\times\left[1 + \frac{\pm(101/48)e^{-i(7/4)}}{(\alpha R)^{1/2}[y-c-(i\alpha^2/\alpha R)]^{3/2}} - \frac{(35905/4608)i}{\alpha R[y-c-(i\alpha^2/\alpha R)]^3} + O[(\alpha R)^{-3/2}]\right].$$

In the same manner, expressions were obtained for the first three derivatives of I_1 and I_2 (differentiating the asymptotic series (18) is not legitimate). Choosing $f_3(y) = I_1$, $f_4(y) = I_2$, the following asymptotic expansion of the secular equation (13) was derived:

$$KC_1 + KC_2(\alpha R)^{-1/2} + C_3(\alpha R)^{-1} + O[(\alpha R)^{-3/2}] = 0, \tag{19}$$

where

$$K = (1-2\alpha)^2 - 4\alpha^2\gamma^2 - e^{-4\alpha}, \qquad \gamma = c + \frac{i\alpha^2}{\alpha R},$$

$$C_1 = 4(1-\gamma^2),$$

$$C_2 = 2e^{i(7/4)}(1-\gamma)[2\alpha(1+\gamma)^{1/2} + (23/24)(1+\gamma)^{-1/2} +$$
$$+ 2e^{-i(7/4)}(1+\gamma)[2\alpha(1-\gamma)^{1/2} + (23/24)(1-\gamma)^{-1/2}],$$

$$C_3 = 16\alpha^2 i\gamma[4\alpha - 1 + 2\alpha^2 - 2\alpha^2\gamma^2] + K\Big\{2i(1-\gamma)\Big[\frac{71}{24}\alpha(1+\gamma)^{-1} +$$
$$+ \frac{4813}{2304}(1+\gamma)^{-2}\Big] - 2i(1+\gamma)\Big[\frac{71}{24}\alpha(1-\gamma)^{-1} + \frac{4813}{2304}(1-\gamma)^{-2}\Big] +$$
$$+ \Big[2\alpha(1-\gamma)^{1/2} + \frac{23}{24}(1-\gamma)^{-1/2}\Big]\Big[2\alpha(1+\gamma)^{1/2} + \frac{23}{24}(1+\gamma)^{-1/2}\Big]\Big\}.$$

Setting $(\alpha R)^{-1/2} = 0$, (19) reduces to $KC_1 = 0$, which yields

$$\alpha c = \pm\tfrac{1}{2}i[e^{-4\alpha} - (1-2\alpha)^2]^{1/2} \tag{20}$$

which is the result of Rayleigh (1945) for the inviscid case and is shown in figure 2.

Equating the sum of the first two terms of (19) to zero yields nothing more than the inviscid solution (20). It is therefore evident that the curves c = constant have a dependence on $(\alpha R)^{-1}$ that is of higher order than one-half.

Three terms of the series (19) are therefore necessary to determine the effect of finite Reynolds number. Equating their sum to zero yields a relation between α, αR and c, which was used to plot c = constant curves in the α, αR plane. These curves are presented in figure 4.

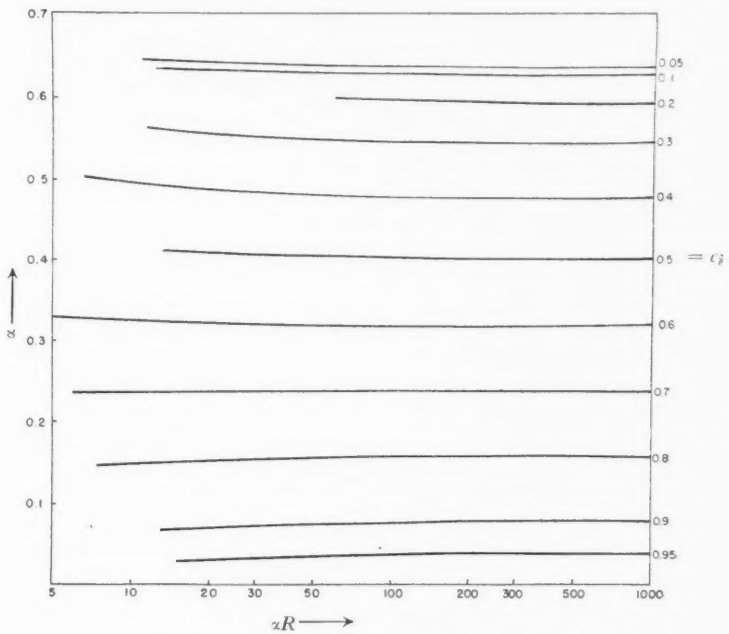

Figure 4. Asymptotic approximations to constant c lines.

From numerical investigations it was concluded that this asymptotic approach was accurate only for $\alpha R > 100$ (a comparison of the $c_i = 0{\cdot}4$ curve with numerical results is shown in figure 5; the values of the integrals (18) were also compared with values obtained by numerical integration). Thus, for $\alpha R > 100$, it may be concluded that there is almost no dependence of $\alpha(c_i, R)$ upon R.

It should be noted that the complex secular equation (13) constitutes in fact two relationships among the four parameters α, R, c_r and c_i. One of these relationships was always found to be satisfied by taking the phase velocity $c_r = 0$. Since the disturbance phase velocity arises from the convection of the disturbance by the steady flow (3), $c_r = 0$ corresponds to a disturbance centred at the midpoint of the shear layer (this interpretation loses its significance for small α, however, since the scale of the disturbance then becomes much larger than the shear layer width). This centring of the disturbance would be expected in the case of the real boundary layer, figure 1 (*d*), because of the point of inflection at the midpoint (cf. Lin 1955). Furthermore, it is found in the inviscid case

(equation (20)) that $c_r = 0$ for all wave numbers α in the unstable range. Though it has of course not been proven that disturbances with $c_r \neq 0$ do not exist, no such roots of the secular equation (13) could be found, even when c_r was deliberately made non-zero in the numerical investigations to be reported below.

A similar set of $c =$ constant curves was obtained for negative values of c_i, i.e. decaying disturbances. For the $c_i = 0$ (neutral stability) case, dependence on αR became of higher order; the only conclusion drawn was that

$$\left[\frac{d\alpha}{d(\alpha R)^{-1}}\right]_{c_i = 0,\,(\alpha R)^{-1} = 0} = 0. \tag{21}$$

(*b*) *Large αR. Numerical method*

In order to determine the region for which the asymptotic approximation is accurate, to extend the solution of the eigenvalue problem to lower values of αR, and to trace the neutral stability curve, a numerical method for large αR was sought. At large αR an error-control problem arises, due to the rapid oscillation both of $f(y)$ and of its Fourier transform. It was decided to integrate the integral representations (17) numerically along the steepest descent paths in the complex s plane. The advantages of this method are: (1) No oscillation of the integrand takes place, since the imaginary part of the exponent is by definition constant on such a path; the error problem caused by such oscillation, which increases in severity as αR increases, is thereby avoided. (2) The modulus of the integrand decreases most rapidly along such a path, allowing earliest termination of the integration. Indeed, because of these two features, the method works best for large αR, the very case for which other methods break down. The disadvantages of the method are: (1) the method is laborious; not only must the integrand be evaluated at each step but so must the quadrature formula coefficients and the integration contour location. (2) The necessity of dealing with complex numbers is expensive in computer time and internal storage space. (3) Auxiliary investigations must be made to find in what direction the steepest descent paths go to infinity, on what sides they pass the poles, and whether they pass too close to a pole.

The following complex generalization of the familiar Simpson's rule was found useful to extend the integration in the complex plane:

$$\left.\begin{aligned}
&\int_{z_0}^{z_2} g(z)\,dz = C_1\,g(z_0) + C_2\,g(z_1) + C_3\,g(z_2) + T,\\
\text{where}\quad &C_1 = \frac{3\Delta_2\Delta_1^2 + 2\Delta_1^3 - \Delta_2^3}{6\Delta_1(\Delta_2 + \Delta_1)},\\
&C_3 = \frac{3\Delta_2^2\Delta_1 + 2\Delta_2^3 - \Delta_1^3}{6\Delta_2(\Delta_1 + \Delta_2)},\\
&C_2 = \Delta_2 + \Delta_1 - C_1 - C_3,\\
&\Delta_1 = z_1 - z_0, \qquad \Delta_2 = z_2 - z_1,\\
&|T| \leqslant (1/24)|g'''|_{\max}(|\Delta_1|^4 + |\Delta_2|^4).
\end{aligned}\right\} \tag{22}$$

The values of $f_3(\pm 1)$ and $f_4(\pm 1)$ found by this method were substituted into (13), and roots of (13) were found by successive approximation. The resulting points are shown on figure 5.

(*c*) *Small* αR. *Numerical method*

A numerical method which was economical for small αR was desired, in order to explore that region numerically, to aid in suggesting the proper approach that should be taken in a small αR analytic theory, and to allow the investigation of other profiles $w(y)$. Therefore a second numerical method, utilizing direct numerical solution of the differential equation (1), was programmed for machine solution.

The roots of the secular equation that were computed by this method are plotted in figures 2 and 5. At $\alpha R = 1$, the maximum growth rate was found to have decreased to less than one-half of its value at $\alpha R = \infty$. It was noted that, for small αR, a good empirical fit to the neutral stability curve is obtained by the curve

$$\alpha/(\alpha R)^{1/2} = \text{constant}, \tag{23}$$

the constant being near 0·4.

Finally, a small number of computations were done with the error-function profile, curve (*d*) of figure 1. The boundary conditions which must be taken for such a calculation require that the function and its first three derivatives, evaluated at $y = \pm A$ (where A is some sufficiently large number), must be continuous with the solutions (9) and (10) valid in the outer regions. The resulting boundary conditions are (12), with the $i\alpha R$ terms deleted, and where f is evaluated at $\pm A$ instead of ± 1.

Due to the lack of availability of machine time, only a single neutral stability point was computed for the error-function profile. It is plotted on figure 5, and is found to lie close to the neutral stability curve of the piecewise linear profile.

(*d*) *Small* αR. *Analytical method*

Since both α and R are small in the low Reynolds number instability region, the choice of a parameter in which to expand (13) is not obvious. The proper approach is indicated by the numerical results mentioned earlier, which suggest that

$$\alpha/(\alpha R)^{1/2} = \delta \tag{24}$$

tends to a non-zero constant as $\alpha R \to 0$ along the neutral stability curve. Consequently the secular equation (13) was re-written with α and R replaced by the parameters αR and δ, and an expansion of the form

$$\sum_{n=0}^{\infty} D_n(\alpha R)^{an} \tag{25}$$

was sought, where a is some simple fraction. The parameter c_i was set equal to zero, in order to obtain the neutral stability curve, and $c_r = 0$ was tried, on the basis of the numerical results reported above.

The differential equation (4), rewritten in terms of δ and αR, is

$$f^{iv} + \alpha R(-2\delta^2 - iy)f'' + (\alpha R)^2(\delta^4 + i\delta^2 y)f = 0. \tag{26}$$

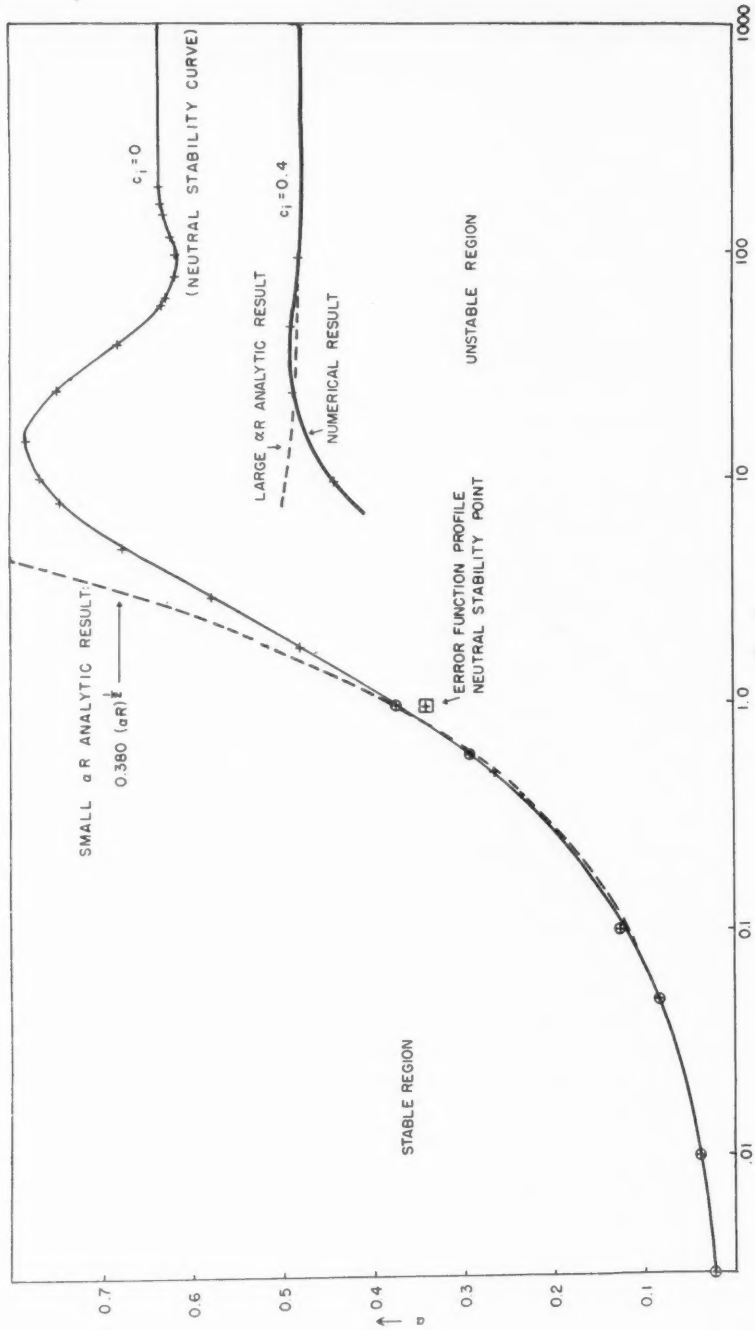

Figure 5. Results plotted in the $(\alpha, \alpha R)$ plane. Results of the numerical method for large αR are indicated by crosses, those for small αR by circled crosses.

Representations of solutions that converge rapidly for αR small at $y = \pm 1$ may be obtained by expanding f in a power series in the independent variable y (the practicability of this approach may be seen by substituting $z = (\alpha R)^{1/2} y$ into (26), and noting the analyticity of $f(z)$; for, as values of $f(y)$ are required at $p = \pm 1$, values of $f(z)$ are required only at the small points $z = \pm(\alpha R)^{1/2}$). In this manner the following particular solutions, linearly independent of the solutions $e^{\pm \alpha y} = e^{\pm \delta (\alpha R)^{1/2} y}$ already used, were obtained:

$$\left.\begin{aligned} f_3 &= 1 - \frac{\delta^4(\alpha R)^2}{24} y^4 - \frac{i\delta^2(\alpha R)^2}{120} y^5 - \frac{\delta^6(\alpha R)^3}{360} y^6 - \frac{i\delta^4(\alpha R)^3}{1008} y^7 + \dots, \\ f_4 &= y - \frac{\delta^4(\alpha R)^2}{120} y^5 - \frac{i\delta^2(\alpha R)^2}{360} y^6 - \frac{\delta^6(\alpha R)^3}{2520} y^7 + \dots . \end{aligned}\right\} \tag{27}$$

The resulting representation of the secular determinant (13) is a series in $(\alpha R)^{1/2}$. The first two terms of this series have coefficients that are identically zero; they may be removed and the algebra may be simplified by judicious manipulation of the rows and columns of the determinant. Equating to zero the first term that does not vanish identically yields the equation

$$2i\delta[\delta + (\delta^2 - i)^{1/2}][\delta + (\delta^2 + i)^{1/2}] + (\delta^2 - i)^{1/2} - (\delta^2 + i)^{1/2} = 0, \tag{28}$$

which for positive real δ has the single root

$$\delta = \frac{\alpha}{(\alpha R)^{1/2}} = 0{\cdot}380. \tag{29}$$

This then must be the asymptotic form of the neutral stability curve as $\alpha R \to 0$. Equation (29) is plotted in figure 5, and is seen to yield a good approximation to the neutral stability curve all the way up to the surprisingly large value $\alpha R = 1{\cdot}0$.

4. Conclusions and discussion

The inviscid theory result (figure 2) has been found to be a good approximation to the true situation for all $\alpha R > 100$. It would seem highly probable that this is not an accident associated with the particular profile investigated, but is true also of related profiles such as that of figure 1 (*d*). Though perhaps not of great theoretical interest, such a result might have considerable practical value.

From the results plotted on figure 5, it is seen that, as αR decreases to smaller values, the neutral stability curve first turns down to smaller wave numbers α. This is in agreement with the results of Lessen (1950) for the boundary layer between free streams. However, beginning at about $\alpha R = 100$, or $R = 170$, the curve turns upwards. A maximum is reached at about $\alpha R = 15$, $R = 20$, with $\alpha = 0{\cdot}78$, which is considerably higher than the asymptote $\alpha = 0{\cdot}64$ at $\alpha R = \infty$. The curve then descends to small values of α as αR is reduced further. Such behaviour is not found in Lessen's results, which are based on asymptotic approximations valid at large αR,

and, of course, on a different steady velocity profile. As shown in figure 5, the present asymptotic theory also fails to predict such behaviour. Consequently there is reason to suspect that the qualitative discrepancy between Lessen's results and the present results is due to inadequacy of asymptotic approximations, rather than to difference in profile. The present asymptotic expansions, which are power series in $(\alpha R)^{-1/2}$, are accurate only for $(\alpha R)^{1/2} > 10$, i.e. $\alpha R > 100$, even though they were carried out to three terms. It might therefore be suspected that the asymptotic approximation techniques conventionally used in parallel flow stability investigations are likely not to be profitable in unbounded shear-flow problems.

It is also fruitful to compare the present results with the results of the analysis of Lin (1955) for the stability of the flat plate boundary layer. The flat plate boundary layer results differ from the present results in that the region of instability in the α, αR plane is smaller, does not extend down to $\alpha = 0$ except at infinite Reynolds number, and does not extend below a minimum 'critical' Reynolds number; however, a relative maximum of the neutral stability curve is found in both cases. The presence of a solid boundary should certainly be expected to have a stabilizing effect; however, the following crude physical reasoning may perhaps further explain the differences. At a given Reynolds number, the amount of energy lost by viscous attenuation increases with wave number; therefore neither flat plate nor unbounded shear layer can be unstable at high α. Small α, on the other hand, corresponds to long wavelength (as seen from (2) the dimensional wavelength is $(2\pi H/\alpha)$, where H is the shear layer half-width). Suppose that a disturbance eigenmode dies out in the direction perpendicular to the shear layer in a distance of a wavelength (or in some distance simply related to the wavelength); then, in the flat-plate case, since the disturbance must be zero at the plate, at small α the main part of a disturbance would be situated entirely outside of the shear layer, a condition unfavourable for the excitation of the disturbance. However, in the absence of a solid boundary, the disturbance could straddle the shear layer in such a way that its excitation was optimized. This would explain the instability at small α, and absence of a positive critical Reynolds number in the present results.

The analytic method making use of ascending power series has been found to give accurate results for $\alpha R < 1$. It should also prove useful in computing growth rates within the unstable region for $\alpha R < 1$.

Although for the present problem there exists no positive critical Reynolds number, i.e. no $R > 0$ below which no instability exists, in practical cases such a critical R will result because an experiment is limited in size. The bounded geometry will imply a maximum disturbance wavelength, and hence a minimum $\alpha > 0$, and the critical R will occur when the neutral stability curve of figure 5 falls to that value of α.

Finally, it may be pertinent to estimate the extent to which the present results apply to related profiles such as figure 1(*d*). By the reasoning of Carrier (1954), it may be argued that agreement among results for related

profiles will be good for small α; for the width of the shear layer will then be small compared to a wavelength, and the motion of the disturbance, which will extend in the y direction effectively the order of a wavelength, will penetrate deeply into the uniform flow layers. In other words, if one wavelength is made the unit of distance, the shear layer becomes very thin, and all profiles on figure 1 look nearly the same. Judging from the inviscid results (figure 2), agreement should be good quantitatively for $\alpha < 0{\cdot}3$. The single neutral stability point calculated for profile (*d*) of figure 1 corroborates this assertion (see figure 5). For $\alpha > 0{\cdot}3$, however, agreement will be only qualitative, the internal structure of the shear layer becoming important.

Most of the work reported here was included in a doctoral thesis submitted in December, 1956, to Harvard University. The problem was suggested by Professor George Carrier, for whose continuing guidance the author is deeply grateful. The advice and help of Professor Sydney Goldstein, Professor Kenneth Iverson, and Mr Peter Neumann are gratefully acknowledged. The machine computations were made possible by the United States Air Force and by the cooperation and help of many members of the Harvard Computation Laboratory. The completion of the work was supported by the Office of Naval Research.

References

Carrier, G. 1954 Interface stability of the Helmholtz type, *Los Alamos Internal Report*.

Lamb, H. 1945 *Hydrodynamics*. New York : Dover.

Lessen, M. 1950 On stability of free laminar boundary layer between parallel streams, *Nat. Adv. Comm. Aero., Wash.*, no. 979.

Lin, C. C. 1955 *Theory of Hydrodynamic Stability*. Cambridge University Press.

Rayleigh, Lord 1945 *Theory of Sound*. New York : Dover.

Watson, G. N. 1944 *Theory of Bessel Functions*. Cambridge University Press.

The effect of a magnetic field on Stokes flow in a conducting fluid

By W. CHESTER

*Guggenheim Aeronautical Laboratory, California Institute of Technology**

(*Received* 23 *July* 1957)

SUMMARY

Low Reynolds number flow of a conducting fluid past a sphere is considered. The classical Stokes solution is modified by a magnetic field which, at infinity, is uniform and in the direction of flow of the fluid.

The formula for the drag is found to be

$$D = D_S\left\{1+\frac{3}{8}M+\frac{7}{960}M^2-\frac{43}{7680}M^3+O(M^4)\right\},$$

where D_S is the Stokes drag and M is the Hartmann number.

INTRODUCTION

We consider the streaming motion of an incompressible, viscous, conducting fluid past a sphere, in the presence of a magnetic field. At infinity the streaming motion and the magnetic field are assumed to be uniform, and their directions are parallel.

For flow in the absence of the magnetic field, the problem was first considered by Stokes (Lamb 1932) on the assumption that the Reynolds number $R = Ua/\nu$ was negligibly small, where U is the undisturbed velocity of the stream, a is the radius of the sphere, and ν the kinematic viscosity. The classical result for the drag force experienced by the sphere is, according to the Stokes approximation,

$$D_S = 6\pi\rho\nu aU,$$

where ρ is the density.

Various writers have refined this result for the case in which R is small but not negligible; in particular Oseen (Lamb 1932) found the formula

$$D = D_S(1+\tfrac{3}{8}R)$$

for the next approximation to the drag. More recently Proudman & Pearson (1957) have obtained the result

$$D = D_S\left\{1+\frac{3}{8}R+\frac{9}{40}R^2\log R+O(R^2)\right\}.$$

It is the purpose of the present paper to investigate the modification of the Stokes formula due to the presence of the magnetic field. Because of the motion of the fluid in the magnetic field, an associated electrical field

* Now at Bristol University.

is produced which, according to Ohm's law, sets up electrical currents in the fluid if the latter is a conductor. The interaction of these currents with the magnetic field then produces a body force which must be included in the Navier–Stokes equations for the motion of the fluid. The effect of this body force is to inhibit the motion of the fluid across the lines of force. Since, as will be shown, the lines of force are approximately in the direction of the undisturbed stream, the natural tendency of the fluid to flow round the sphere is opposed and the result is an increase in drag. The possibility of separation behind the sphere will also be enhanced, and then the present theory will no longer apply. However, there is presumably a certain range in which there is no separation, as in the Stokes problem. In this range, the theory will be valid.

The problem also seems amenable to experiment, and investigations are to be conducted at the Guggenheim Aeronautical Laboratory, California Institute of Technology, on the motion of small spheres in a column of mercury, the magnetic field being produced by a surrounding coil carrying a current.

Governing equations

The flow is assumed to be steady and parallel to the negative x-axis at infinity. The equations to be solved are then, using m.k.s. units (Cowling 1957), and with the usual notation for electromagnetic quantities,

$$\operatorname{curl}\mathbf{H} = \mathbf{j}, \qquad \operatorname{div}\mathbf{H} = 0, \tag{1}$$

$$\operatorname{curl}\mathbf{E} = 0, \tag{2}$$

$$\mathbf{j} = \sigma(\mathbf{E} + \mu\mathbf{V}' \times \mathbf{H}), \tag{3}$$

$$\operatorname{div}\mathbf{V}' = 0, \tag{4}$$

$$\rho(\mathbf{V}' \cdot \nabla)\mathbf{V}' = -\nabla p' + \rho\nu\nabla^2\mathbf{V}' + \mu\mathbf{j} \times \mathbf{H}, \tag{5}$$

where $\mathbf{V}'$ is the velocity of fluid and p' is the pressure.

From the first three equations we deduce that

$$\mu\sigma \operatorname{curl}\mathbf{V}' \times \mathbf{H} = \operatorname{curl}\operatorname{curl}\mathbf{H}. \tag{6}$$

Let U be the speed of the uniform stream at infinity parallel to the negative x-axis, and let a be the radius of the sphere. The space coordinates may then be made non-dimensional with the factor a^{-1} and the pressure and velocity as follows,

$$p = \frac{a}{\rho\nu U}p', \qquad \mathbf{V} = \frac{\mathbf{V}' + U\mathbf{i}}{U},$$

where $\mathbf{i}$ is a unit vector along the x-axis. Note that the boundary conditions on $\mathbf{V}$ are now $\mathbf{V} = 0$ at infinity and $\mathbf{V} = \mathbf{i}$ at the sphere.

Equations (4), (5) and (6) then become

$$\operatorname{div}\mathbf{V} = 0, \tag{7}$$

$$R(\mathbf{V} \cdot \nabla)\mathbf{V} = -\nabla p + \nabla^2\mathbf{V} + (\mu a^2/\rho\nu U)\mathbf{j} \times \mathbf{H}, \tag{8}$$

$$R_m \operatorname{curl}\mathbf{V} \times \mathbf{H} = \operatorname{curl}\operatorname{curl}\mathbf{H}, \tag{9}$$

where
$$R = \frac{Ua}{\nu} = \text{Reynolds number},$$
$$R_m = Ua\mu\sigma = \text{magnetic Reynolds number},$$

and all the operators now refer to non-dimensional coordinates.

As in the classical Stokes problem we assume that R is small. In addition we assume that R_m is small. In most practical problems the first condition implies the second. For example, for mercury, $\nu \doteqdot 10^{-2}$ and $\mu\sigma \doteqdot 10^{-5}$, so that $R_m/R \doteqdot 10^{-7}$.

If the term containing R_m in (9) is neglected we get

$$\operatorname{curl}\operatorname{curl}\mathbf{H} = 0,$$

and so the magnetic field is independent of the fluid velocity to this approximation. In practice the permeabilities of the fluid and the sphere will be effectively equal provided both are non-magnetic, so that we may take the magnetic field to be uniform and parallel to the x-axis at all points. This makes $\mathbf{V}\times\mathbf{H} = 0$ both at the sphere and at infinity. Hence equation (2), and the boundary conditions on $\mathbf{E}$ and $\mathbf{j}$, are satisfied by

$$\mathbf{E} = 0, \qquad \mathbf{j} = U\mu\sigma\mathbf{V}\times\mathbf{H}. \tag{10}$$

The problem is now reduced to the solution of equations (7) and (8) for $\mathbf{V}$ and p, with $\mathbf{j}$ given by (10) and with a prescribed value for $\mathbf{H} = H\mathbf{i}$.

It should be noted that some of the complications which arise from boundary conditions in magneto-hydrodynamics are conveniently absent in this problem. Moreover the displacement currents are identically zero, since the motion is steady. Nor is there an electric field required to prevent a pile-up of charge on the sphere, for the current filaments, like the vortex filaments, form closed circuits coaxial with the sphere and vanish on its surface.

Solution of the equations

In equation (8) we omit the left-hand side, since it contains the factor R. The equations are then

$$\nabla\cdot\mathbf{V} = 0, \tag{11}$$
$$-\nabla p + \nabla^2\mathbf{V} - M^2\{\mathbf{V} - (\mathbf{V}\cdot\mathbf{i})\mathbf{i}\} = 0, \tag{12}$$

where M denotes the Hartmann number $\mu Ha(\sigma/\rho\nu)^{1/2}$ and is essentially non-negative.

We assume the following terms for $\mathbf{V}$ and p:

$$\mathbf{V} = e^{Mx}\nabla\phi_1 + e^{-Mx}\nabla\phi_2, \tag{13}$$
$$p = M\left(e^{Mx}\frac{\partial\phi_1}{\partial x} - e^{-Mx}\frac{\partial\phi_2}{\partial x}\right). \tag{14}$$

where ϕ_1 and ϕ_2 are to be determined. It will appear (see equations (19) and (18) below) that both ϕ_1 and ϕ_2 are $O(M^{-1})$ as $M\to 0$, so that the limiting value for the pressure (the classical Stokes solution) is non-zero.

Moreover, the singular terms in equation (13) cancel each other, so that a finite limiting value for the velocity is also obtained.

Equations (11) and (12) now become

$$\nabla . \mathbf{V} = e^{Mx}\left(\nabla^2\phi_1 + M\frac{\partial\phi_1}{\partial x}\right) + e^{-Mx}\left(\nabla^2\phi_2 - M\frac{\partial\phi_2}{\partial x}\right) = 0,$$

$$-\nabla p + \nabla^2\mathbf{V} - M^2\{\mathbf{V} - (\mathbf{V}.\mathbf{i})\mathbf{i}\} = e^{Mx}\nabla\left(\nabla^2\phi_1 + M\frac{\partial\phi_1}{\partial x}\right) + e^{-Mx}\nabla\left(\nabla^2\phi_2 - M\frac{\partial\phi_2}{\partial x}\right) = 0,$$

and so both equations are satisfied provided that

$$\nabla^2\phi_1 + M\,\partial\phi_1/\partial x = 0, \tag{15}$$

$$\nabla^2\phi_2 - M\,\partial\phi_2/\partial x = 0. \tag{16}$$

Solutions of equations (15) and (16) may be written in the form

$$\phi_1 = (\pi/Mr)^{1/2}e^{-\frac{1}{2}Mx}\sum_{n=0}^{\infty} A_n K_{n+\frac{1}{2}}(\tfrac{1}{2}Mr)P_n(\cos\theta), \tag{17}$$

$$\phi_2 = (\pi/Mr)^{1/2}e^{\frac{1}{2}Mx}\sum_{n=0}^{\infty} B_n K_{n+\frac{1}{2}}(\tfrac{1}{2}Mr)P_n(\cos\theta), \tag{18}$$

where (r, θ) are non-dimensional spherical polar coordinates, K_n is the modified Bessel function and P_n is the Legendre polynomial.

Considerations of symmetry also imply that $B_n = (-1)^{n+1}A_n$; for example the x-component of the velocity must be an even function of x.

It remains to obtain the coefficients A_n by imposing the boundary conditions that the x-component of $\mathbf{V}$ as given by (13) shall be unity and the component perpendicular to the axis zero at the sphere. For values of M which are not too large this can be done numerically, approximating to the resulting series by a finite number of terms. The expansion of $e^{\xi\cos\theta}P_n(\cos\theta)$ in terms of spherical harmonics is required, and will be found in Goldstein (1929). However, values of M which are $O(1)$ and smaller are reasonable in laboratory experiments. For example, the Hartmann number for a sphere of radius 0·1 cm in mercury subject to a field of 100 gauss is about 0·1. Thus a solution in powers of M is not without interest. For this purpose, solutions of (15) and (16) of a different form were used in order to avoid the algebraical manipulation of Bessel functions, Legendre polynomials and their derivatives.

Fundamental solutions of equations (15) and (16) are, respectively

$$r^{-1}e^{-\frac{1}{2}M(r+x)}, \qquad r^{-1}e^{-\frac{1}{2}M(r-x)},$$

and further linearly independent solutions can be formed, having the required symmetry about the x-axis and the correct behaviour at infinity,

by successive differentiation with respect to x. Thus we may write

$$\phi_1 = \sum_{n=0}^{\infty} C_n \left(\frac{\partial}{\partial x}\right)^n (r^{-1}e^{-\frac{1}{2}M(r+x)}),$$

$$\phi_2 = \sum_{n=0}^{\infty} (-1)^{n+1} C_n \left(\frac{\partial}{\partial x}\right)^n (r^{-1}e^{-\frac{1}{2}M(r-x)}),$$

$$\mathbf{V} = e^{Mx}\nabla\left\{\sum_{n=0}^{\infty} C_n \left(\frac{\partial}{\partial x}\right)^n (r^{-1}e^{-\frac{1}{2}M(r+x)})\right\} - e^{-Mx}\nabla\left\{\sum_{n=0}^{\infty} (-1)^n C_n \left(\frac{\partial}{\partial x}\right)^n (r^{-1}e^{-\frac{1}{2}M(r-x)})\right\},$$

$$p = Me^{Mx}\sum_{n=0}^{\infty} C_n \left(\frac{\partial}{\partial x}\right)^{n+1} (r^{-1}e^{-\frac{1}{2}M(r+x)}) + Me^{-Mx}\sum_{n=0}^{\infty} (-1)^n C_n \left(\frac{\partial}{\partial x}\right)^{n+1} (r^{-1}e^{-\frac{1}{2}M(r-x)}).$$

For small values of M the exponential terms may be expanded in series. The differentiations are easily performed and the first few coefficients calculated so as to be consistent with the boundary conditions. The details are straightforward and are omitted. When the coefficients are obtained, the drag may be computed from the stress across the surface of the sphere using the formula (Lamb 1932)

$$rp_{rx} = -px + \{r(\partial/\partial r) - 1\}(\mathbf{V}.\mathbf{i}) + \partial(\mathbf{r}.\mathbf{V})/\partial x.$$

The final result for the drag is

$$D = D_S\left\{1 + \frac{3}{8}M + \frac{7}{960}M^2 - \frac{43}{7680}M^3 + O(M^4)\right\}.$$

The author would like to express his thanks to Professor H. W. Liepmann for suggesting the problem and for several profitable discussions. The research was carried out with the support of the Office of Naval Research.

References

Cowling, T. G. 1957 *Magnetohydrodynamics*. New York : Interscience.

Goldstein, S. 1929 *Proc. Roy. Soc.* A, **123**, 225.

Lamb, H. 1932 *Hydrodynamics*, 6th Ed. Cambridge University Press.

Proudman, I. & Pearson, J. R. A. 1957 *J. Fluid Mech.* **2**, 237.

The impact of a shock wave on a movable wall

By R. F. MEYER
Department of the Mechanics of Fluids, University of Manchester

(*Received* 29 *August* 1957)

SUMMARY

An approximate solution is devised for the one-dimensional motion following the impact of a shock wave on a wall which is free to move. The approximate solution neglects changes in entropy occurring through the reflected and transmitted shocks, thus reducing the problem to one of a simple wave type. The asymptotic behaviour of the system is considered and it is shown by exact physical argument that the transmitted shock eventually attains the same strength as the incident shock and that the reflected shock ultimately decays to a sound wave.

An experimental investigation of the interaction was made, using thin walls of cellulose acetate, in a shock tube at an incident shock Mach number of 1·50. Agreement between the theoretical and experimental results, especially for the path followed by the wall, was found to be good.

1. INTRODUCTION

When a wall of small mass, initially at rest and free to move under impact, is struck head-on by a plane shock wave, the resulting difference in pressure between the two sides of the wall causes it to accelerate in the direction of the initial motion of the incident shock wave and thereby to send out compression waves into the region ahead of the wall and rarefaction waves into the region behind it. The compression waves overtake and eventually coalesce to form a shock, whereas the rarefaction waves catch up the reflected shock and weaken it. The appropriate wave diagram, for the interaction is sketched in figure 1, where x and t designate distance and time respectively. Ultimately the pressure difference across the wall vanishes, so that the wall and the transmitted shock attain constant speeds; the reflected shock on the other hand decays to a sound wave.

This paper describes a theoretical and experimental study of the problem, which will be treated as essentially one-dimensional.

The complete analytical problem of determining the motion of the wall, the behaviour of the transmitted shock and the behaviour of the reflected shock, is difficult and not attempted here. Courant & Friedrichs (1948) state, when discussing the strong shock produced by an accelerating piston, that "the problem is an initial boundary value problem with an unknown boundary and that no direct theoretical treatment seems possible". Pillow & Levey (1947) and Pillow (1949) found an analytical solution for the shock

produced by a *uniformly* accelerating piston, which is correct to the first order in entropy changes through the shock. It would seem difficult, however, to extend their method to a problem involving a more general motion of the piston and more difficult still to extend it to the present problem in which the motion of the piston is unknown to start with. Courant & Friedrichs (1948), Friedrichs (1948) and Rudinger (1955) indicate that the problem could be solved numerically by a step-by-step integration by the method of characteristics, but since the motions of the wall, the transmitted shock and the reflected shock are all interdependent such a solution would be lengthy and tedious.

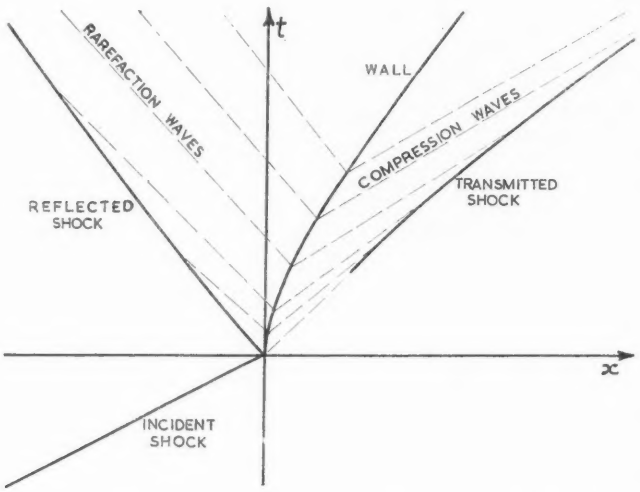

Figure 1. Wave diagram for the motion following the one-dimensional impact of a shock wave on a movable wall.

The theoretical solution given in this paper is approximate. The changes in specific entropy occurring through the transmitted and reflected shocks are neglected, so that the problem reduces to one of a simple wave type in which it is possible to determine the motion of the wall independently of the transmitted and reflected shocks. Having determined the path followed by the wall, the transmitted and reflected shocks are determined by Friedrichs' (1948) theory. Such a theory is accurate to the second order in shock strength and should therefore be reasonably accurate provided that the incident shock is not too strong.

The asymptotic behaviour of the system is considered and is shown to be exactly determinable independently of the approximate theory. Comparison is made, for varying shock Mach numbers, between the asymptotic speed of the wall as determined exactly and as determined by the approximate theory, the difference between the two giving a measure of the accuracy of the approximate theory.

The experimental investigation was made using movable walls of thin cellulose acetate, in a shock tube at an incident Mach number of 1·5. The ideal one-dimensional conditions of the theory could not be reproduced exactly because of the difficulty in avoiding a small amount of leakage past the edges of the wall, but results of the experiment show that the approximation to the one-dimensional problem was quite good, and in particular, that the motion of the wall was, for some time at least, little affected by the small amount of leakage. The agreement between theory and experiment for the path followed by the wall was excellent; for the shocks some discrepancies between theory and experiment were observed which could be attributed, in part at least, to the leakage past the edges of the wall.

2. Theory

The full characteristic equations for the regions between the shocks and the wall are

$$\frac{\partial}{\partial t}\left(\frac{2}{\gamma-1}a\pm u\right)+(u\pm a)\frac{\partial}{\partial x}\left(\frac{2}{\gamma-1}a\pm u\right)=\pm\frac{a^2}{(\gamma-1)c_p}\frac{\partial s}{\partial x}$$

and $Ds/Dt = 0$, where a, u, s are respectively the velocity of sound, particle velocity and specific entropy. If the changes in specific entropy through the transmitted and reflected shocks are neglected, the flow in the regions ahead of and behind the wall is isentropic and the characteristic equations reduce to

$$\frac{\partial}{\partial t}\left(\frac{2}{\gamma-1}a\pm u\right)+(u\pm a)\frac{\partial}{\partial x}\left(\frac{2}{\gamma-1}a\pm u\right)=0.$$

We then have that

$$P=\frac{2}{\gamma-1}a+u=\text{constant along}\ \frac{dx}{dt}=u+a,$$

and

$$Q=\frac{2}{\gamma-1}a-u=\text{constant along}\ \frac{dx}{dt}=u-a.$$

P and Q are the Riemann invariants. Since the change in specific entropy through the transmitted shock is neglected it follows that Q must be constant through the transmitted shock. Q is everywhere constant ahead of the transmitted shock and so must be everywhere constant ahead of the wall. Similarly it may be argued that P is everywhere constant behind the wall. Since Q is constant in the flow region between the wall and the transmitted shock, the positive characteristics (lines along which P is constant) are straight lines along which the flow properties are constant. In other words, the compression waves are simple waves. Similarly the negative characteristics in the region between the wall and the reflected shock are straight lines along which the flow properties are constant.

Consider some general point *ef*, figure 2, on the wall, where *f* refers to the conditions on the leading side of the wall and *e* refers to conditions on the trailing side. Ahead of the wall

$$Q_f=\frac{2}{\gamma-1}a_f-u_f=\text{constant}=Q_1,$$

which, together with the isentropic relation, leads to

$$\frac{p_f}{p_1} = \left(\frac{a_f}{a_1}\right)^{2\gamma/(\gamma-1)} = \left(\frac{Q_1 + u_f}{Q_1}\right)^{2\gamma/(\gamma-1)},$$

where p is the pressure and the suffix 1 denotes the uniform initial conditions ahead of the wall.

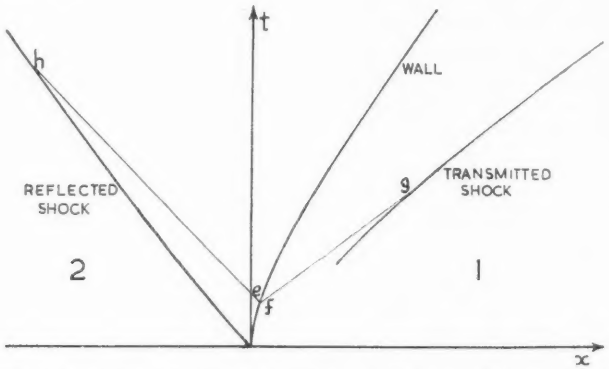

Figure 2. Wave diagram 1 denotes the region of uniform conditions into which the transmitted shock is advancing and 2 denotes the region of uniform conditions into which the reflected shock is advancing.

Similarly we have for the pressure on the trailing side of the wall

$$\frac{p_e}{p_{e0}} = \left(\frac{P_2 - u_e}{P_2}\right)^{2\gamma/(\gamma-1)};$$

hence

$$p_e - p_f = p_{e0}\left(\frac{P_2 - u_w}{P_2}\right)^{2\gamma/(\gamma-1)} - p_1\left(\frac{Q_1 + u_w}{Q_1}\right)^{2\gamma/(\gamma-1)},$$

where the suffix 0 denotes the conditions at $t = 0$, and $u_e = u_f = u_w$. Thus

$$\frac{du_w}{dt} = \frac{p_e - p_f}{p_{e0} - p_1}\left(\frac{du_w}{dt}\right)_{t=0}$$

$$= \left(\frac{du_w}{dt}\right)_{t=0}\frac{p_1}{p_{e0} - p_1}\left[\frac{p_{e0}}{p_1}\left(\frac{P_2 - u_w}{P_2}\right)^{2\gamma/(\gamma-1)} - \left(\frac{Q_1 + u_w}{Q_1}\right)^{2\gamma/(\gamma-1)}\right]. \qquad (1)$$

Before integrating (1) it is convenient to introduce the non-dimensional variables

$$U = u/a_1, \qquad A = a/a_1, \qquad \xi = x/a_1 t_c, \qquad \tau = t/t_c,$$

where $t_c = 2a_1/(\gamma+1)b$ and b is the initial acceleration of the wall. The reason for selecting this particular form of t_c as a reference time will become apparent later. In terms of these variables (1) becomes

$$\frac{dU_w}{d\tau} = \frac{2}{\gamma+1}\frac{p_1}{p_{e0} - p_1}\left[\frac{p_{e0}}{p_1}\left(\frac{P_2' - U_w}{P_2'}\right)^{2\gamma/(\gamma+1)} - \left(\frac{Q_1' + U_w}{Q_1'}\right)^{2\gamma/(\gamma+1)}\right]. \qquad (2)$$

p_{e0}/p_1, P_2' are constants which can be determined from the shock equations. Because of the particular way in which the system is made non-dimensional, Q_1' is a constant equal to $2/(\gamma - 1)$. Equation (2) can be integrated twice

with the boundary conditions $\xi = U_w = 0$ at $\tau = 0$ to determine the path of the wall. From this and the flow variables at the wall the transmitted and reflected shocks can be determined.

Consider first the transmitted shock. It starts at the point which defines the cusp at the beginning of the envelope of the positive characteristics. Courant & Freidrichs (1948) show that this cusp occurs at $\tau = 1$, $\xi = 1$. The shock is then determined as follows. Neglecting entropy changes, the equation of the positive characteristic fg (see figure 2) is

$$\xi - \xi_f = (\tau - \tau_f)(U_f + A_f).$$

This must hold at the shock, whence

$$\xi_g - \xi_f = (\tau_g - \tau_f)(U_f + A_f). \tag{3}$$

Also

$$d\xi_g/d\tau_g = M_{Sg}, \tag{4}$$

where M_{Sg} is the shock Mach number at g. Since U is constant along fg,

$$M_{Sg} = \left(\frac{\gamma+1}{4}\, U_f\right) + \left[1 + \left(\frac{\gamma+1}{4}\, U_f\right)^2\right]^{1/2} = F(U_f). \tag{5}$$

Since ξ_f, A_f, U_f are known functions of τ_f, (3) and (4) can be integrated to find the coordinates of the transmitted shock. The boundary conditions are $d\xi_g/d\tau_g = \xi_g = 1$ at $\tau_g = 1$.

Similarly, for the reflected shock,

$$\xi_h - \xi_e = (\tau_h - \tau_e)(U_e - A_e)$$

and

$$\frac{d\xi_h}{d\tau_h} = U_2 - A_2 M_{Sg} = U_2 - A_2 F\left(\frac{U_2 - U_e}{A_2}\right),$$

where F is defined by (5). The appropriate boundary conditions are

$$d\xi_h/d\tau_h = U_2 - A_2(M_{Sh})_{\tau=0}, \qquad \xi_h = 0 \quad \text{at } \tau_h = 0.$$

The equations for the wall and those for the transmitted and reflected shocks are easily integrated numerically. Analytical solutions for the paths followed by the wall and shocks can be obtained, however, since the speed of the wall is conveniently represented by the series

$$U_w = D_0 + D_1 e^{-k\tau} + D_2 e^{-2k\tau} + D_3 e^{-3k\tau} + \ldots, \tag{6}$$

where D_0, D_1, D_2, D_3, ... and k are constants. k is positive. The form of (6) is suggested by the fact that the solutions of (2) show the behaviour $U_w \to 0$ as $\tau \to 0$ and $U_w \to$ constant as $\tau \to \infty$, together with the fact that for a weak incident shock

$$U_w = C(1 - e^{-k_1\tau}),$$

where

$$C = \frac{\gamma-1}{2\gamma}\,\frac{(p_{e0} - p_1)P_2' Q_1'}{p_{e0} Q_1' + p_1 P_2'}, \qquad k_1 = \frac{4\gamma}{\gamma^2 - 1}\,\frac{p_{e0} Q_1' + p_1 P_2'}{(p_{e0} - p_1)P_2' Q_1'}.$$

The boundary conditions combined with the relations obtained by substituting (6) in (2) are sufficient to determine the constants in (6). For moderate Mach numbers of the incident shock, only a small number of terms are required, three or four being sufficient for a Mach number of 1·5. The wall path is then obtained by integrating (6). The procedure for

determining the paths of the transmitted and reflected shocks is more complicated and in general it is simpler to calculate such paths by numerical integration.

3. The asymptotic behaviour of the system

The asymptotic speed of the wall can be determined from (2). This equation indicates that as the speed of the wall increases the acceleration decreases and eventually becomes zero. The final strengths of the shocks can be obtained from the final speed of the wall, since the fluid behind the shocks will be moving at the same speed as the wall. However, the asymptotic behaviour of the system can be obtained exactly, and independently of the above analysis, by one of a number of physical arguments which are true for any strength of incident shock. Such an argument is as follows. For a given incident shock Mach number, the only fundamental length in the problem is $\rho_w r/\rho_1$, where ρ_w is the density of the wall material, r the thickness of wall and ρ_1 the density of the fluid initially in the channel ($a_1 t_c$ is simply a constant multiple of $\rho_w r/\rho_1$). The strength of the transmitted shock can then depend only on the distance parameter $\xi' = x\rho_1/\rho_w r$, and its asymptotic value is obtained when $\xi' \to \infty$. This shows that the same shock strength is obtained whether $x \to \infty$ or $\rho_w r \to 0$. The case $\rho_w r = 0$ corresponds to the flow without the wall present and it can therefore be concluded that as $x \to \infty$ the strength of the transmitted shock tends to the strength of the incident shock. The reflected shock eventually becomes vanishingly weak. Although the transmitted shock eventually attains the same strength as the incident shock it will not at a given instant of time have reached the position that the incident shock would have reached if it had not encountered the wall. When the quasi-steady state is attained there will be a constant displacement between the position of the transmitted shock and the position that the incident shock would have reached. An expression for the amount of the displacement can be found as follows.

Figure 3 (*a*) shows a piston moving in a channel of uniform cross-section. The piston is started impulsively from rest at time $t = 0$ and continues to move with a constant speed u_2. A shock is generated which moves away from the initial position of the piston face with a constant speed w until it encounters a movable wall situated sufficiently far ahead of the piston to ensure that no disturbance travels back to the piston. Figure 3 (*b*) illustrates the case in which no wall is encountered. An expression is sought for the final value of the displacement δ between the two shocks. It will be supposed that in (*a*) the transmitted shock has not quite attained the strength of the incident shock. Define for (*a*) a velocity u_2' such that

$$u_2' = \frac{\int_0^{L-\delta} \rho u \, dx + \rho_w r u_w}{(L\rho_2 - \delta\rho_1) + \rho_w r},$$

$(L\rho_2 - \delta\rho_1)$ being the mass of the fluid between the shock and the piston in (*a*). u_2' will be close to the linear mean velocity of the fluid between the

shock and the piston in (*a*). Since the pressure on the pistons in both cases is the same and constant, the momentum contained between the pistons and some control surface ahead of the shocks must, at any instant of time, be the same for both systems. Therefore

$$L\rho_2 u_2 = [(L\rho_2 - \delta\rho_1) + \rho_w r]u_2',$$

and so

$$\delta = \rho_w r/\rho_1 - L\rho_2(u_2 - u_2')/u_2'.$$

Put $u_2 - u_2' = \Delta u$, where $\Delta u/u_2 \ll 1$, and note that $L = (w - u_2)t$ and $(w - u_2)\rho_2 = w\rho_1$, where w is the speed of the incident shock and t is the time measured from the instant at which the piston commenced to move. Then

$$\delta = \rho_w r/\rho_1 - wt\Delta u/u_2. \tag{7}$$

Now suppose that $\Delta u = B/t^n$, where n is positive. Equation (7) shows that, if $n < 1$, $\delta \to -\infty$ as $t \to \infty$, which is clearly impossible. If $n = 1$, δ is independent of t and therefore independent of Δu. This is also impossible since $d\delta/dt$ is a function of Δu. Or, more simply, if Δu is not zero the shocks are not of equal strength and δ must change with time. Therefore $n > 1$ is the only case admissible. As $t \to \infty$, $\delta \to \rho_w r/\rho_1$.

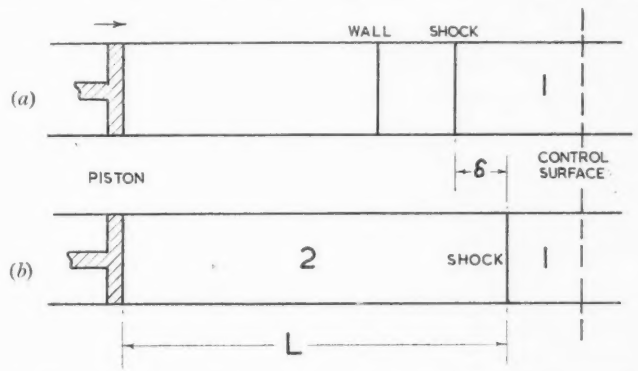

Figure 3. The displacement of the transmitted shock from the position that the incident shock would have attained if it had not encountered the wall.

The fact that the transmitted shock must eventually become equal in strength to the incident shock provides a useful check on the approximate theory. It also gives an indication of how p_{e0}/p_1, which appears in (2), should be determined. Consistently with the approximate theory, p_{e0}/p_1 may be calculated assuming isentropic compression through the reflected shock, or alternatively, the shock relations may be used to determine the exact value of p_{e0}/p_1. On first thoughts it might appear that there would be some advantage in having the initial pressure difference across the wall correct. Figure 4 shows plots of the ratio $(U_w \text{ approx.})_{\tau\to\infty}/(U_w \text{ true})_{\tau\to\infty}$ against incident shock Mach number. The upper curve is obtained using the 'isentropic' value of p_{e0}/p_1, whereas the lower curve is determined with the exact value of p_{e0}/p_1. The approximate theory appears to be

best if the 'isentropic' value of p_{e0}/p_1 is used, although the additional error introduced by using the exact value of p_{e0}/p_1 is not great. Figure 4 also indicates that the approximate theory predicts $(U_w)_{\tau\to\infty}$ fairly accurately even when the incident shock Mach number is far from unity.

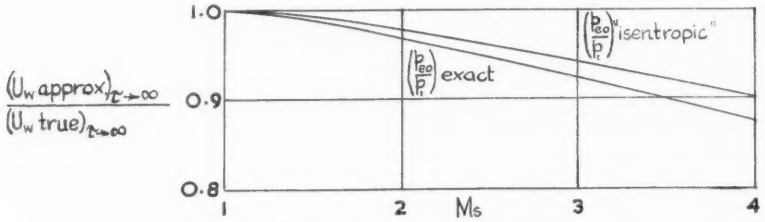

Figure 4. Error in the approximate theory.

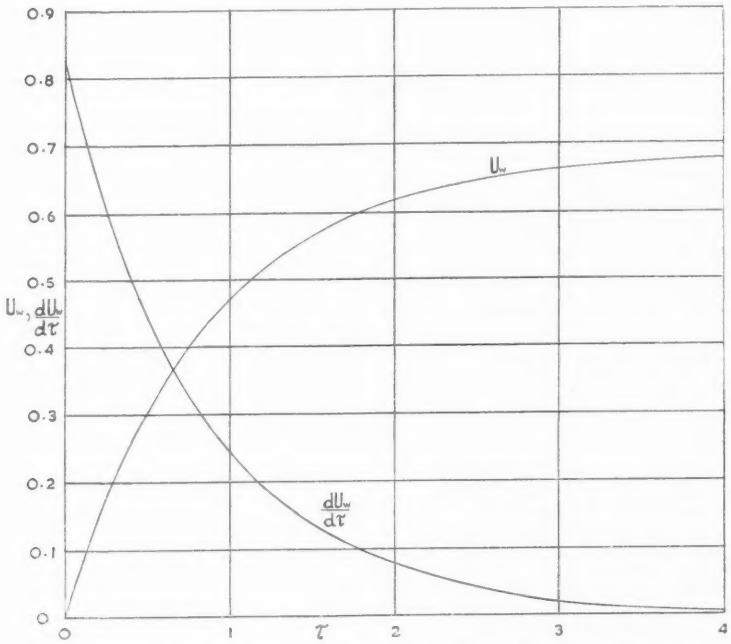

Figure 5. Variation with time of the wall speed and the wall acceleration.

The behaviour of the wall, the transmitted shock and the reflected shock have been computed for an incident shock Mach number of 1·500. Figure 4 shows that at this incident shock Mach number the final speed of the wall as predicted by the approximate theory differs from the true final speed by about 1%. The computed results are summarized in figures 5, 6 and 10. In figure 10, where the experimental results are compared with the theory, the paths of the wall, the transmitted shock and the reflected shock are

shown. Figure 5 shows the variation with time of wall acceleration and of wall speed. Figure 6 shows how the strengths of the transmitted and reflected shocks vary as they propagate, together with the asymptotic values of $M_S - 1$. The fact that these asymptotic values differ by only small amounts

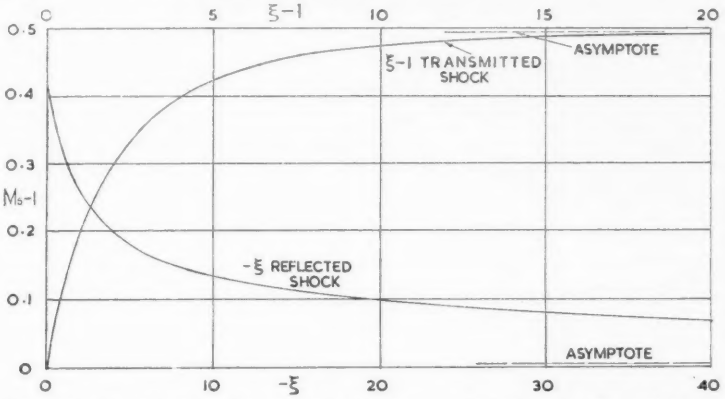

Figure 6. Variation in the strength of the transmitted and reflected shocks.

from 0·500 and 0 respectively is a further indication that the error in the approximate theory for an incident shock Mach number of 1·500 is small.

4. The shock tube

The shock tube at the Mechanics of Fluids Laboratory is of rectangular cross-section 5·785 in. deep and 1·500 in. wide; it is 13 ft. 6 in. long and closed at one end. The diaphragm is 12 ft. from the closed end and the high pressure section is maintained at atmospheric pressure. The required pressure ratio across the diaphragm is achieved by evacuating the low pressure section of the shock tube. The shock speed is measured by timing the passage of the shock between two schlieren light screens placed 1 ft. apart. Investigations are usually made by schlieren spark photography, and photographs, only one per run, can be taken at known pre-set delays after the shock passes the second light screen. The use of the shock tube is limited to a shock Mach number below about 1·9, because above this the density in the shock tube becomes too low for the light screens to function. A general description of the tube together with its instrumentation is given by Lapworth (1954).

5. Experiments

The object of the experimental study was to determine the motions of the wall, the transmitted shock and the reflected shock by taking photographs of the interaction at various known time intervals after the incident shock had passed the second light screen.

The experimental conditions were chosen to make the scale of the experiment suit the size of the shock tube ($a_1 t_c \doteqdot 4$ in. or $b \doteqdot 3 \times 10^6$ ft./sec^2).

For an incident shock Mach number of 1·500 a cellulose acetate sheet 0·0017 in. thick gave $a_1 t_c = 4{\cdot}025$ in. and $b = 3{\cdot}100 \times 10^6$ ft./sec^2. Some experiments were carried out with walls of 0·0010 in. and 0·0030 in. thick cellulose acetate, using the same incident shock Mach number, to check that the results (in non-dimensional form) were, as the theory suggested, independent of the mass of the wall.

Owing to the difficulty of mounting the wall in the full cross-section of the shock tube it was decided to use a channel of reduced cross-section, obtained by inserting liners in the working section. This scheme also had the advantage that the holding device for the wall could be shifted simply by moving the liners along the shock tube. The reduced channel was 2·830 in. deep and 1·500 in. wide.

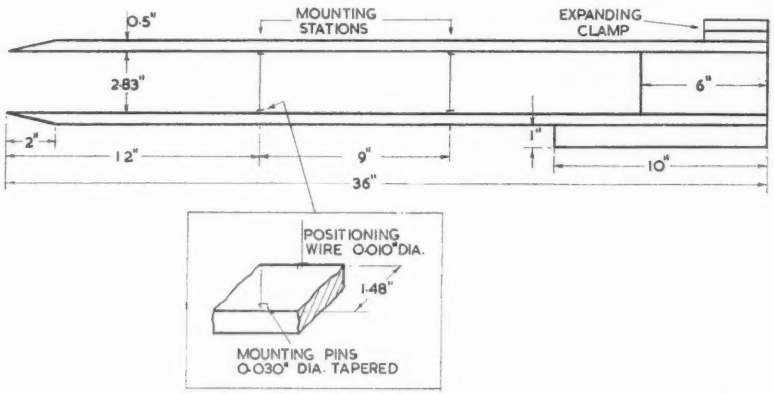

Figure 7. Liners, together with details of mounting pins and positioning wires.

Lack of stiffness made it necessary to support the wall until it was struck by the shock. Support was provided by impaling each corner of the wall on a slender pin pointing in the direction in which the wall was to move. Figure 7 is a diagram of the liners showing details of the mounting pins. The vertical wires alongside the pins were provided so that the wall could be placed in the same position, against the wires, for each run. In mounting the wall it was required that the wall should as nearly as possible fill the cross-section of the working channel and also that it should be as plane as possible. Meeting these requirements was the most difficult part of the experiment. Figure 8 shows the device that was eventually used in mounting the sheet cellulose acetate. Strips of the wall material 1·500 in. wide were stretched and accurately held on the device by the movable clamp. The device was then carefully placed between the liners and the strip of wall material accurately positioned on the pins. A sharp knife was used to cut the wall to size in position. The wall was left with some wrinkles when the mounting device was removed, but when the shock tube was closed and the

pressure reduced the cellulose acetate dried slightly, shrinking in the process, and was left stretched plane on the pins*.

Experiments were carried out to measure the loss of mass of the cellulose acetate due to drying which was found to be of the order of 1%. Account was taken of this loss of mass.

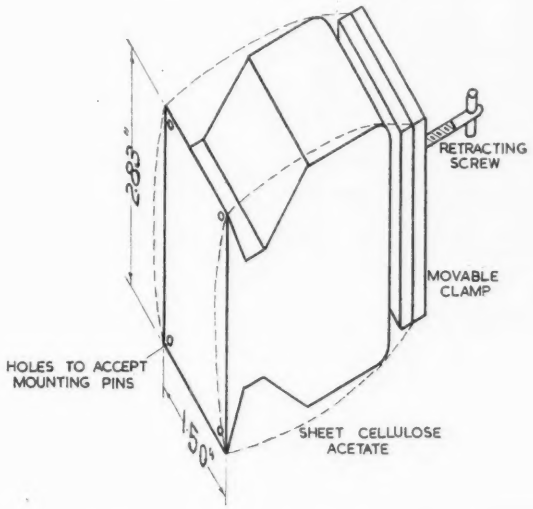

Figure 8. Device for positioning the wall.

Measurements of the photographic negatives, 0·6 full size, were made with a travelling microscope accurate to $\pm 0{\cdot}0005$ in. All measurements were made on the centre line of the working channel. The pressure in the shock tube was measured with a mercury manometer accurate to $\pm 0{\cdot}2$ mm Hg. The ambient temperature was measured with a mercury thermometer accurate to $\pm 0{\cdot}1^{\circ}$ C. Throughout all experiments an endeavour was made to keep the variations of incident shock Mach number to within 1% and this was nearly always achieved.

6. Experimental results and discussions

Figure 9 (plate 1) shows the wall in several positions after it has been struck by the shock. In figure 9(*a*) the mounting pins, the positioning wires and the wall are seen, while in the others only the wall appears. During the early stages of its motion the wall remains very flat, but as it progresses away from its initial position the edges are observed to lag behind the main body of the wall. The curling of the edges increases as the motion of the wall proceeds, although the extent of the curling is not

* The artifice of allowing material like cellulose acetate to dry in order to produce a taut diaphragm is well known domestically in the preparation of covers for jam-jars.

considerable until the wall has moved some distance. At $x = 3{\cdot}583$ in., figure 9(*d*), the shape of the wall is still a good approximation to the ideal plane moving wall, but at $x = 6{\cdot}726$ in., figure 9(*e*), this is no longer the case since the wall has become distinctly curved. When the wall reaches $x = 6{\cdot}726$ in. it has attained a speed which is about 90% of its final speed, and from then on its speed is changing only slowly so that most of the interesting part of the wall path has already been covered. It should be remembered that the plates showing the wall are photographs of different walls at the various distances and not photographs of the same wall at these distances. No attempt should therefore be made to follow too closely the distortions of the wall from one photograph to the next for it may occur that photographs of different walls in the same position are different in detail. The curling of the edges of the wall needs some explanation.

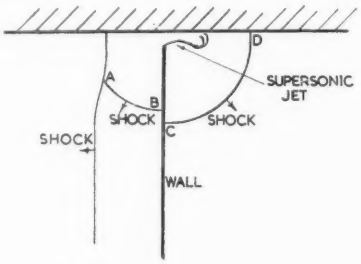

Figure 10. Diagrammatic sketch of the shock wave pattern near a gap at the edge of the wall from which a shock wave is reflected.

It appears that the curling of the wall edges results mainly from leakage past the edges of the wall. Figure 13 (plate 2) shows the interaction of a shock with a movable wall in which large gaps have intentionally been left at the top and bottom edges of the wall and figure 10 is a diagrammatic sketch of the interaction in the neighbourhood of a gap. Part only of the shock *AB* is seen in figure 13 (*a*) since it is very weak and since the schlieren photograph was taken with the knife edge perpendicular to the direction of flow. Approximate analysis of the normal reflection of a shock at a wall with a slit in it, by Whitham's (1957) theory, together with the results of an experimental investigation by the author, suggest that the shocks *AB* and *CD* are too weak at the wall to be responsible for the observed curling. Modification of the pressure forces near the edges of the wall by the flow past the edges is thought to be the main cause of the curling. The fluid approaches the gap, accelerates, passes through the gap, separation occurs at the edge of the wall and a small supersonic jet forms. The decrease in pressure of the fluid approaching the gap reduces the pressure difference across the wall in the neighbourhood of the gap, causing the edges to lag behind the main body of the wall. Provided that the gaps are small and the curling slight, leakage should have only a small effect on the motion of the wall as a whole.

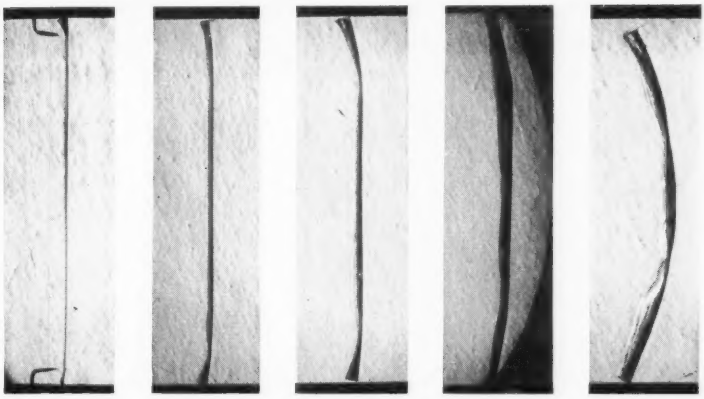

(*a*) (*b*) (*c*) (*d*) (*e*)

Figure 9. The moving wall in several positions after being struck by the shock wave.

(*a*) $\tau = 0{\cdot}300$, $\xi = 0{\cdot}034$, $x = 0{\cdot}144$ in. ;
(*b*) $\tau = 0{\cdot}947$, $\xi = 0{\cdot}250$, $x = 1{\cdot}035$ in. ;
(*c*) $\tau = 1{\cdot}751$, $\xi = 0{\cdot}644$, $x = 2{\cdot}684$ in. ;
(*d*) $\tau = 2{\cdot}076$, $\xi = 0{\cdot}859$, $x = 3{\cdot}583$ in. ;
(*e*) $\tau = 3{\cdot}280$, $\xi = 1{\cdot}659$, $x = 6{\cdot}726$ in.

(*a*) (*b*) (*c*) (*d*) (*e*)

Figure 11. The transmitted shock in various stages of formation.

(*a*) $\tau = 1{\cdot}140$, $\xi = 1{\cdot}242$, $x = 5{\cdot}122$ in. ;
(*b*) $\tau = 1{\cdot}275$, $\xi = 1{\cdot}396$, $x = 5{\cdot}678$ in. ;
(*c*) $\tau = 1{\cdot}670$, $\xi = 1{\cdot}847$, $x = 7{\cdot}627$ in. ;
(*d*) $\tau = 2{\cdot}520$, $\xi = 2{\cdot}897$, $x = 11{\cdot}987$ in. ;
(*e*) $\tau = 3{\cdot}228$, $\xi = 3{\cdot}983$, $x = 16{\cdot}183$ in.

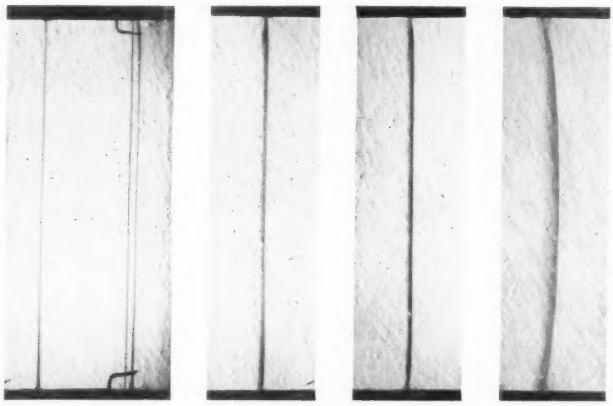

(*a*) (*b*) (*c*) (*d*)

Figure 12. The reflected shock at several distances from the initial position of the wall.

(*a*) $\tau = 0{\cdot}178$, $\xi = -0{\cdot}170$, $x = -0{\cdot}685$ in. ;
(*b*) $\tau = 0{\cdot}358$, $\xi = -0{\cdot}325$, $x = -1{\cdot}312$ in. ;
(*c*) $\tau = 0{\cdot}688$, $\xi = -0{\cdot}611$, $x = -2{\cdot}474$ in. ;
(*d*) $\tau = 3{\cdot}388$, $\xi = -2{\cdot}573$, $x = -10{\cdot}494$ in.

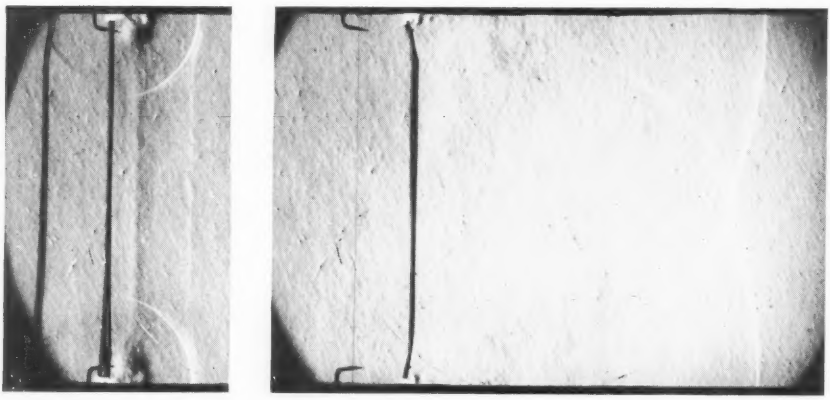

(*a*) (*b*)

Figure 13. Two stages in the motion following the impact of a shock wave on a movable wall along the top and bottom edges of which large gaps have been left.

Figure 11 (plate 1) shows the transmitted shock at various stages during its formation. Figures 11 (*a*) and (*b*) show that during its initial stages the transmitted shock is far from plane and its ends are forked. This is due to the fact that the transmitted shock is composed not only of compression waves coming from the accelerating wall but also of weak shocks which originate at the gaps around the edges of the wall. The transmitted shock is thus the result of the interaction of four approximately cylindrical shocks, some of which may be stronger than others, and the compression waves coming from the accelerating wall. The nature of the shocks coming from the gaps and their interaction are shown in figure 13 (plate 2). Figures 11 (*c*), (*d*) and (*e*) (plate 1) show that as the transmitted shock propagates it soon takes up the stable plane form for a shock travelling in a straight duct of uniform cross-section.

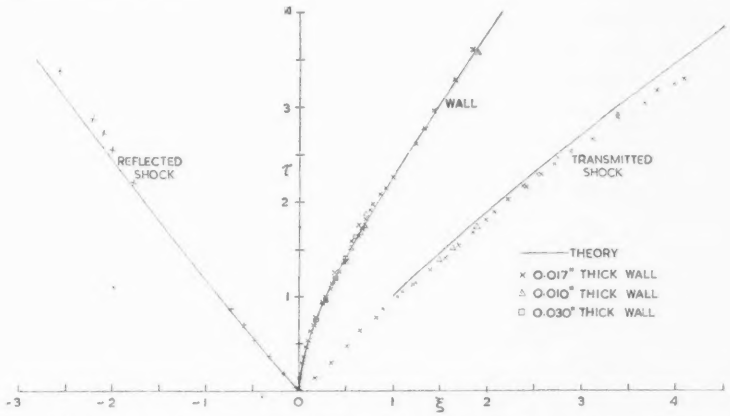

Figure 14. Comparison of the theoretical and experimental results.

Figure 12 (plate 2) shows the reflected shock at several distances from the point at which the incident shock struck the wall. In figure 12 (*a*) the mounting pins, the positioning wires and the reflected shock are seen while in the others only the reflected shock appears. The reflected shock is plane to start with, but as it moves away from the initial position of the wall it becomes curved at the channel walls and woolly in appearance. The curving and the woolly appearance are due to the growth of the boundary layer on the channel walls. In figure 12 (*d*) the boundary layer on the channel walls appears to be relatively thick.

Figure 14 compares the theoretical and experimental results. Before discussing the comparison in detail it would be as well to consider the relative sizes of the errors in the theory and those in the experimental technique. It has already been stated that for an incident shock Mach number of 1·500, the approximate theory predicts the final speed of the wall with an error of the order of 1%. Figure 6 indicates that the final

Mach numbers of the transmitted and reflected shocks are also given with an error of approximately 1%. If it is assumed that the approximate theory gives the wall speed and the shock Mach numbers correct to 1% for all times, then the displacements of the wall, the transmitted shock and the reflected shock will also be given with an error of only 1%. Since the errors in the experimental technique are about 1% the errors in the approximate theory are not thought to be significant in the comparison of the theoretical and experimental results.

Referring again to figure 14, it will be seen that there is good agreement between the theoretically determined curve for the path followed by the wall and the experimentally determined points. It is also apparent that the results are, as expected, independent of the mass of the wall. The experimental points for the reflected shock agree well with the theoretical curve for the initial part of the shock path, but for larger times the shock lags behind the position predicted by theory. Part at least of this lag is due to leakage past the edges of the wall and leakage past the sides of the liners, which were made 0·20 in. narrower than the shock tube to avoid damaging the working section windows. The experimental results for the transmitted shock show two distinct departures from the theoretically determined shock. In the first place, a shock appears in the region $0 < \xi < 1$ where theory predicts none and, secondly, the experimental points appear consistently ahead of the theoretically determined shock. The appearance of shocks in the region $0 < \xi < 1$ is due simply to shocks getting past the edges of the wall. The displacement is probably due to leakage past the edges of the wall and to leakage past the sides of the liners; the displacement at $\xi = 1$, $\tau = 1$, where, in theory, the transmitted shock wave should just begin to form, is mainly due to the former type of leakage. It is difficult to give a detailed analysis of the effect of leakage, but a simple model can be imagined which will probably yield an answer of the correct order of magnitude. Assume that the gap is uniformly distributed over the wall or, in other words, that the wall is porous. Further assume that the leakage through the wall and the wall acceleration remain constant for a short time. The contact surface, which separates the gas which has passed through the wall and that which has not, moves away from the wall with a constant speed, and so the transmitted shock can be imagined as resulting from the motion of a piston which is impulsively given a small speed and then accelerates with the acceleration of the wall. The transmitted shock starts at $\xi = 0$, $\tau = 0$, and by using Friedrichs' (1948) theory, the position of the transmitted shock at $\tau = 1$ can be found for a given initial velocity of the contact surface. Or, given the position of the shock at $\tau = 1$, the initial velocity of the contact surface can be found. From this, assuming isentropic expansion through the wall, the leakage area of the wall can be determined. According to this argument the observed displacement was consistent with a leakage area equivalent to a gap of 0·005 in. along all edges of the wall. This appears to be of the correct order of magnitude, bearing in mind the difficulty of arranging the flimsy wall-material, 0·0017 in.

thick, to fill completely the cross-section of the tube and the gap of 0·01 in. between the liners and the walls of the shock tube.

The author wishes to acknowledge much helpful advice and constructive criticism given him by Dr N. H. Johannesen and Professor P. R. Owen. He is also grateful to the Defence Scientific Corps, Royal New Zealand Air Force, for making his period of study at Manchester University possible.

References

Courant, R. & Friedrichs, K. O. 1948 *Supersonic Flow and Shock Waves.* New York : Interscience.

Friedrichs, K. O. 1948 Formation and decay of shock waves, *Comm. Pure Appl. Math.* **1,** 211.

Lapworth, K. C. 1954 M.Sc. Thesis, Manchester University. (Precis available in *Aero. Res. Counc., Lond., Rep.* no. 17328.)

Pillow, A. F. 1949 The formation and growth of shock waves in the one-dimensional motion of a gas, *Proc. Camb. Phil. Soc.* **45,** 558.

Pillow, A. F. & Levey, H. C. 1947 The formation and growth of shock waves in the one-dimensional motion of a gas, *Aus. Counc. Sci. Indus. Res., Div. Aero. Rep.*, no. A47.

Rudinger, G. 1955 *Wave Diagrams for Non-steady Flow in Ducts.* Princeton : Van Nostrand.

Whitham, G. B. 1957 A new approach to problems of shock dynamics, *J. Fluid Mech.* **2,** 145.

REVIEWS

Gas Dynamics, by KLAUS OSWATITSCH; English version by Gustav Kuerti. New York: Academic Press Inc., 1956. 610 pp. $12.00.

The original German version of this book was published in 1952; the English version under review bears the date 1956 and one's first and immediate reaction is to ask whether or not the subject has grown to such an extent in the intervening four years as to make profitable this reissue in translated form. Quite obviously in such a rapidly growing subject it is not every book that can stand up to such a time lapse.

In an attempt to decide whether Professor Oswatitsch's book has withstood it, one must examine in some detail its objects and scope. These are set out in prefaces to the translated edition. As far as the objects are concerned, Professor Kuerti says, in his preface, "There is still a place in the literature of the English language for a book of moderate length on gas dynamics, combining a thorough and imaginative account of the fundamentals with a survey of the advanced methods of analysis that are beyond the scope of the usual textbooks of aeronautical engineering". As far as the scope is concerned, Professor Oswatitsch says "Gas dynamics deals with the flow of compressible media. It represents the *general* form of hydrodynamic theory and includes as a special case the classical hydrodynamics of liquids.... In this book the flowing medium will be treated as a continuum; considerations that belong to the field of kinetic theory of gases will be omitted. Even so the range of topics remains very large indeed.... This makes further restriction necessary, arbitrary to the extent that a clear cut boundary between gas dynamics and its neighbour sciences cannot be drawn.... The *typical problems of gas dynamics* always involve considerable changes of density" (author's italics).

In fact the subject as presented is perhaps more restricted than even this last sentence suggests, for the emphasis is very largely on inviscid flows, as will emerge when we go on to consider the detailed contents. In addition to the publisher's agreement to the references being brought up to date, one final quotation from the preface is relevant; Professor Oswatitsch says "In preparing the English text improvements have been made and many formulations have been rendered more precise. Thus the substance of the book has in my opinion profited by the translation."

The first chapter entitled thermodynamics is perhaps too short to be really successful. It is difficult to avoid feeling that it raises in the reader's mind more problems than it answers and does not pay enough attention to dynamical processes which should after all be the prime concern here. Even at the time it was first written, the ideas of the classical thermodynamics of media at rest had been successfully extended in part at least to gases in motion by such writers as Tolman and Fine (see for example *Rev. Mod. Phys.* **20,** 1948, 50–77), but I suspect that the passage of four more years has made the omissions seem more glaring.

The next two chapters are devoted to steady and unsteady one-dimensional flows respectively and here one feels that the book can stand up to any examination. Although the author makes no claim to an encyclopaedic completeness the accounts here are full and illuminated by appropriate and interesting examples, including, for instance, the effects of combustion, detonation and condensation, as well as an account of Lagrange's problem in internal ballistics.

Two chapters follow on general equations and theorems and on the application of the integral theorems in particular cases. Here the general differential equations of motion and energy are derived and from them similarity rules are obtained. Perhaps rather more would have been said about the second coefficient of viscosity had the book been written today, but this is not a serious criticism. An interesting point of nomenclature arises. The word homentropic as originally suggested by the Fluid Motion Sub-Committee of the Aeronautical Research Council has been adopted for flows in which the entropy is constant in a region of space and the word isentropic for a process in which the entropy of an individual element remains constant, as for example in some steady flows along a streamline. However, when it comes to energy considerations, where again the same distinction can usefully be drawn between regions in which the energy is constant and processes in which the energy of an element remains constant, the corresponding nomenclature homenergic has been spurned in favour of isoenergetic.

The integral theorems are primarily concerned with the forces experienced by bodies immersed in streams, and their application to specific problems show the book at its best.

Chapters 6 to 10 inclusive, rather more than half the bulk of the book, are devoted to inviscid flows steady and unsteady, subsonic, transonic and supersonic in two and three dimensions. Whilst it is true, as Professor Oswatitsch himself comments in the preface, that much has been achieved since the original version appeared, particularly in linearized theories, yet even faced with complete freedom in 1956 some drastic selection would be necessary to keep the book within its avowed limits. Professor Oswatitsch's original selection was weighted very much towards discussion of the basic physical phenomena and typical results rather than on mathematical techniques for dealing with specific problems. It is an over-simplification to say that all the recent developments have taken place in this latter field, but certainly the book has been saved by its approach from being as outdated as some of its contemporaries. This is not to say that the passage of four years has left the book unscathed; one would imagine that the area rule would have been seized on by Professor Oswatitsch had he been writing today and that he would have said more about transonic flows, for example. However, the fact remains that chapters of the book have still much to offer and my most serious criticism is that more has not been made of the permission to bring references up to date.

Chapter 11, devoted to viscous and turbulent flows, is the one where in your reviewer's opinion it least measures up to its task. There is so

much more that should be said even accepting the exclusion of all flows in which the density changes are small. It might, one feels, have been better to limit the stated objectives even further and to omit this chapter altogether rather than give the impression of such an unbalanced treatment. Here again many more references might have been added.

Chapter 12, the final chapter, gives a brief account of experimental methods and is open to the same type of criticism as those levelled against Chapter 11.

The final conclusion I reach is that apart from the first chapter, and the last two particularly, which unbalance it, the book has much to commend it. A detailed study of it will reward any serious student and lead, as Professor Oswatitsch states as his intention, to an insight and understanding of many of the fundamental aspects of gas dynamics.

L. HOWARTH

Wing Theory, by A. ROBINSON and J. A. LAURMANN. Cambridge University Press, 1956. 569 pp. 75*s.* or $13.50.

The publication of a new book on wing theory by the Cambridge University Press is surely an important event for many of us, especially when we reflect that the same Press published Glauert's *Aerofoil and Airscrew Theory* some thirty years ago, and that that famous volume has been almost the only book on the subject in all the intervening years. One is led to speculate on whether the new work will be as useful to new generations of aerodynamicists as 'Glauert' has been. To do so, it would have to combine as effectively the physical explanation and the mathematical development.

The content of the new book is impressive, representing as it does the increased scope of the subject: aerofoils in two- and three-dimensional flow at low speeds, aerofoils in compressible flow (subsonic, transonic, and supersonic), and aerofoils in unsteady motion. All this is preceded by an introductory chapter entitled "Foundations" in which the fundamental ideas of fluid mechanics are reviewed, with emphasis on such concepts as source, doublet, and vortex distributions, particularly useful in wing theory. This chapter also includes a concise discussion of viscosity and of the assumptions of the Navier–Stokes equations. This provides the basis for some dimensional analysis and the boundary-layer approximations, including the momentum-integral equation. Turbulence is also described, Reynolds' equations are derived, and the turbulent boundary layer briefly discussed. These real-fluid phenomena are to prepare the reader for the subsequent discussions of wakes and trailing-edge conditions that are central to the subject of wing theory, but so often glossed over in textbooks.

Two-dimensional aerofoil theory for low speeds is, of course, largely a matter of complex-variable techniques and the thin-aerofoil theory. These matters seem to be handled competently. There is a purely

mathematical section on conjugate functions. Theodorsen's method for arbitrary profiles is given, and so are Lighthill's procedure for prescribed pressure distribution and Goldstein's approximate calculations. Cascades of aerofoils are also treated briefly, and there is an explanation of profile-drag determination by Pitot-traverse methods. The latter includes discussions of boundary-layer calculations (turbulent and laminar) and the Pohlhausen procedure.

The chapter on three-dimensional aerofoils in low-speed flow begins with considerable generality, for singular behaviour of the velocity at the leading edge is assumed from the beginning and the force formulas are accordingly complicated. Lifting-line theory appears as a special case; the reviewer remarks that present authors do not seem able to recapture the clarity of Prandtl's original presentation. Among other computational schemes, the one attributed to Multhopp (but actually originated by I. Tani) is given. The theory of minimum induced drag for general multiplane arrangements is included. The lifting-surface approximations of Falkner, Weissinger, and others are presented, and then R. T. Jones's theory for small aspect ratios. Wind-tunnel-wall interference is calculated in detail, for open, closed, and slotted boundaries.

The reader of this review will recognize from what has been said already that the scope of the book is ambitious. The chapter on aerofoils in compressible steady flow is comparable in size and in scope to some of the monographs on the subject that have appeared. Almost everything is included: source-sink methods, conical flow, Evvard's technique, higher-order approximations, transonic similitude, the shock polar—even hodograph theory. It is surprising, in view of this thoroughness, that the energy equation of compressible flow is never mentioned; the isentropic equation of state appears as an unexplained assumption, and the generalized Bernoulli equation then follows, of course, from the equations of motion.

Finally, there is the chapter on aerofoils in unsteady motion. This begins with an exceptionally fine introduction, and proceeds to the classical theory of two-dimensional thin aerofoils. The usual vertical-gust cases, however, are contained in a rather complicated section devoted to " motions with non-uniform average velocity ". The subject of three-dimensional wings in unsteady flow is handled principally by discussion and some references. For two-dimensional compressible flow the Lorentz transformation is used, following Küssner, to set up elementary solutions; this leads to Possio's integral equation, approximate solutions of which are discussed briefly. Supersonic unsteady aerofoil theory is a somewhat simpler affair, and here, for oscillating aerofoils, the solution is actually carried out. The chapter includes a considerable portion of new material, previously unpublished.

This book has been carefully planned and written. The authors' attention to the published literature, both old and new, is very impressive; it includes, incidentally, an appended bibliography of over 100 more recent titles. The index seems complete and well organized. The

character of the book, it seems to this reviewer, is something like this. After a clear, physical, but concise introduction of each new subject, the mathematical argument appears and often becomes rather elaborate and, especially, lengthy. Conclusions are reached, graphs are sometimes provided, and experimental confirmation and references to literature are not omitted. But one wonders whether a graduate student (for whom, among others, the volume is intended) may not get lost in the intervening analysis. One therefore feels somewhat more confident in recommending this volume as a reference book for engineers and research workers than as a textbook, even for graduate students. It may be argued that wing theory is naturally a highly mathematical subject—practically a minor branch of mathematical analysis, once the fundamental assumptions are set down and the boundary conditions established—and that a textbook of this character is therefore appropriate. Perhaps the correct answer depends on whether we intend our students to become masters of the mathematical art of applying established theories or the successors of Prandtl, Munk, Ackeret, and R. T. Jones, who originated the theories but whose greatest contributions to wing theory were not essentially mathematical. If the latter is our goal (and admittedly it is a ridiculously optimistic one!) we might prefer a textbook with a slightly different emphasis. But this is not a severe criticism of Robinson and Laurmann, especially since the other textbooks, with slightly different emphasis, are non-existent. Their volume will be widely used and much appreciated.

W. R. SEARS

CORRIGENDUM

" On the hydrodynamic stability of two viscous incompressible fluids in parallel uniform shearing motion ", by S. FELDMAN (*J. Fluid Mech.* **2,** 1957, 343).

Page 358. In the second line below figure 3, replace $F = W = 0$ by $F = W = \infty$.

Page 368. The expressions within large round brackets in equations (88) and (89) should read as

$$\frac{\phi^{\mathrm{iv}}\bar{\phi} - 2\alpha^2\phi''\bar{\phi} + \alpha^2\phi\bar{\phi}}{U-c} + \text{complex conjugate.}$$

The expression within the first pair of square brackets on the right-hand side of equation (91) should read as

$$\phi^{\mathrm{iv}}\bar{\phi} + \bar{\phi}^{\mathrm{iv}}\phi - 2\alpha^2(\phi''\bar{\phi} + \bar{\phi}''\phi) + 2\alpha^2\phi\bar{\phi}.$$

JOURNAL OF FLUID MECHANICS

Volume 3, Part 3 December 1957

CONTENTS

Some shock tube experiments on the chemical kinetics of air at high temperatures
by SAUL FELDMAN 225

The diffraction of a rarefaction wave by a corner
by J. B. L. POWELL 243

A note on Mott-Smith's solution of the Boltzmann equation for a shock wave
by AKIRA SAKURAI 255

The flow of swirling water through a convergent–divergent nozzle
by A. M. BINNIE, G. A. HOOKINGS and M. Y. M. KAMEL .. 261

The structure of a shock wave in a fully ionized gas
by J. D. JUKES 275

On fully-dispersed shock waves in carbon dioxide
by WAYLAND C. GRIFFITH and ANNE KENNY 286

The instability of a shear layer between two parallel streams
by ROBIN E. ESCH 289

The effect of a magnetic field on Stokes flow in a conducting fluid
by W. CHESTER 304

The impact of a shock wave on a movable wall
by R. F. MEYER 309

Reviews 324

Printed in Great Britain by Taylor & Francis Ltd.